Università degli Studi di Udine
Dipartimento di Matematica e Informatica
Dottorato di Ricerca in Informatica

Ph.D. Thesis

First Quantization Table Detection in Double Compressed JPEG Images

Candidate
Fausto Galvan

Supervisor
Prof. Alberto Policriti

Co-Supervisor
Prof. Sebastiano Battiato

Cycle XXVII — A.Y. 2014-2015

Institute Contacts
Dipartimento di Matematica e Informatica
Università degli Studi di Udine
Via delle Scienze, 206
33100 Udine — Italia
+39 0432 558400
http://www.dimi.uniud.it/

Author's Contacts
Via Molin Nuovo, 88
33100 Udine — Italia
+39 3313689868
fausto.galvan@giustizia.it

Ai miei molti maestri,
consapevoli e non.

Acknowledgements

First and foremost I would like to thank my advisors, Prof. Sebastiano Battiato and Prof. Alberto Policriti, for their advice, guidance and support over the years.
A special thanks also to Prof. Giovanni Puglisi and Arcangelo R. Bruna for their technical and theoretical advices, to Federico Costantini who helped me for the Section about the digital evidence and to AMPED SRL [1] for providing useful code for DCT coefficient manipulation and a big collection of quantization matrices.
And finally, it' impossible not to thanks my wife for her endless patience and encouragement, my daughters for giving me so many tender reasons to distraction, and my parents for their never ending trust in me.

Abstract

In order to efficiently check the originality of images and videos from the all-day context, in the last ten years the scientific discipline known as Image Forensics, whose goal is exploit the knowledge from the science of Image Processing to answer questions that arise in the forensic scenario, has developed at a growing rhythm. The objective of this doctoral study is to actively contribute to this research field developing an approach devoted to recover the coefficients of the JPEG quantization matrix used to compress an image at the time of shooting (i.e., when the image has been created), when for some reasons this information is no more available in the Exif metadata. This scenario may include the primary quantization coefficients of an image that has been doubly JPEG compressed, or the retrievial of the compression matrix of an uncompressed image previously JPEG compressed, since in both these cases the values of the primary compression steps are lost.
Once we are able to distinguish which is the "compression history" of a digital image, in particular the quantization matrix used for the first compression, it is possible to exploit this information both for Image Forgery Identification and Image Source Identification, two of the main areas of Multimedia Forensics science.
Although some papers allow taking an overview to the state of the art about Image Forensics methods, the need to include all the approaches in the various subsets of this research area necessarily prevents to explore in depth every one of them. Our purpose is to fill this gap regarding the approaches in the DCT domain, that has never been covered as a stand-alone topic.
The impact of visual information in everyday life, and the main problems that arises in a forensics scenario dealing when the so-called "digital evidences", will be exposed in the introductory sections of this thesis. It will follow a short look to the JPEG compression algorithm, the DCTransform and the traces (that we will call "errors") left during the various stages of a typical forgery pipeline, since they will be used in a lot of approaches illustrated in the following sections. The work will go on with a chronological list of the most important papers in the field of interest, before its core part exposed in Chapter 5, whose contents has been published in the three following papers:

- Fausto Galvan, Giovanni Puglisi, Arcangelo R. Bruna and Sebastiano Battiato: *First quantization coefficient extraction from double compressed JPEG images.* Presented to International Conference on Image Analysis and Processing - ICIAP Naples (Italy), vol. 8156, pp 783 - 792, (2013).

- Giovanni Puglisi, Arcangelo R. Bruna, Fausto Galvan and Sebastiano Battiato: *First JPEG quantization matrix estimation based on histogram analysis.* Presented to the 20th International Conference on Image Processing - ICIP Melbourne

(Australia), pp. 4502 - 4506, (2013).

- Fausto Galvan, G. Puglisi, A.R. Bruna, and Sebastiano Battiato. *First quantization matrix estimation from double compressed JPEG images.* In IEEE Transactions on Information Forensics and Security, 9(8):1299 - 1310, (2014).

The work ends with a list of open problems in this research field, followed by some conclusive considerations.

Contents

1

The increasing importance of images in everyday life

Prima ancora che nella realtá la storia, a volte, nasce nella nostra testa.
Solo successivamente diviene un fatto storico.

A.Prosperi

Nowadays our whole life is becoming increasingly more reliant upon images, and virtually all our video memories are stored in real-time in our devices, to the cloud (often without the user realizing it), and possibly shared through the web. As an example, in 2013 426 Million Photos were upload to Facebook everyday [2], that means 8.254 PB (PetaBytes) every month. This enormous pervasiveness of images (in addition to the web, images taken by cameras are getting more and more extensive in our cities, see Fig. 1.1, especially for private or public security purposes) has a lot of consequence in all the aspects in our everyday life. Today, like never before, people has the possibility to choose between a lot of methods and software, free of charge, built for image editing. This method of recording and representing the reality can be defined as "liquid knowledge" [3], and collaborates to form our beliefs about the best product to buy, about the best politician to vote and generally about every occurrence in the world around us, being able to ascertain the originality of in image, or in general of a visual document has become crucial in different fields.
If it's true that "a picture is worth a thousand words" [61], is also true that in most of the cases simply there is no time to investigate if a visual information is true or false, so people simply trust what sometimes is fake (see Fig. 1.2), and once an opinion is rooted is really difficult to remove it [4, 127, 147] (see Fig. 1.3). The lack of human ability


Messaggero Veneto EDIZIONE UDINE

HOME CRONACA SPORT TEMPO LIBERO ITALIA MONDO FOTO VIDEO RISTORANTI ANNU

SI PARLA DI INCIDENTI STRADALI MALTEMPO UDINESE SANITÀ REGIONE FVG GRANDE GUERRA FURTI

Scopri il territorio su pietra-lenta.dolomitifriulane.com

Sei in: UDINE > CRONACA > CI SONO 340 TELECAMERE PER VIGILARE...

Ci sono 340 telecamere per vigilare su Udine

Entrano in gioco anche gli occhi elettronici a circuito chiuso dei palazzi comunali Polizia, Carabinieri, Guardia di Finanza e Vigili condivideranno le registrazioni

di Renato D'Argenio

Figure 1.1: In this headline of a local newspaper [5] an example on the increasing diffusion of cameras for security purposes is shown. As the number human eyes decrease, automatic systems for monitoring the streets and the strategic locations in our cities are increasing, thanks also to the performances of the image processing methods.

to distinguish between tampered and original images [149] helps to increase the risk for mankind to be fooled by malicious agents. During the 2013 World Photo Awards, World Press Photo said that Paul Hansens photo of mourners in Gaza (see Fig. 1.4) was "retouched with respect to both global and local color and tone", despite that there was no evidence of manipulation. A long and interesting debate took place about whether this is a good thing for photojournalism. Even our health, see Fig. 1.5, and the way we communicate our information (as exposed in Fig. 1.7, an image can contain malicious code hiding a malware exploit that can hack the machine) can be sometimes affected by a wrong use of corrupted visual information. In a few years, also due to the opportunities offered by modern miniaturization technologies, wearable cameras (Fig. 1.6) that nowadays are part of the normal equipment of a law enforcement agent in U.S.A. [6] will probably become a standard also for other police corps.
A natural consequence of the above considerations and examples is that more and more likely images or video will become fundamental evidences to determine the result of a large and heterogeneous set of legal trials. In these cases, the reconstruction of the history of a visual document is often the main effort that an Image Forensics expert must face. In particular, before performing common tasks such as image enhancement or any kind of information retrieval, it's first of all important to ascertain if the document is original and, if not, recovering useful information about its possible manipulations. In this complex environment, sometimes also determined by the difficulty of combining the results of several methods [68, 86], JPEG[164] has emerged as the world's most

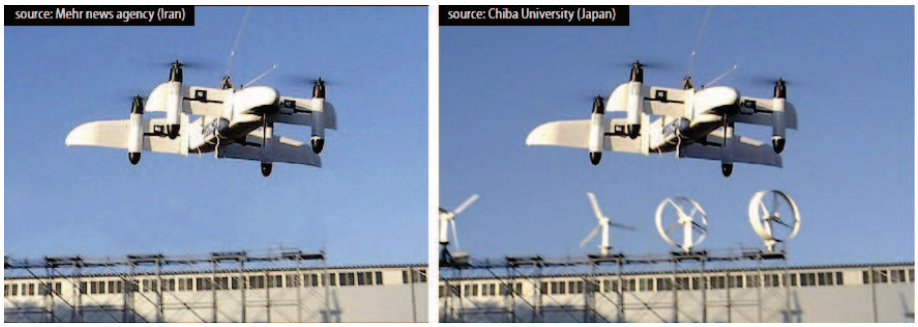

Figure 1.2: On the left a "new" sophisticated Iranian drone, according to the official Iranian news agency (November 2012). On the right the same flying object (apart from some details in the background), whose first flight was in 2008, developed by The Chiba University in Japan [7].

Figure 1.3: The image on the left is the one that the Kenyan politician Mike Sonko posted on Facebook just immediately after the death of Nelson Mandela (December 2013). Knowing that it was a doctored version of the original, on the right, in which Mandela was actually embracing boxer Muhammad Ali[8] really removes from our memory the impression created when it has been seen for the first time?

popular compression standard for images. It is widely used (about 70% of the total amount) to share images on the net [11, 12], on the biggest social networks [48], and it is employed by the majority of cameras and devices at the entry and mid-high level [52, 105] (professional cameras usually shoot in RAW format). Consequently, Discrete Cosine Transform (DCT from here on), the mathematical tool used inside JPEG to shift

Figure 1.4: With the above image, the Swedish photojournalist Paul Hansen won the World Press Photo of the Year 2013 [9]. After a few days, Neal Krawetz, a forensic analyst, commented on this by saying that "This year's 'World Press Photo Award' wasn't given for a photograph. It was awarded to a digital composite that was significantly reworked...the modifications made by Hansen fail to adhere to the acceptable journalism standards used by Reuters, Associated Press, Getty Images, National Press Photographer's Association, and other media outlets". The World Press Photo invited two independent experts (Eduard de Kam from the Nederlands Instituut voor Digitale Fotografie, and Hany Farid and Kevin Connor of image forensics and authentication startup Fourandsix.) to forensically analyze the photograph. The outcome was that no traces of composite has been found.

from the spatial to the frequency domain, has been then deeply investigated by Image Forensics community. In DCT domain is somehow easier "to see", as reported in [119], if a JPEG image has been or not doubly compressed (double compression, as we will discuss in the following, is one of the consequence of a forgery). In more detail it is possible to retrieve (some of) the traces leaved from a tampering operation, and also some fingerprints about the camera that shoot the image. Beyond that, some of the methods and results in this field are also applied to Anti-Forensic[66, 73, 74, 154, 156, 157, 163], Watermarking[70, 104, 150], and also to Steganalysis [129, 133, 160], when the hidden information is embedded inside of a JPEG image.
The overall feeling for the importance of the issues connected with the Integrity Verification in Multimedia is constantly increasing. The scientific european community accepted the challenge and joined its forces around the following four major projects:

- Rewind [13]. It is finalized to develop approaches in three main directions of research: the use of Watermarking as a tool for the validation of the autenticity on an image, and revealing traces of resampling and copy-move operations as a

«Truccate le foto delle cellule» Il prof universitario sotto accusa

I pm: ricerche sul cancro aggiustate al computer per ottenere fondi

16/10/2013 A A

Tweet 9 Condividi Stampa Invia ad un amico

CORRIERE DELLA SERA

MILANO — C'è un doping fotoinformatico che trucca persino gli studi sulle malattie? Una inchiesta delle Procure di Milano e Napoli mostra come le immagini destinate a comprovare gli esiti di ricerche sul cancro, pubblicati da primarie riviste scientifiche e utilizzati per rafforzare il curriculum dei ricercatori in concorsi pubblici e per concorrere a finanziamenti erogati dall'Associazione italiana ricerca sul cancro (Airc), in alcuni casi sono stati manipolati al computer con uno sconcertante photoshop.

Il caso concreto all'esame della magistratura, segnalato dall'esposto di un biologo molecolare ricercatore del Cnr che ha trovato conferma nella consulenza informatica affidata dai pm milanesi Maurizio Romanelli, Francesco Cajani e Antonio D'Alessio al professor Sebastiano Battiato dell'Università di Catania, riguarda otto pubblicazioni prodotte fra il 2001 e il 2012 dal gruppo di lavoro del professor Alfredo Fusco, ordinario di patologia generale, direttore a Napoli dell'Istituto di endocrinologia e oncologia sperimentale del Cnr, socio corrispondente dell'Accademia dei Lincei e membro della commissione scientifica consultiva dell'Airc, da tempo impegnato sui meccanismi molecolari alla base di varie forme tumorali.

Figure 1.5: A recent survey of the Public Prosecutors of Milan and Naples shows how images designed to demonstrate the outcomes of cancer research, published by leading scientific journals and used to strengthen the curricula of researchers in competitions and compete for loans made by the Associazione Italiana per la Ricerca sul Cancro (AIRC), in some cases have been tampered through the use of software for photo editing [10].

means of image forgeries.

- S-FIVE [14]. Dedicated to face problems related to standardisation in Forensic Image and Video Enhancement, it has its main focus on the developing of techniques for improving the quality of surveillance video data and other types of images.
- Reveal [15]. The project has the aim in developing tools and services that aid in Social Media verification from a journalistic and enterprise perspective.
- Maven [16]. The project addresses the issue of the efficient management of large amounts of multimedia files and of the extreme volatility of every digital asset, by using some of the latest technologies, powering integrity and authenticity verification tools. Its goals ranges from face detection and recognition to image source verification.

1.1 Outline of the work

This thesis is composed by six parts. After the present introductory section, in which the importance of image and video memories in various fields of our everyday life is highlighted, Chapter 2 consists on a brief exposition of the main legal aspects and definitions which compose the forensics science known as Image/Video Forensics. Chapter

Figure 1.6: When police forces will be equipped with wearable cameras, that will possibly record every actions the single police officers is involved with, a huge amount of images and footage will be available for help law enforcement in their investigations. At the same time, the originality of all these visual documentation need to be certified for legal usage.

Figure 1.7: As reported in [17], always more frequently the malicious code can be embedded in an image, rather than hiding it in email attachments, pdfs or other types of files that are typically used for this purposes.

3 explores the technical details underneath the JPEG compression algorithm, with a focus upon the importance of the Discrete Cosine Transform and the various kind of errors that arises during a typical compression-decompression-compression procedure, that usually characterizes a forgery pipeline in case of JPEG images. Chapter 4 contains a list of the most important methods that, in the last fifteen years, tried to model the behavior of DCT coefficients during a (single or multiple) JPEG compression. The common goal of these approaches, and the problem that we faced in our research path, is the recovery of the majority of the compression coefficients, which compose the quantization matrix in a JPEG compression, when for some reason they have been lost.
In the Chapter 5, the main part of this work, throught the content of three papers we mean to give our contribute to this research field. The works expose the application of a brand new error function that includes the DCT coefficients of a doubly compressed JPEG image before and after a third and fourth quantization. The steps of the method presented in Sect.5.3 are the results of a continued improvement and refinement, developed from the use of the stand-alone error function, to the addition of a prefiltering stage. Chapter 6 is devoted to list some open problems before the conclusive remarks.

2

From Digital Evidence to Digital Forensics

Physical evidence cannot be wrong, it cannot perjure itself, it cannot be wholly absent. Only human failure to find it, study and understand it can diminish its value.

Paul L. Kirk

In the last twenty years the increasing development of information technologies brought a lot of positive contributions to our society, allowing the creation of new "virtual lands" on the web where is possible to move or create our interests and activities. Consequently, also the way used by the criminals to implement their actions, and even the actions themselves, are very different compared to those existing before this revolution. Lawmakers by various countries had to conform to this evolution, often defining new types of crimes and trying to upgrade their legislation consequentely. In this Chapter some definitions are given with the goal to fix the new concepts in their right environment, starting from the definition of digital evidence.

2.1 The notion of digital evidence

After the premise that data stored inside a computer are grouped together with all the documentary evidence, since they represents "things" [18], it's necessary to point out that, in the Italian trial system, the term "evidence" generally indicates everything that can (in some way) contribute to form the convincement of the judge upon some given event, and collaborate to its final decision. It can be a single material object, i.e. a weapon or a footprint found on crime scene, but it can also be a person, i.e. a witness.

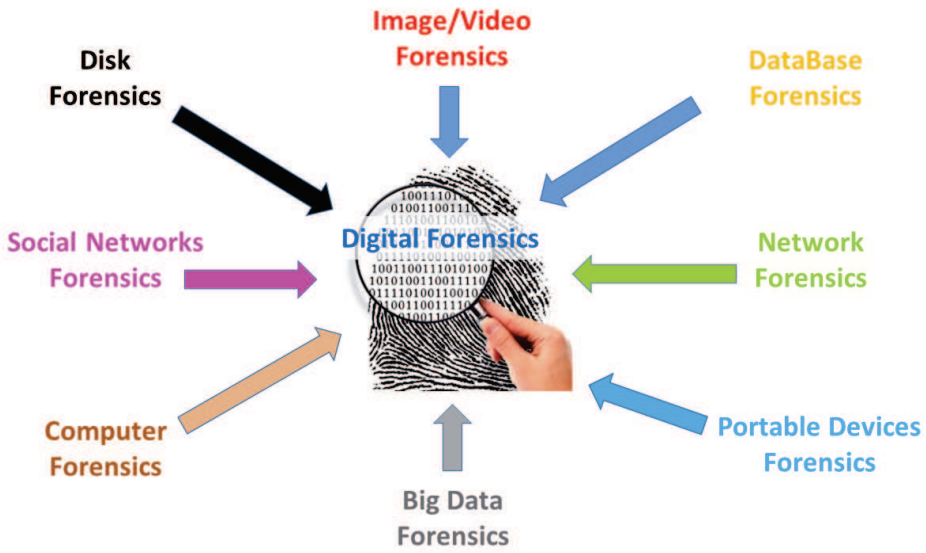

Figure 2.1: An example of possible division of Digital Forensics in sub areas [19]. It's very difficult to separate these components, since often they are closely connected. As an example, if we have to extract a chat session made using WhatsApp stored inside a smartphone (a Portable Devices Forensics's issue), we surely must use Computer Forensics's rules, adding some attentions related to the fact that information in that kind of device may changes during the analysis (if the cell phone is connected to the net). The extracted information is then examined according to DataBase Forensics

The digital evidence belongs to the group of the scientific evidences, it is defined as: *evidences that are provided by some scientific-technical tool with the addition of specific technical skills, possibly with the intervention of an expert in the specific field* [44], and correnspponds to the scientific area indicated as Digital Forensics.
This science includes many subareas, as exposed in Fig. 2.1, and can in turn be described in two different ways, with respect to different important aspects:

- **The purposes**: *the use of scientifically derived and proven methods toward the preservation, collection, validation, identification, analysis, interpretation, documentation and presentation of digital evidence derived from digital sources for the purpose of facilitation or furthering the reconstruction of events found to be criminal, or helping to anticipate unauthorized actions shown to be disruptive to planned operations* [55].
- **The intervention of an expert**: *the science of locating; extracting and analyzing types of data from different devices, which are interpreted by specialists in order to be used as legal evidence* [84].

The following formal definition of digital evidence is widely accepted: [62, 63]: *digital data that establish that a crime has been committed can provide a link between a crime*

and its victim, or between a crime and the perpetrator. From a practical point of view, a digital evidence is composed by a digital content, often stored in a file of whatever format or kind, and it's characterized by the following attributes:

- **Volatility**, such as residues of gunpowder. Think about a chat with an internet browser setted in private browsing;
- **Latency**, such as fingerprints or a DNA evidence. This is the case of data that have been erased or hidden (like steganography);
- **Easy to modify or to spoil** since reliability of digital data are intrinsically fragile. Indeed, with a simple copy-paste operation could affect the strength of a digital evidence;

For the Italian law [20], any kind of digital data involved in a trial is regarded as "atypical evidence" (evidences that are not explicitly prescribed by law) and so considered by art.189 c.p.p. To be admitted in the court, as prescribed by art.190 c.p.p. this kind of evidence has to be accepted by the judge.

- **Admittable**, which means that it has to comply the precepts of the Italian Code of Criminal Procedure (Codice di Procedura Penale), namely that can be evaluated during the trial. Case law by the Italian Supreme Court (Corte di Cassazione) recognizes to image and video the value of figurative document [21].
- **Authentic**, namely data must be the same as the one that was on the physical devices from where is has been taken. If for a bit stream copy of an hard disk this definition is clear, in case of an image this may give rise to very interesting and nontrivial questions, about the philosophical and conceptual meaning of the term "Authenticity": which one of the images in Fig. 2.2 is authentic? Which is the difference between Authenticity and Originality? Switching from abstract forensics theory to practical Digital Forensics rules, we often encounter some problems. Borrowing the definition of authenticity for an audio file by AES (Audio Engineering Society) [22], we can state: *we are allowed to state that an image is authentic when it can be ascertained that was made simultaneously with the visual event that aims to get registered, and in a manner fully consistent with the acquisition method reported by the party collecting the 'image; an image without artifacts, additions, deletions or every kind of changes.*
  Recently some experts tried to face these questions defining the "best practices" that must be followed to certify the authenticity of an image in a forensics scenario [53].
- **Complete**, namely all the information about the acquisition mode, availability and location of the data must be given, without simply describing data and certifying that it was in that given device.
- **Reliable**, which means give enough elements to ensure the chain of custody for the data, to save its authenticity from the time of acquisition to its submission as an evidence.

(a) (b)

Figure 2.2: On the left a joke acted on the set of the movie Jaws [23], on the right a famous doctored image created by pasting a photo of a shark from South Africa (by Charles Maxwell) into a U.S. Air Force photo taken near San Francisco's Golden gate Bridge (by Lance Cheung). Even if the left image has not been modified after the shoot, in which sense we can state that it is original?

- **Understandable**, namely give the right motivations for the relevance of the evidence acquired with the present investigation, understandable also to people who are not highly skilled in computer science, as very likely is the judge. The ability, often missing, of the magistrate to understand any technical explanations involving informatics is another key issue in Digital Forensics, but it is out of the purposes of this thesis.

2.2 The visual evidences and their usability in a court: Image and Video Forensics

Like all the finds used as evidence in a trial, images and footage to be declared valid, and therefore admissible, must have to be acquired, processed and stored according with the required procedures[69, 84, 121, 153]. Even when facing with analog technologies, predominant until just over 10 years ago, this problem was known, but at that time editing a photo or video required the intervention of experts and traces left by modifications were easily identifiable. In the digital age instead, an user with almost rudimentary knowledge of Photoshop [24] or other photo editing software can make changes on an image without any perceptible trace.
Forensic analysis of images is a forensic science carried out since the very first photos were made. In 1851 Marcus A. Root conducted the first documented example of forensic authentication of images: by microscopic examination, Root revealed that the applied procedure for coloring images, developed by the Reverend Levi Hill, was actually a result of hand coloring, and not the result of an improvement in the picture [25]. The first "photo tampering" are dated 1860 as reported in [26]. The Scientific Working Group on Imaging Technology's web site [27] reports the following definition of Image/Video

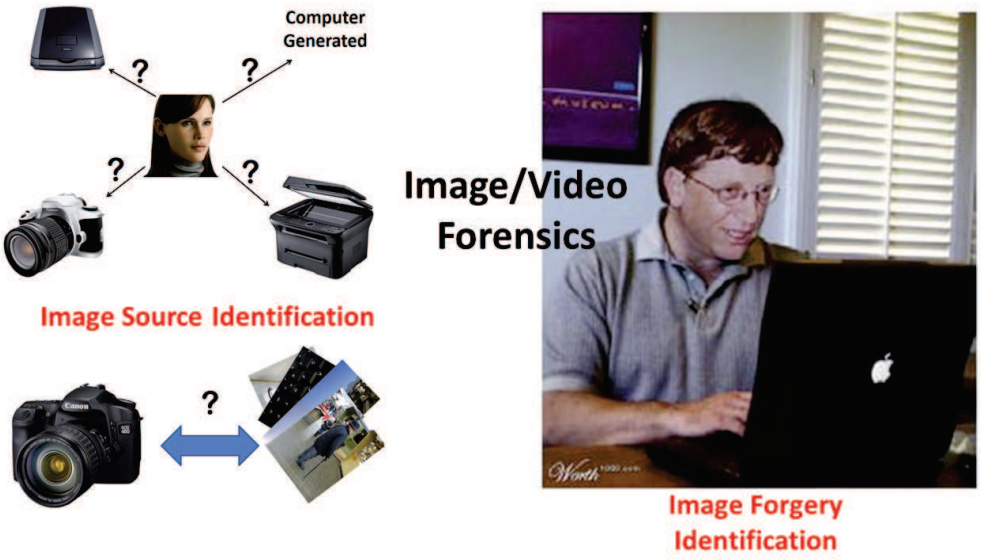

Figure 2.3: The Image/Video Forensics can be divided in two main areas, depending upon the question to answer: Image Source Identification has the goal to associate an image to the devices that created it, whereas Image Forgery Identification searches for evidences of tampering.

Forensics: *The application of image science and domain expertise to discern if a questioned image or video is an accurate representation of the original data by some defined criteria. These criteria usually involve the interpretability of the data, and not simple format changes that do not alter the meaning or content of the data.* From FBI web site [28], we can read that *Forensic Image Analysis is the application of image science and domain expertise to interpret the content of an image or the image itself in legal matters.* From both these definitions, we can identify the main points that should characterize every forensics approach to the analysis of an image. It must be provided by someone with adequate technical skills in Image Processing, but also is able to interpret the extracted information inside a legal and judicial framework.

Image/Video forensics methods are grouped in six main categories, related with the goal that they aim to achieve [135]. The first two of the list are the one more closely connected to forensics issues (see Fig. 2.3), whereas the others are general-purposes approaches:

- **Image forgery identification**: identification of manipulations in an image, given by inclusion or removal of part of the informative content of an image. These methods are divided itselfes in Pixel Based (to detect cloning, resampling and splicing operations), Statistical Based, Format Based (to detect, for example, single or multiple JPEG quantizations), Camera Based (that specifically model artifacts introduced by various stages of the imaging process), Physics Based (that leverage the inconsistencies introduced in the tampered image when its parts are coming

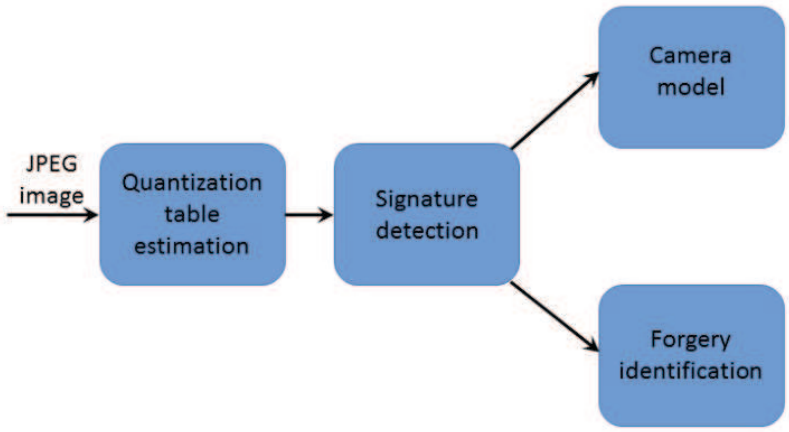

Figure 2.4: The retrieved quantization table used for the first JPEG compression in doubly compressed JPEG images can be compared with the ones of a given set of cameras, for Source Camera Identificaton pourposes. Alternatively, for Image Forgery Identification, different values highlighted in some parts of an image can be a signal that it has been tampered.

by different environments), and finally Geometric Based (aimed to find inconsistencies connected to the formation of the image inside the camera) [80].

- **Source camera identification**: identification of the device (hopefully the exact one, more often the brand of device) that generated the image. Sometimes the first step is devoted to discriminate between natural or artificial (also known as Computer Generated) images. In general, the methodology switches to the identification of the source that generated the image, ascertaining the type of device (scanner, camera, copier, and printer) and then trying to determine the particular device.

- **Image reconstruction/restoration/enhancement**: restoration and improvement of quality of deteriorated images in order to identify, even partially, the original content and/or retrieve useful information [95].

- **Image/video analysis**: dynamic or behavioral analysis, for example with the aim to identify the consecutio temporum of an event of interest.

- **3D reconstruction and comparison**: bi/three-dimensional information extraction to derive measures or reference values (for example the height of an individual) and for the comparison between images (for example to compare the identity of a subject with the known offender from a footage taken by a video surveillance system).

- **Steganalysis**: detection of hidden information within an image with steganographic techniques, for example by changing the least significant bit in the number that defines the color of a pixel (LSB approach).

The focus of this thesis is upon methods to retrieve information about the first JPEG compression in doubly compressed JPEG images. According to the diagram showed in Fig. 2.4, this kind of informations can be used as a signature to be matched with the compression table of a specified camera, for Source Camera Identification pourposes, or in order to determine if the image of interest could have been downloaded from a Social Network [124]. Alternatively, if these coefficients are calculated in different parts of an image under analysis, can form a part of a Image Forgery Identification pipeline. Before exposing the core of this work, some theoretical concepts are provided.

3

JPEG compression algorithm and DCT Transform

Numbers are like people; torture them enough and they will tell you anything.

Gregg Edmund Easterbrook

3.1 The JPEG standard

In 1986, the Joint[1] Photographic Experts Group (JPEG), officially known as ISO/IEC JTC 1/SC 29/WG 10, was formed with the purpose to establish a standard for the sequential progressive encoding of continuous tone grayscale and colour images.
As a result of this mission, starting from 1987 JPEG conducted a selection process, whose main requirements was the followings [164]:

- be at or near the state of the art with regard to compression rate and accompanying image fidelity, over a wide range of image quality ratings;
- the encoder should be parameterizable, so that the application (or user) can set the desired compresslon/qualiy tradeoff;
- be applicable to practically any kind of continuous-tone digital source image (i.e, not be restricted to images of certain dimensions, color spaces, pixel aspect ra-

[1]The word "joint" refers to the collaboration between ISO (International Standard Organization) and CCITT (Commi-tee Consultatif Internationale des Telephones et Telegraphs) which, in turn, operates in close collaboration with the group CCITT/SGVIII.

tios,etc.), and not be limited to classes of imagery with restrictions on scene content, such as complexity, range of colors, or statistical properties;

- have tractable computational complexity, to make feasible software implementations with viable performance on a range of CPUs, as well as hardware implementations with viable cost for appliations requiring high performance;
- have the following mode of operation:
  - Sequential DCT-based encoding (the most used): each image component is encoded in a single left-to-right, top-to-bottom scan;
  - Progressive DCT-based encoding: the image is encoded in multlple scans for appliations in which transmission time is long, and the viewer prefers to watch the image buil up in multlple coarse-to-clear passes;
  - Lossless encoding: the image is encoded to guarantee exact recovery of every source image sample value (even though the result is low compression compared to the lossy modes);
  - Hierarchical encoding: the image is encoded at multlple resolutions, so that lower-resolution versions may be accessed without first having to decompress the image at its full resolution.

In 1988, at the end of a challenging iter, the Group stated that the proposal given in [111], based on the 8×8 DCTransform, had produced the best picture quality.
From 1988 to 1990, JPEG undertook a huge set of tests and validating procedures to ensure the interoperability and universality of the method.
The JPEG standard (ISO/IEC 10918 - Recommendation T.81) [164, 142] was created in 1992[2] (latest version, 1994) as the result of that collaboration.
Its large and fast diffusion is mainly due to the fact that this standard allows higt compression ratios on natural images compared to a loss of quality within acceptable limits. Besides, the standard is "open, and everyone can implement its own JPEG ceder/decoder for free. The responsible for the reference implementation of the original JPEG standard is the Independent JPEG Group (IJG) [29].

3.2 Overview of the JPEG compression engine

As pointed out in Chapter1, the reason for the persisting interest upon JPEG demonstrated by the Image Forensics community, is the widespread diffusion of this format both on the web, and on the majority of the image acquisition devices circulating at the present time. Though JPEG compression algorithm is not the main topic of this work, and even if there is a huge amount of pubblications about it (starting from the above cited [164]), we decided to give a brief introduction to its basic fundation steps since some of them leave useful footprints for Image Forensics applications. Its main stages are showed in Fig. 3.1.
Since human visual system is more sensitive to luminance than to chrominance [60],

[2] approved on 18th September 1992

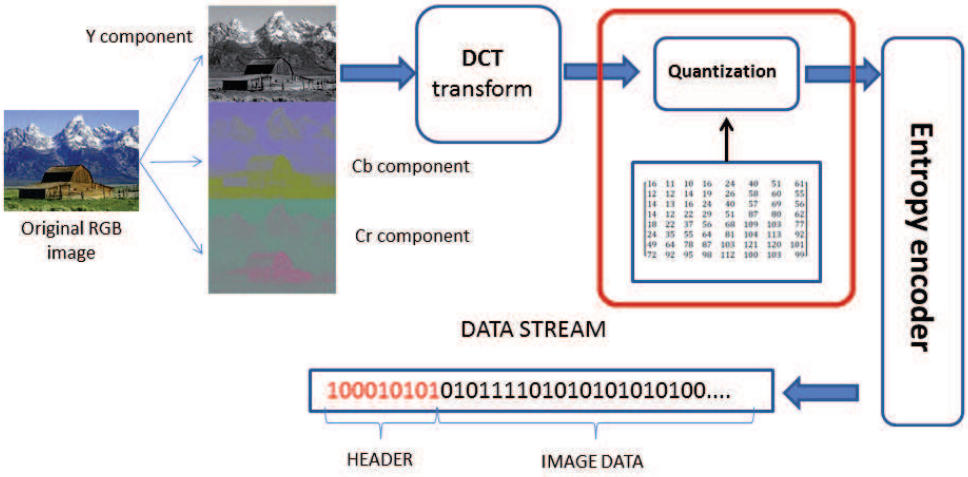

Figure 3.1: Synthetic scheme of the basilar steps in the JPEG compression pipeline. The steps corresponding to the DCT transform, quantization and entropy encoder, here shown only for the Y (Luminance) component, are replicated also for C_b and C_r (Chrominance) components. The results of the three channels are then joined to form the data stream.

instead of working on (native) *RGB* color space, where the two components, or "channels", are mixed together, the first step is devoted to convert the image to the YC_bC_r space. This is done with the following transformation [164, 142]:

$$\begin{pmatrix} Y \\ C_b \\ C_r \end{pmatrix} = \begin{pmatrix} 0.299 & 0.587 & 0.114 \\ -0.1687 & -0.3313 & 0.5 \\ 0.5 & -0.4187 & -0.0813 \end{pmatrix} \begin{pmatrix} R \\ G \\ B \end{pmatrix} + \begin{pmatrix} 0 \\ 128 \\ 128 \end{pmatrix} \tag{3.1}$$

At this point it is possible to separate the Y (luminance channel) from C_bC_r (chrominance), in order to further process them separately and obtain higher compression maintaining the visual information unaltered. To this aim, the chroma channels are usually subsampled and compressed more strongly compared to the luminance one.

Besides being more sensitive to luminance compared to chrominance, the human visual system, looking at a scene, perceives more accurately the variations in low-frequency areas, respect to changes in high-frequencies areas. Again, being able to process in a different way the parts of an image with different frequency values, is possible to further reduce the size of the compressed image. It is therefore necessary moving from the spatial domain to the frequency domain. Accordingly, for every channel of the resulting image a DCT transform is applied to each one of its (8×8 non-overlapping) blocks, after having converted their values from unsigned integer in the range [0,255] to signed values belonging to the range [-127,128].

The next step is a *deadzone quantization*, whose effect is illustrated in Fig. 3.2. It is obtained dividing each DCT coefficient in the same position of the 8×8 block for the

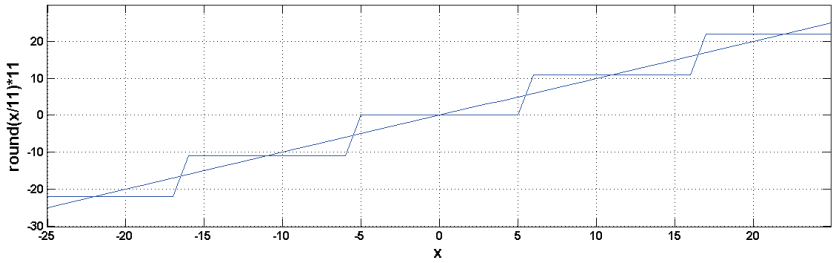

Figure 3.2: The effect of the deadzone quantization for $q = 11$: all the DCT coefficients lying in a certain range around a multiple of the quantization step whose extension depends on q, namely the dead zone, are forced by the joint effect of the quantization (i.e., division by a quantization coefficient), of the round function, and of the dequantization step, to be all equal to that multiple of q.

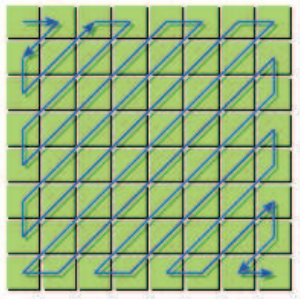

Figure 3.3: The zig-zag order followed during the entropic coding of the JPEG compression algorithm. The coefficients are sorted in a 1D vector from the lowest (DC) to the highest frequencies. Source image from [30].

same integer value[3] belonging to a 8×8 quantization matrix [54]. The results of the ratio between the original DCT coefficients and the corresponding quantization steps are then rounded. This last part of the algorithm is responsible, at the same time, for the powerful compression obtained by JPEG (because the joint effect of the quantization-rounding step, causes the reset of many DCT coefficients) and for the loss of information that it causes (because the rounding function it isn't perfectly reversible). For this reason the entire procedure is said to be *lossy*.
The quantized and rounded coefficients are then transformed into a data stream, following a zig-zag order as illustrated in Fig. 3.3, by mean of a classic entropy coding (i.e., run length/variable length). As can be noted, DCT transform plays a central role in JPEG compression pipeline.
Coding parameters and other metadata [97, 138] are embedded into the header of the JPEG file to allow a proper decoding. These informations, that in JPEG images are stored in Exif format [72], include details upon the compression parameters, about the kind of camera that took the image (with a lot of its setting parameters), the time of

[3] from here on indicated generically as q, or q_{ij} to indicate the specific quantization step in position (i, j)

the shoot, and so on. In some cases, if the GPS module is embedded in the acquisition device, the Exif metadata contain the exact position where the picture has been shoot. These data, although very useful for general purposes, are not so robust to tampering [31, 32], so are very weak if presented in a court as evidences. For this reason they are not widely used for forensics analysis.
In case of a forgery operation the entire compression process needs to be inverted, since to visualize the image it has to be decompressed. The decompression path starts with dequantization (see Sect. 3.4.1), and it's followed by the Inverse DCT (IDCT) that brings the coefficients from the frequency domain back into the spatial domain. Finally, to get the visible image ready to be modified, the information in the YC_bC_r space is converted back to its RGB version with the following transformation, that is the reverse version of (3.1), :

$$\begin{pmatrix} R \\ G \\ B \end{pmatrix} = \begin{pmatrix} 1 & 0 & 1.402 \\ 1 & -0.34414 & -0.71414 \\ 1 & 1.772 & 0 \end{pmatrix} \begin{pmatrix} Y \\ C_b - 128 \\ C_r - 128 \end{pmatrix} \tag{3.2}$$

Once manipulated the image is compressed again, most probably with a different compression coefficient (it's very unlikely that the editing software is set with the same parameters as the camera's inner software). The entire pipeline of a forgery operations on a JPEG image is exposed in Fig. 3.4.

3.3 Terminology.

Although the number of papers which over the past years covered these topics is quite remarkable, none of them tried to uniform the great variety of terms used to define the various components of the theory. The need to standardize our exposure between all the papers to which we will refer later, led us to overcome this problem with the following definitions of the various features that will be take under consideration. We first discuss the different choices found in literature, and then will give our view to be used in the rest of the work:

- the terms "quantization" and "compression" lead to some confusion in their interpretation. The core of JPEG algorithm is the reduction of size of the considered image file. This reduction, often called *compression* with a clear figurative meaning, is obtained with a mathematical operation called *quantization*, which consists in dividing (and rounding) DCT coefficients for specific integer values, namely the coefficients of a 8×8 matrix called *quantization matrix*. Every one of them is singularly referred as *quantization step*, but sometimes also as *compression step*. For these reasons the two terms are used indifferently. We suggest to use "compression" to denote the abstract concepts, like the kind of algorithm or its propriety, and "quantization" when we refer to concrete numbers, so we will use "quantization step", "quantization matrix", and so forth.

- In many papers in this specific field the terms "image noise" and "image error" are often used with the same meaning. The reason is the following: in the world of photography, the noise is something that affects the image quality. As an example,

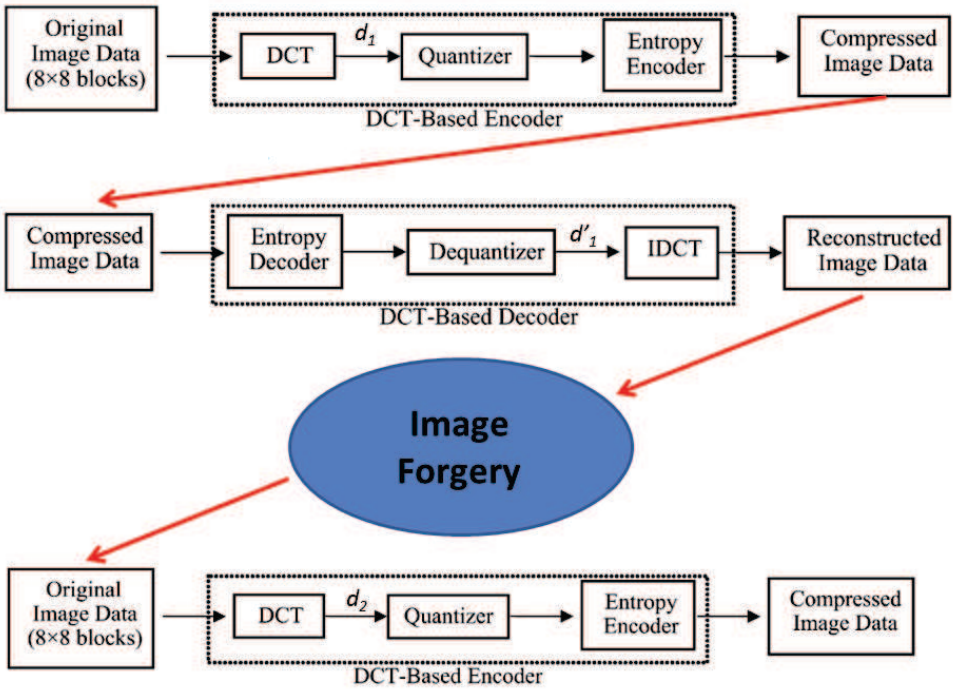

Figure 3.4: The complete pipeline for a forgery operation in case of a JPEG image: the first JPEG compression, the decompression of the image, the forgery, and finally the second JPEG compression. d_1, d_1' and d_2 are the distributions of the terms in that point of the pipeline.

the one known as Picture Response Non Uniformity (PRNU) noise [67, 71] is inducted at the time of shooting by imperfections on the silicon components of the camera sensor, some others are introduced during the quantization/dequantization phases of the JPEG algorithm. These latter are frequently also named as errors, and are of great importance for Image Forensics, as we will see in Sect. 3.5.

- The way to indicate the quantization step is generally not yet uniformed. The authors often refer to it as q when it doesn't matter neither how many times the JPEG algorithm is applied, nor which is its position in the quantization matrix. If the number of JPEG compression matters, the quantization step of the *n-th* compression is denoted as q_n, or q^n. Instead, if the exact position (i, j) in the quantization matrix of a generic quantization step is important, the term mostly used is $q_{i,j}$, or $q^{i,j}$, with or without parenthesis. Finally, if the level of detail is so high that both the number of JPEG compression and the position of the quantization step inside the quantization matrix must be defined, in literature can be found indifferently $q^n_{i,j}$, or $q^{i,j}_n$, again with or without parenthesis. We will denote the three conditions, respectively $q, q_n, q^{i,j}$ and $q^{i,j}_n$.

- The whole quantization table referred to the *i-th* compression is universally indi-

cated as Q_i.

- As illustrated in the previous section, the JPEG algorithm maps the values of the image from the spatial to the frequency domain. Since every step of the algorithm (both during the coding and the decoding phase) has got his own characteristics that can be leveraged for Image Forensic purposes, every feature of the image data stream (i.e., the distribution of the DCT terms) in a particular phase of the image forgery pipeline needs to be examined separately. For this reason, the way the terms are named varies with the step in which they are discussed, and every author made his own choices in this regard, so the same term and its features are indicated in many different ways over different papers. In consideration of the part of the JPEG algorithm that we will leverage, and with the goal to maintain a clear and unambiguous terminology, our choice is to use the following (see Fig. 3.5):
  - $x_{i,j}^{(n)}$ indicates a single element in the spatial domain in position (i, j) of a certain 8×8 image block of an uncompressed image, yet subjected to n JPEG compressions ($n = 0$ means that the image has never been compressed);
  - $\tilde{x}_{i,j}^{(n)}$ indicates a term (in the spatial domain of an image that has been compressed n times) during the decompression phase, just after dequantization and IDCT steps;
  - $y_{i,j}^{(n)}$ indicates a single element in the frequency domain in position (i, j) of a certain 8×8 image block of an uncompressed image yet subjected to n JPEG compressions, just after the DCT transform ($n = 0$ means that the image has never been compressed);
  - $y_{(q)i,j}^{(n)}$ indicates a single element in the frequency domain in position (i, j) of a certain 8×8 image block of an uncompressed image yet subjected to n JPEG compressions, just after the quantization ($n = 0$ means that the image has never been compressed);
  - $j_{i,j}^{(n)}$ indicates a single element in the frequency domain in position (i, j) of the n-times compressed JPEG image.
- with regard to the statistical distribution of the terms in the various steps of the JPEG algorithm (both in the coding and in the decoding pipeline), we will use (see Fig. 3.4):
  - d_n is the distribution of the terms just after the DCT transform during the *n-th* encoding phase, and $p_n(x)$ its Probability Density Function (PDF);
  - $d_n^{'}$ is the distribution of the dequantized DCT terms just before the IDCT transform during the *n-th* decoding phase, and $p_n^{'}(x)$ its PDF;
- the rounding function is indicated either with the word *round* or with the square brakets $[\ldots]$;
- ϵ_q is the quantization error;
- ϵ_r is the rounding error;

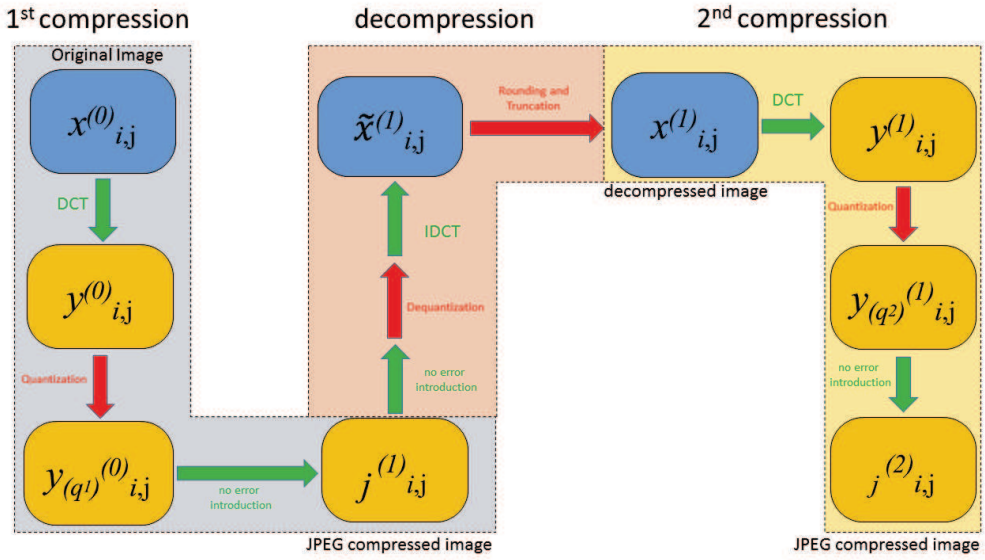

Figure 3.5: The transformations of a single value of a 8×8 block in a uncompressed grayscale image subjected to a double JPEG compression. Operations that are source of error are depicted in red, while the completely reversible ones are green. The blue boxes contain terms in the spatial domain, whereas the orange boxes are for the terms in the frequency domain. The operations with "no errors introduction" are referred to the Entropic coding and decoding phases. The terms q_1 and q_2 refer to the (very high) possibility to have two different quantization steps.

- ϵ_t is the truncation error;

Our hope is that the above choices, to which we will refer in the rest of the thesis, can be used in the future as a guideline for the specific literature.

3.3.1 Strengths and utility of the Discrete Cosine Transform

Starting from the paper by Ahmed, Natarajan and Rao that firstly developed the DCT in 1974 [46] (in this regard, an interesting historical note on this milestone article is reported in [45]), the increasingly rapid growth of image processing algorithms, and in particular of compression methods like JPEG for images or MPEG [141] for videos, has led to the success of this transform. A lot of books [47], tutorials [106], papers [146, 158, 169] and webpages [33] defined the mathematical details concerned the DCT, and also its applications to solve real problems [82]. This literature have been chosen as a main guideline for our following considerations to briefly summarize its intrinsic details.
From a mathematical point of view, the DCT block transform is a linear and invertible function belonging to the family of the *Discrete Trigonometric Transforms* (DTTS). It can be defined as a finite length mapping from a $L^2(R)$ space to another $L^2(R)$ space, generally defined as:

$$\mathcal{F} : \mathbb{R}^n \longrightarrow \mathbb{R}^n, n \in \mathbb{R}. \tag{3.3}$$

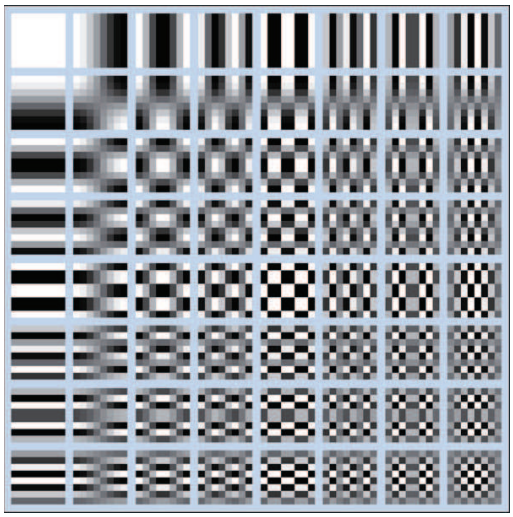

Figure 3.6: The set of 64 basis functions corresponding to the 2-D discrete cosine transform, taken from [146]. As can be seen they exhibit a progressive increase of the frequency component. The DC term has no frequency component.

In the JPEG algorithm the entire image matrix is divide into smaller matrix with a dimension of 8×8 before the DCT, which maps the values from the spatial to the frequency domain; this effect is obtained using two 8×8 *kernels*, or *basis functions* M_c and M_r. Indeed, if y is the image matrix in the spatial domain, the DCT is obtained with the following linear transformation:

$$Y = M_c \cdot y \cdot M_r^T \tag{3.4}$$

Where T indicates the matrix transposition, and $\cdot$ the matrix product.
Some of the most important motivation for the use of DCT in image compression are the following:

- **It decorrelates the image data**: normally an image contains areas with uniform brightness, or slowing varying. These areas are bounded from the so called *edges* which instead cover a limited area. Therefore, neighboring pixels are strongly correlated. The idea is expressing the image values through a linear combination of coefficients that are (ideally) not correlated. This particular Fourier Transform [134] is able to remove redundancy between neighboring pixels, so that the obtained uncorrelated coefficients can be independently encoded, thus reducing the total entropy of the image data, then allowing a higher compression efficiency. As an example, in Fig. 3.7 is clearly visible that the amplitude of the autocorrelation after the DCT is highly reduced. Regarding the entropy, in particular its use as an indicator of the average number of bits required for representing a signal [96], it is heavily reduced by the ability of DCT transform in discarding some high frequency parts, as showed with some practical examples in [106]. The advantages in a compression procedure are straightforward.

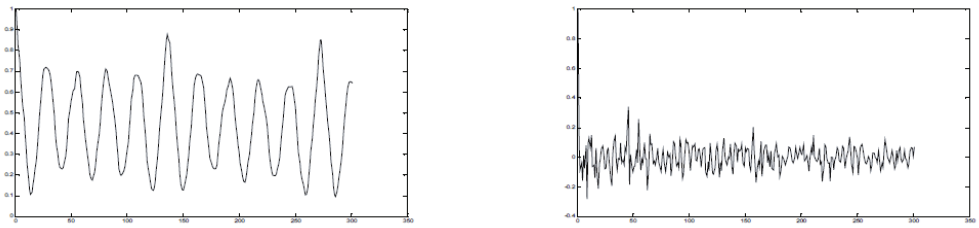

Figure 3.7: The effect of DCT transform on normalized autocorrelation of correlated image: before (sx) and after (dx). Image from [106].

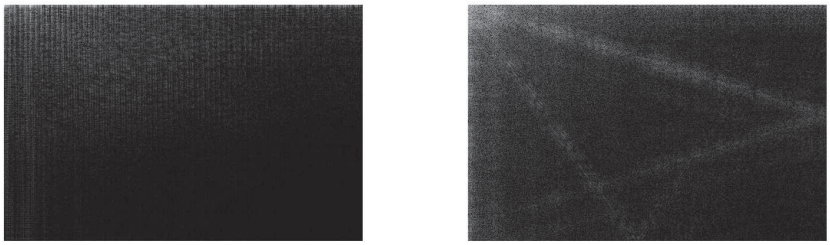

Figure 3.8: The effects of DCT applied to an uncorrelated image (left) and to a correlated image (right). In both cases is clearly visible the effect of energy compaction: the most quantity of data (whose presence is indicated by white/gray colored pixels) are grouped in a small part of the image (almost exclusively in the upper left corner) that is referred to low frequencies. Images from [106].

- **It packs data (thus energy) into as few coefficients as possible**: as clearly visible in Fig. 3.8, both in uncorrelated and correlated images, DCT groups information on the upper left part of the resulting image (the lower order coefficients). In the frequency domain, this area corresponds to the low-frequency content of the image. This situation allows discarding (through a strong quantization) the part of the image corresponding to high-frequency content without losing relevant information. The more quantity of data that can be discarded, the higher the compression that can be achieved. Obviously, this is strictly related to the frequency content of the image itself.

- **It is computationally efficient**: it can be computed symmetrically and separately, distinguishing successive operations on rows and columns. Recall from 3.2 that DCT, in JPEG pipeline, is applied to every single 8×8 image block. If $f(x, y)$ is the coefficient of the image in the spatial domain at position (x, y), the formula to calculate the generic coefficient in the frequency domain in position (i, j) is:

$$y_{i,j}^{(n)} = \frac{1}{4} C(i) C(j) \left[\sum_{x=0}^{7} \sum_{y=0}^{7} f(x, y) cos \frac{(2x+1)i\pi}{16} cos \frac{(2y+1)j\pi}{16} \right] \tag{3.5}$$

with

$$\begin{cases} C(i), C(j) = \frac{1}{\sqrt{2}} & i, j = 0 \\ C(i), C(j) = 1 & \text{otherwise} \end{cases} \tag{3.6}$$

The separability allows to transform (3.5) in:

$$y_{i,j}^{(n)} = \frac{1}{4} C(i) C(j) \sum_{x=0}^{7} cos \left[\frac{(2x+1)i\pi}{16} \right] \sum_{y=0}^{7} f(x,y) cos \left[\frac{(2y+1)j\pi}{16} \right] \tag{3.7}$$

This allows $y_{i,j}^{(n)}$ to be computed in two steps, precisely first on the row and then on the column, since the operations on the rows and on the columns are functionally identical as can be seen in (3.7).

- **It is an orthogonal transformation**: this property, that can be proved in different ways[47, 158] arises from the fact that the transformation matrix is composed by orthogonal columns and so it is orthogonal itself. This is one of the reasons for its computational efficiency.
- **Normalization**: for each column vector v_j of any discrete cosine transform kernel matrix holds the following:

$$\|v_j\| = 1, i \in [1, \ldots, 8] \tag{3.8}$$

- **Orthonormalization**: Since both the columns and the rows of the transformation kernel are orthogonal and normalized, this matrix is said to be *orthonormal*. This results in a significant decrease of the computational complexity, being the matrix inversion reduced to a matrix transpose.
- **Efficient algorithms for its computation are available**: the separability together with the symmetry and the orthogonality allows building a fixed transformation matrix that can be computed separately. Moreover it is not a complex transform, (compared, i.e., with DFT) so there is no need to encode information about its phase.

3.3.2 JPEG quantization matrices: from a standard to an adaptive approach

The "quality" of a compressed image is intended as its capability to show as much information as possible with respect to the original one. Historically, starting from the first implementation of the JPEG encoder by the IJG group [29] in October 1991 (the last version, 9b, is currently in development and is planned for release in January 2016), the index of this feature is denoted as Quality Factor (QF from here on). Ranging from 1 to 100, it indicates how much a compressed image is similar to its uncompressed version. JPEG algorithm, by definition devoted to reduce the bit size of an image as already exposed in the previous subsection, achieves its purpose during the quantization step, so the correct choice of these values becomes crucial. The quantization tables showed in Fig. 3.9 are the most commonly used for the two channels of Luminance and Chrominance. They have been developed by the Independent JPEG Group (IJG) in

16	11	10	16	24	40	51	61
12	12	14	19	26	58	60	55
14	13	16	24	40	57	69	56
14	17	22	29	51	87	80	62
18	22	37	56	68	109	103	77
24	35	55	64	81	104	113	92
49	64	78	87	103	121	120	101
72	92	95	98	112	100	103	99

17	18	24	47	99	99	99	99
18	21	26	66	99	99	99	99
24	26	56	99	99	99	99	99
47	66	99	99	99	99	99	99
99	99	99	99	99	99	99	99
99	99	99	99	99	99	99	99
99	99	99	99	99	99	99	99
99	99	99	99	99	99	99	99

Figure 3.9: The two standard JPEG tables, for the Luminance (left) and Chrominance (right) channels. Properly scaled, every one of them can cover 100 different Quality Factors.

1998 [34] following the contents of [164] and [89]. These tables correspond to a QF of 50 and are used as basis for the derivation of every other possible QF. Indeed, starting from them is possible to derive the matrices required to obtain the desired QF in a JPEG image following a two steps algorithm [107, 118]:

1. computation of the scaling factor Z from every QF:

$$Z = \begin{cases} 5000/QF & \text{if} \quad QF < 50 \\ 200 - 2QF & \text{otherwise} \end{cases} \tag{3.9}$$

2. the $(i, y) - th$ element of the desired matrix Q^* for every channel is obtained from the corresponding position in the basis matrix Q with the following map:

$$Q^*(i, j) = \frac{Q(i, j) * Z + 50}{100} \tag{3.10}$$

In addition to the standard set, all the programs devoted to digital image editing possess their own non-IJG quantization tables[77]. For example, when Adobe Photoshop[35] saves an image in JPEG format, in addition with other different settings it allows the user to select one among 12 quality level. Even the most popular Social Network platform, aside from deleting the majority of Exif metadata from every uploaded image, compress it with its own tables [124]. Concerning the acquisition devices, both digital cameras and smartphones use their own custom base quantization table, again different from the IJG matrices and scaling methods [78]. In general, from their definition until the present days, the challenge is to develop quantization tables that are self-produced by the devices after a process of advanced scene-context classification, possibly taking into account also the needs of the visual human system [54].
Regarding the magnitude of the quantization steps, with the increasing availability of low-price storage space inside the acquisition devices, the trend leads to ever smaller values, as can be seen in Fig. 3.10. Indeed, thanks to the collaboration with AMPED srl [1] we had the possibility to study and classify the quantization tables of more than 7000

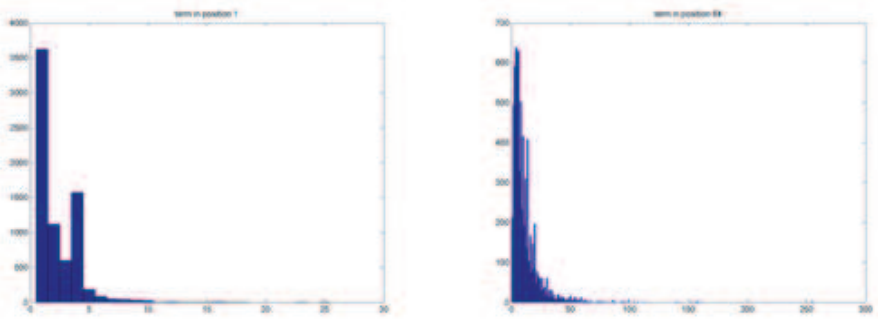

(a) (b)

Figure 3.10: Histogram a) shows the distribution of the values assumed in the quantization matrices by the terms in position 1, considering the usual zig-zag order. Histogram b) is referred to the position 64. Note that the two images have different scales.

kind of cameras, smartphone and tablet of about 70 different brands. Considering only the Luminance channel, we isolated about 1500 different matrices. The most widely used (222 occurrences coming from devices of 14 different brands) is the one showed in Fig. 3.11 a).
Fig. 3.11 b) shows another interesting result of this survey, namely in the firts 15 positions of the compression matrices of the examined database (considering the zig-zag order of the JPEG algorithm, exposed in Sect 3.2), the percentage of values of the quantization steps in the range [1:30] is never under 99%. This result, as pointed out in Sect. 5.3.4, will be used in [90, 91, 140] to justify the choice of the range of variability in the values of a third quantization step applied to the image.

3.3.3 Statistical distribution of the DCT coefficients

In the present section we will expose the works that, over the years, allowed to have a clear cognition of the statistical distribution fo the DCT coefficients for all the 64 positions of the 8×8 image block. These preliminary studies are the necessary prelude to the methods illustrated in the following of this thesis. The first insight on the distribution of DCT coefficients were given in [137] and [126], even if until [144] substantially there were only a lot of proposals and hypothesis not supported by real scientific reasons. In their paper instead, Reininger and Gibson performed a set of Kolmogorov-Smirnov [151] goodness-of-fit tests to compare the various options: Gaussian, Laplacian, Gamma and Rayleigh distributions. Their results allowed concluding that:

- the distribution of the DC coefficients (the one in position $(0, 0)$ in every (8×8) block, see the upper left sub-image in Fig. 3.12), which represents the average value of the input sequence in the corresponding block, follows a Gaussian law;

- the distribution of the AC coefficients (see Fig. 3.12, apart from the image in the upper left) follows a Laplacian law.

1	1	1	1	1	1	3	4
1	1	1	1	1	2	4	6
1	1	1	1	2	3	5	6
1	1	1	2	3	4	5	6
1	2	2	3	4	5	6	7
2	3	3	5	7	6	7	6
3	4	4	5	6	7	7	6
4	3	3	4	5	6	6	6

(a)

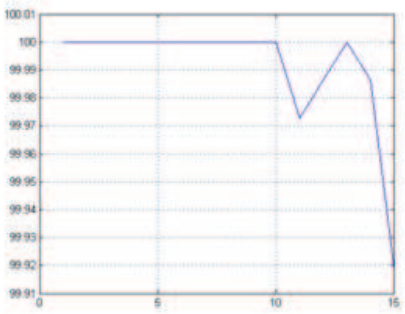

(b)

Figure 3.11: On the left the most widely used compression matrix considering a database of about 7000 image acquisition devices kindly provided by Amped srl [1]. The map on the right represents the percentage of quantization coefficients below 30, considering the first 15 positions, according to the zig-zag order exposed in Fig. 3.3. In abscissa is the position of the coefficients in the matrix, in ordinate the value in percentage.

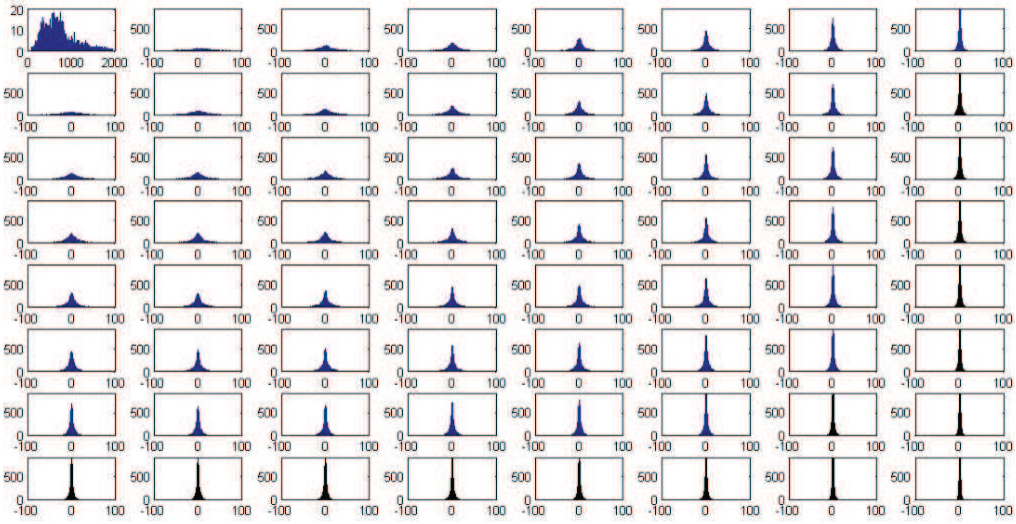

Figure 3.12: Histograms of the values of the DCT coefficients in all the positions of the 8×8 block for an image taken from the Kodak Dataset[43] after a shift from the spatial to the DCT domain using the Matlab[36] function `dct2`*. The difference in the slope of the histograms for the AC terms, as the frequency changes, as well as the particular behavior of the DC term are clearly noticeable.*

For a complete and exhaustive analytical discussion about the topic, we instead refer to [110]. In the paper, Lam and Goodman firstly pointed out that in every 8×8 image block pixel values can reasonably be thought as identically distributed random variables, generally with no (or with a weak) spatial correlation. Since the central

limit theorem[85] states that the weighted summation of identically distributed random variables can be well approximated as having a Gaussian distribution[4] with zero mean and variance proportional to the variance of pixels in the block (note that the above characterization perfectly match with DCT terms as defined in (3.5) and (3.7)), and using conditional probability, they define:

$$d_n = p(y_{i,j}^{(0)}) = \int_0^\infty p(y_{i,j}^{(0)}|\sigma^2)p(\sigma^2)d(\sigma^2) \tag{3.11}$$

They also hypothesized that, considering typical images, the variance of the Gaussian distribution of the terms through the 8×8 image blocks also varies as a random variable. This last distinction turns out to be the determining factor for the shape of the coefficients distributions, as we will see. They finally concluded that, for these two reasons, the image can be represented with a doubly stochastic model and, since the PDF of σ^2 in case of natural images has been proved to be exponential with parameter λ, is possible to write the distribution of the coefficient as:

$$p(y_{i,j}^{(0)}) = \frac{\sqrt{2\lambda}}{2} exp\{-\sqrt{2\lambda}|y_{i,j}^{(0)}|\} \tag{3.12}$$

Recalling that the PDF of a Laplacian distribution is defined as:

$$p(y) = \frac{\mu}{2} exp\{-\mu|y|\} \tag{3.13}$$

it is straightforward to conclude that the PDF in (3.12) is Laplacian with parameter $\mu = \sqrt{2\lambda}$. As a corollary it is possible to state that, since the constant of proportionality that link the variance of the Gaussian distribution with the variance of the block becomes smaller as we move to higher frequency, the amount of DCT coefficients equal (or very near) to 0 increase as the positional index approaches to the high frequencies, i.e. the lower right part of the 8×8 block. Incidentally, as discussed further in Sect. 4.1 and clearly visualized in Fig. 4.4, this is the reason why in a context of First Quantization Step Estimation it will be almost impossible to discover all the terms of the quantization matrix.

As an application of these results, a recent work by Farinella et al.[81] analyzes DCT coefficients distribution to discover semantic patterns useful for scene classification. In these particular cases, it is observed that different scene contexts present differences in the Laplacian scales, and therefore the shape of the various Laplacian distributions can be used as an effective scene context descriptor.

Even if, historically, about the PDF of the DC term there is a general accordance, alternative proposals for better representing the statistical behavior of AC coefficients by Muller[125] and Chang et al.[64], which proposed (respectively) the Generalized Gaussian Model and the Generalized Gamma Model. Although the exposed results are to some extent remarkable, scientific community defining PDF of DCT terms is yet used to refer to Laplacian distribution, that in any case is a special case of the Generalized Gaussian distribution. In our opinion this is justified from several reasons:

[4] note that the central limit theorem holds even when the image pixels are spatially correlated, as long as the magnitude of correlation is less than one.

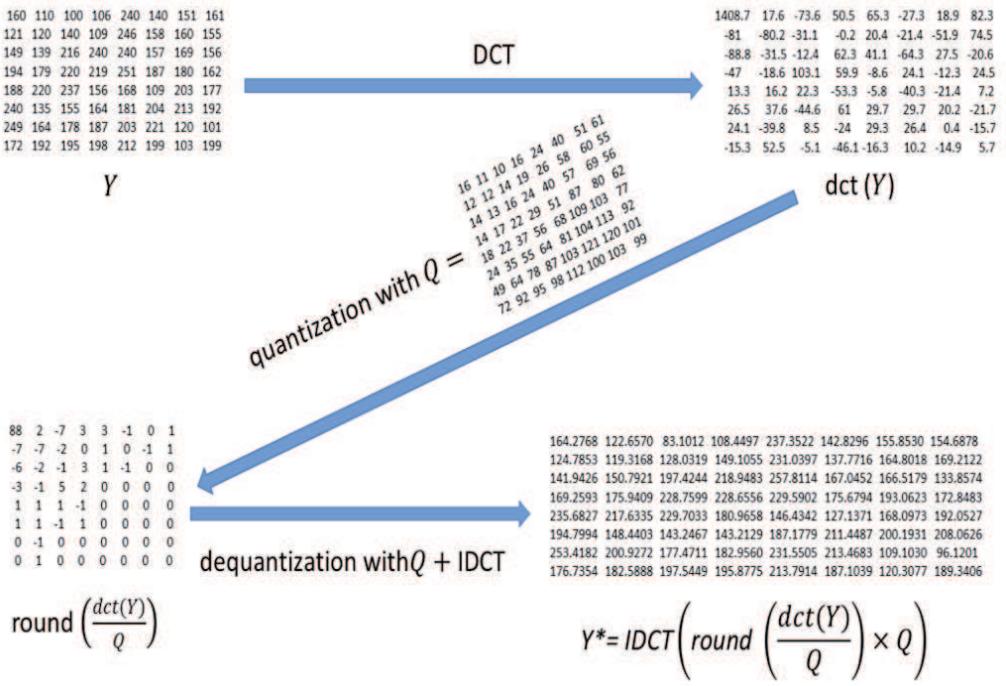

Figure 3.13: In the above toy example is possible to follow step by step what actually happens during a quantization/dequantization process, to a term in a generic position (i, j) in the 8×8 base block, starting immediately after the conversion from RGB to YC_bC_r color space. After the DCT transform (note the value assumed from the DC term) it is quantized with a compression matrix Q corresponding, following the standard introduced by JPEG Group exposed in Sect. 2.2, to QF=50. Subsequently the rounding function is applied. This is the end of the first compression stage, since the other operations have only the task to encapsulate the values in a data stream to form the JPEG file. Here it is possible to appreciate what happens to the file when it is "opened": the obtained matrix Y^* after dequantization and IDCT is yet considerably different from Y.

the Generalized Gaussian Model, as exposed in [110], is a better model only when the kurtosis has a high value (that is not true for all kind of images), these models require in general more complex expressions and extra computational cost compared with the Laplacian one. Besides, these latter approaches are not based on mathematical analysis and empirical tests, thus having the drawback of a lack of robustness.
Finally, always about different ways to model the distribution of DCT terms, in 2004 Lam[109] pointed out that, in case of text documents, a Gaussian distribution is a more realistic model.

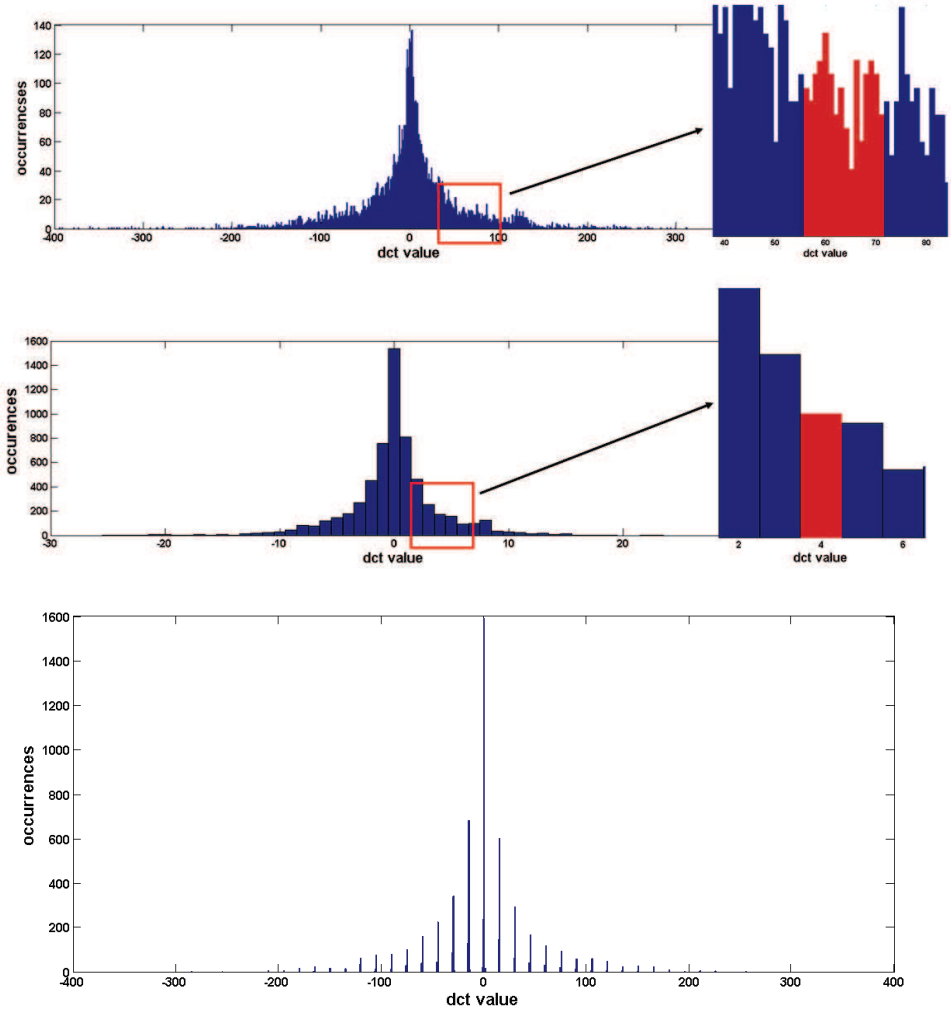

Figure 3.14: Loss of information caused by quantization error in case of an uncompressed image subjected to a (almost exactly reproduced) JPEG compression. The histogram of a generic AC term after the DCT transform (to the left in the upper row) reveals a high variability (highlighted in the same row in the histogram on the right). After a quantization with quantization step $q = 16$ *all the bins in the range* $[nq - \frac{q}{2}, nq + \frac{q}{2} - 1]$ *are mapped to* n*, for some appropriate* $n \in \mathbb{Z}$*. In the example, for* $n = 4$*, all the bins in [56,71] are mapped to the bin located in* 4 *(histogram on the right in the center row). When the image will be decompressed, the bin in* 4 *will be transferred in* 64*. The lower row shows what happens to the information after the dequantization. Since the rounding step is not yet executed, in some bins we can note the effects of the rounding error*

3.4 The sources of error in the JPEG algorithm: formal definitions

As previously mentioned, the JPEG algorithm is classified as *lossy* because the compression process applied to the image is not fully reversible. Although this loss of information can be unpleasant, with Image Forensics domain this shortcoming becomes useful for investigative purposes. Indeed, in analogy to the cues left by the criminal on the crime scene, some traces left in an image from JPEG compression algorithm can be used to get useful information to reconstructing the history of the document. Cues or "evidences" are usually related on the "difference between the image quality *before* and *after* the JPEG compression". For this reason they are known as "errors", and will be the topic of the following pages. In Fig. 3.5 can be appreciated in detail what happens to a single value of an originally decompressed image, while in Figs.3.13 and 3.16 a numerical example allows to see the errors resulting when an image undergoes to a compression/decompression procedure.

3.4.1 Quantization Error

This is the main source of error, and arises when a DCT coefficient is divided by the corresponding term of the quantization matrix, and the result is then rounded to the nearest integer. Indeed, it is formally defined as:

$$\epsilon_q = |y_{(q)i,j} \times q - y_{i,j}| = |round\left(\frac{y_{i,j}}{q}\right) \times q - y_{i,j}| \tag{3.14}$$

where $i, j = (0 \dots 7)$, $|\dots|$ is the *abs* function, q is the quantization step (i.e., the $(i,j)^{th}$ term of the 8×8 quantization matrix), and $y_{i,j}$ is the $(i,j)^{th}$ DCT term of a generic 8×8 image block.
Unlike the others two kind of errors illustrated in the following, whose definitions in the various papers are always the same, so obtaining a sort of "global acceptance" inside the scientific community, in case of the quantization error the bibliography has showed different points of view, that we will expose in the next section for every single paper. The only aspect with a general agreement is that (3.14) it's a *non-linear* operation and that we can model its output as a random variable. Our choice about the way to express this error is motivated to the fact that it better allows to highlight the joint effect of the quantization and the rounding steps in terms of information loss. In addition, and as further proof that this point of view is the most agreed, we can see that recent papers facing this kind of error [112, 166] made our same choice.
There are two different ways to consider (and therefore define) this error:

- difference between the values *exactly before and exactly after the mathematical function that generated it* (i.e., the quantization step and the rounding operation).
- difference between the DCT terms *in the same condition (i.e., dequantized)* before and after the quantization step. This one represent our point of view.

To support and clearly motivate our choice in more detail, we expose an example. Starting from any position in the 8×8 block of DCT values of a given image, showing

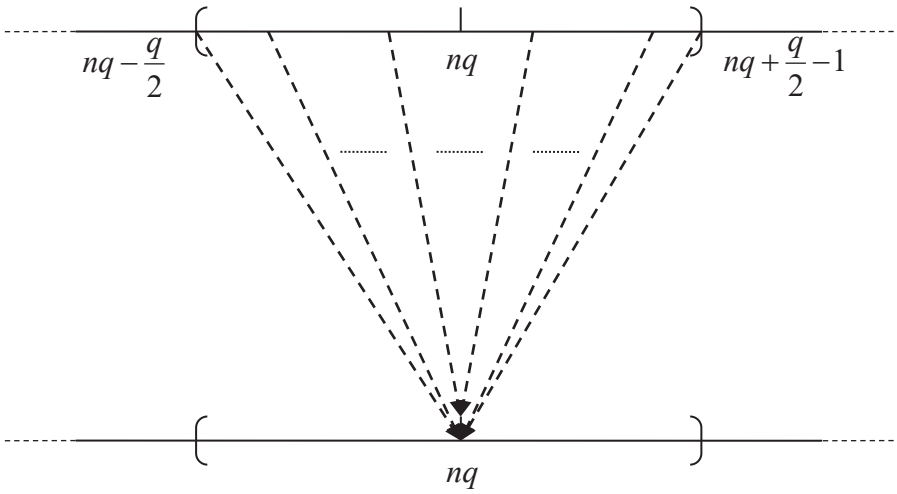

Figure 3.15: The effect of quantization and dequantization for a generic term $c \in [nq-\frac{q}{2}, nq+\frac{q}{2}-1]$ *in case of* q *even. All the terms in that range will be cast in* nq.

on the horizontal axis all the numerical values assumed by all the DCT terms in that position through all the image blocks, and in the vertical axis their occurrences, we can derive the histogram illustrated in the upper subfigure of Fig. 3.14. At this point we quantize all the terms with a quantization step $q = 16$. Due to the *round* function, during this step the values in the range [56,71] are all mapped in the bin located in 4, as showed in the center histogram of the same figure. When the image is decompressed (i.e., all the coefficients will be multiplied for 16), all the terms will assume the value of 64 ($= 16 \times 4$) and the situation is the one showed in the lower subfigure of Fig. 3.14. As clearly illustrated in Fig. 3.15, the joint action of quantization and dequantization steps takes a generic DCT term in the range $[nq - \frac{q}{2}, nq + \frac{q}{2} - 1]$ if q is even, or in $[nq - \lfloor \frac{q}{2} \rfloor, nq + \lfloor \frac{q}{2} \rfloor]$ if q is odd, and casts it in nq ($n \in \mathbb{Z}$ for a proper range around 0, in the numerical case just exposed, $n = 4$).
According with this point of view, the loss of information is the difference between the "old" values of the DCT terms (between 56 and 71) and the only "new" value after the dequantization, i.e. 64, for all of them.

3.4.2 Rounding and Truncation Errors

These two other sources of error, which are accomplished inside the box indicated as "DCT-Based Decoder" in the tampering pipeline exposed in Fig. 3.4, both arises after the IDCT, the inverse DCT transform that drives back the values from the frequency to the spatial domain once the image must be visualized. The reason is that the output values of this operation must be transformed in format (from double to 8-bit unsigned integer) and range (from a larger range to [0,255]) to be correctly visualized. Despite they are generally discarded during every mathematical modeling of the JPEG algorithm,

nevertheless their effects are not totally negligible, as can be appreciated in Fig. 3.16. The formal definitions are as follows:

- Rounding Error: The float numbers after the IDCT must be rounded to the nearest integer value to reconstruct the image in the spatial domain. The difference between the values before and after this process is called rounding error. Always referring to Fig. 3.5, and after the above considerations about the truncation error, it is defined as:
$$\epsilon_r = |\tilde{x}_{i,j} - x_{i,j}| \tag{3.15}$$
As exposed in [171], it can be considered as a special kind of quantization were $q = 1$.
Fan and de Queiroz in Ref. [76] modelled rounding errors as Gaussian distribution with zero-mean around each expected quantized histogram bin, as can been graphically appreciated in the zoom and detail of the right subfigure of Fig. 3.17, and in the lower subfigure of Fig. 3.14.

- Truncation Error: After the rounding step, again with the goal to reconstruct the image data, the values that are less than 0 needs to be *truncated* to 0, whereas the ones larger than 255 are truncated to 255. The difference between the values before and after this cutoff is the truncation error. It's highly dependent on the quality factors used in JPEG compression, and on the tested image dataset[103, 118]. More precisely, the smaller the quality factor (that means high quantization values), the higher the probability that it arises. Since nowadays the quality factors are, by default, considerably high (see what exposed in Sect. 3.3.2), this kind of error generally occurs with very low probability (less than 1%, as reported in [118]), and can be reasonably discarded during a mathematical modeling.

3.5 The sources of error in the JPEG algorithm: a timeline of the main approaches

Among the papers which in the latest decade tried to set up methods to reconstruct the history of a JPEG image, some of them moved from the study of the errors mentioned in the previous section. In particular, observing and discussing their effects on the distribution of the DCT coefficients in various points of the JPEG (single or multiple) compression pipeline, the authors tried to understand their influence on the performances of the proposed Image Forensics approach.
In the present section, we critically illustrate the most significant works in this topic, trying to follow their evolution among the years and using the uniformed terminology exposed in Sect. 3.3.
In [145] the authors, assuming to start from an observed quantized DCT value $y^{(1)}_{(q)i,j}$, studied the quantization error focusing on three different hypothesis:

- To enable the determination of expectations for the quantization error, pixel values in images are viewed as random rather than as deterministic;

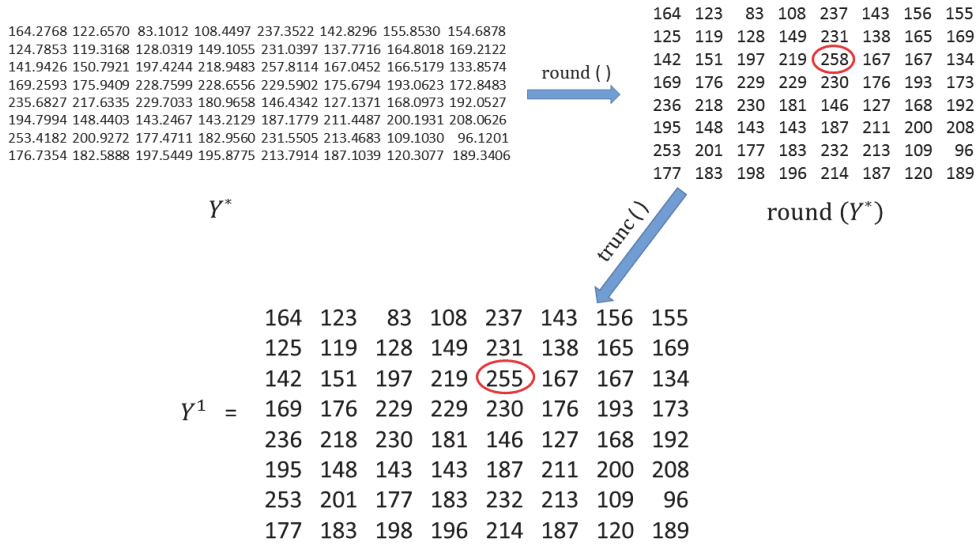

Figure 3.16: Starting from Y^*, obtained after the pipeline depicted in Fig. 3.13, it is possible to appreciate the effects of the rounding and truncation steps. The corrections made, respectively to the floating point values and to the values out of the range [0,255], create the matrix Y^1 in YC_bC_r space, now ready to be shifted in RGB space just before its visualization. Note that while the rounding function influence all the terms, the truncation one changes only one value (the one circled in red).

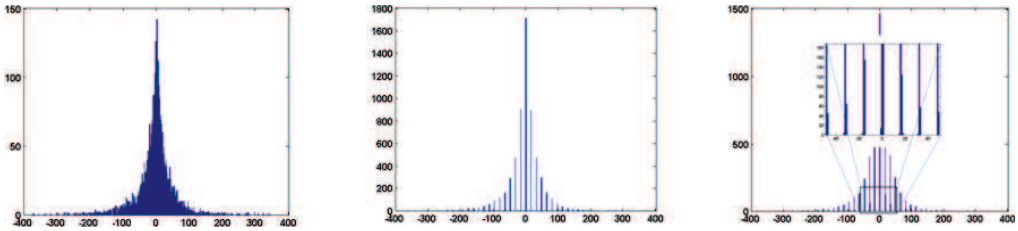

Figure 3.17: The distributions of a same coefficient in three different moments of a double compression algorithm: (left) histogram of the original uncompressed image just after the DCT, (center) histogram after the first compression, (right) histogram just before the second JPEG compression (color conversions, rounding and truncation of the values to eight bit integers have been already performed). A detail was also over imposed for a better visualization of the rounding error.

- If no prior knowledge about the value of the original frequency DCT coefficient $y_{i,j}^{(0)}$, they model the quantization error defined in (3.14) as a uniformly distributed random variable, allowing an easy derivation of the variance of the DCT-quantization error. Although mathematically easy to handle, this approach is not always appropriate, as simulations have shown in case of images with most of their energy concentrated at low frequencies with little energy at high frequencies, like the ones consisting primarily in large areas of uniform color.
- Starting from some prior knowledge about the distribution of the DCT coefficients, in particular supposing that they follow a Laplacian distribution, a different expression for the variance is obtained.

They concluded observing that simulations proved that neither of the two models are the right choice to accurately predict the spatial-domain quantization noise. Indeed, the Laplacian model works well for quantized DCT coefficients that are observed to be zero whereas when non-zero quantized DCT coefficients are observed, the uniform model is a better choice. In this paper the quantization error is defined as "*the difference between the quantized and non-quantized DCT terms.*"
In [103], one of the few works that studies the behavior of the terms of an image after two JPEG quantization with the same quantization matrix, there is another different definition of quantization error. It is defined as "*the difference between the actual float value of the divided DCT coefficients and the rounded integer value.*" In this case this definition is very similar to the one we gave in Sect. 3.4.2 for the rounding error.
The paper in [118] starts its part devoted to distinguish between JPEG image and uncompressed ones, with a mathematical derivation of the distribution d_2 of the DCT terms of an image that have been already JPEG compressed and decompressed (i.e., before the second quantization), starting from the distribution of d_1 of the DCT terms just before the first quantization. The authors stated that:

$$d_2 = DCT(IDCT(d_1^{'})) + DCT(\epsilon_r) = \left[\frac{d_1}{q_{i,j}} \times q_{i,j} + DCT(\epsilon_r)\right] \tag{3.16}$$

restricting their discussion to the AC terms and to a quantization step ≥ 2, and assuming that ϵ_r is an independent and identically distributed random variable with uniform distribution in the range of $[-0.5, 0.5]$, use the Central Limit Theorem to state that $DCT(\epsilon_r)$ has a 0-mean Gaussian distribution with variance amounting to $\frac{1}{12}$.
Then, looking at (3.16) and recalling that d_1 is approximately Laplacian, they observed that:

- $p_1^{'}(x)$ is a multiple of the quantization step q;
- p_2 is obtained from $p_1^{'}(x)$ adding some (rounding) noise around the multiples of q. This is in accordance with our[90] filtering approach, further exposed in Sect. 5.2;
- the $99,95\%$ of the the above mentioned rounding noise is spread in the range $[kq-1 : kq+1]$ of every value $kq, (k \in \mathbb{Z})$, thus allowing to conclude that $p_2(x) \approx p_1^{'}(x)$.

In this paper, the quantization error is not exactly defined, but only cited as *the error introduced when the DCT coefficients are quantized.*

In [112] Li and al., moving from the results of [145] and [118], faced the study of the rounding and quantization errors (here called *noises*) for a double JPEG compression pipeline in a very complete and exhaustive way. In particular, their mathematical definition of the latter is consistent with our point of view, as exposed in Sect. 3.1. The key points of this work, relatively to the topic exposed in the present section are:

- The distribution of the quantization error defined in (3.14) depends upon the distribution of the DCT terms, which in turn depends upon their position inside the single 8×8 block. Precisely, for the (i, j)-th term of the first JPEG cycle, and supposing that $y_{i,j}^{(1)}$ has a Laplacian distribution with 0 mean and λ as a parameter, it has the following distributions:

$$\epsilon_q(i,j) \sim \begin{cases} U\left(-\frac{q_1}{2}, \frac{q_1}{2}\right) & \text{for} \quad (i,j) = (0,0) \\ Q^L\left(\lambda_{y_{i,j}^{(1)}}, q_1\right) & \text{for} \quad (i,j) \neq (0,0) \end{cases} \tag{3.17}$$

  where q_1 is the quantization step, U indicates a uniform distribution and Q^L is a so-called Quantized-Laplacian distribution. As a personal contribution to these conclusions, in Fig. 3.18 we show graphically (in the paper these figures are missing) the application of the error function defined in (3.14) for an image taken from the Kodak Dataset [43], for a given quantization step and in four different position of the 8×8 image block. We observe that, whereas the histogram of the DC is very similar to an uniform distribution pattern in the expected range (i.e., $[-\frac{q}{2} : \frac{q}{2})$), the change towards a Laplacian behavior in case of an AC term is not as straightforward as in (3.17) would seem. This aspect, i.e. the relation between the variance of a random variable, the magnitude of the quantization step and the behavior of the distribution, is highlighted by the the authors when they state that "*the quantization noise distribution will approach uniform distribution as the quantization step is small when compared to the variance of the random variable*".

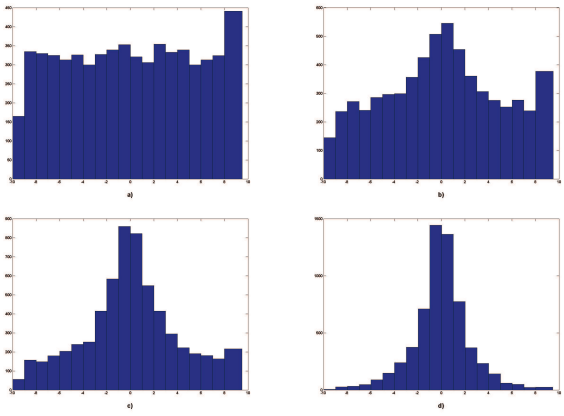

Figure 3.18: Distribution of the quantization error as defined in (3.14) for $q = 19$ in four different positions of the 8×8 block with respect to the zig-zag order showed in Fig. 3.3: a) position 1 (the DC term), b) position 20, c) position 40, and d) position 64.

- The rounding error defined in (3.15) for the (i, j)-th term of the first JPEG cycle has the following distributions:

$$\epsilon_r(i,j) \sim Q^N\left(\sigma_{\bar{x}_{i,j}^{(1)}}, 1\right) \tag{3.18}$$

  where $\bar{x}_{i,j}^{(1)}$ is defined as the difference between the original luminance value $x_{i,j}^{(n)}$ and $\tilde{x}_{i,j}^{(n)}$, that is the value of the same term after DCT, compression, decompression and IDCT. Both terms are in the spatial domain.

In addition and beyond these important results, the authors also expose considerations about the distributions of the quantization and rounding errors in case of multiple quantizations, using their observations to develop methods for quantization step estimation and identical recompression detection in these scenarios. As an application of the above theory, in [59] Li et al. proposed an approach useful to extract traces left by JPEG compression in uncompressed images, and use this information as a proof to classify the originality of a visual document. This paper is important mainly because it faces the problem in case of high-quality JPEG compressions, very common in the standard settings of a lot of cameras at the present time, as highlighted in our survey exposed in Sect. 3.3.2 .

4

Quantization Step Estimation Approaches for JPEG Images in DCT Domain

The voyage of discovery is not in seeking new landscapes but in having new eyes.

Marcel Proust

This Chapter is devoted to list, and in some cases briefly expose, the major results obtained in the last fifteen years by the international research community in the estimation of the Quantization Table used in a first JPEG compression, when the image to examine has been decompressed, and then saved in some kind of uncompressed format or again in JPEG. Since some of the the Image Forensics methods exposed in the following move by the assumptions that the non-originality of the image has already been established, before the following list we will briefly illustrate how this starting point can be achieved, in case of double compressed JPEG images.
This ability can be very useful, especially in a forensics scenario. Indeed, if we are able to demonstrate that a JPEG image used as an evidence in a court has been doubly compressed, we have the clear proof that the image under analysis is not the one stored by the acquisition device just after the shoot. This because the presence of the second compression, proofs beyond every doubt that the image has been decompressed and (possibly after some kind of operation) compressed again. In some case this could be enough to invalidate the entire outcome of a trial.
The most robust detector of this chain of quantizations is based upon the analysis of the DCT coefficients, since their histogram in case of doubly compressed images assumes a

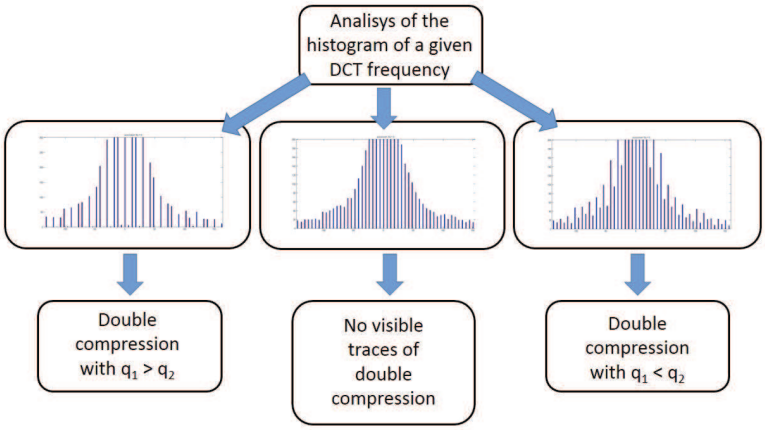

Figure 4.1: The pipeline to distinguish between single vs double compressed JPEG images. The different shapes of the periodical patterns that characterize the two histograms on the left (obtained from a double compression with $q_1 = 10$ and $q_2 = 6$), and on the right (obtained with $q_1 = 4$ and $q_2 = 6$) not only highlight a double compression, but also if the first compression is stronger than the second one. The central histogram is the outcome obtained plotting the values of an AC coefficient after a single quantization (in this example with $q = 6$). The lack of "strange" features can be indeed used as a proof of singly compressed image, even if the same result could be obtained also after two compressions with identical quantization steps.

characteristic shape, that it is called "Double Quantization Effect".

4.1 Verify the originality of a JPEG image by means of the Double Quantization Effect

Even if a detailed study of the response of DCT coefficient histograms in the frequency domain can be also in [92], the Double Quantization Effect was firstly cited in 2003 by Lukáš and Fridrich [117], and a more complete description has been done by Popescu and Farid[136] in 2005. In this paper, the authors illustrated a set of possibilities that arise from the observation of the statistical properties of a digital image for a forensics analysis. This analysis was followed by others, providing with more mathematical details, namely He et al. [99] and some years later Lin et al. [115]. In the latter exposition, where is proposed a method to build a probability map for the automatic localization of tampered regions in JPEG images, the authors begin from the extraction of the histogram of the DCT coefficients before the first quantization (named h_1), and proceded investigating how the two quantizations with steps q_1 and q_2 change the shape of the histogram obtained after the second quantization (named h_2).
The first two important results, summarized in Fig. 4.1, are the following:

- the shape of the histogram of a single AC term allows to understand if the image under analysis has been singly or doubly compressed;

- in case of doubly compressed image, the relationship between the two successive quantization steps changes the pattern of the histogram for a certain range around 0. In particular, if the bins are located in multiples of q_2 with some empty positions, and if the height of the bins follows a decreasing monotonous trend moving away from 0, is possible to assert that the first quantization step was bigger than the second one, whereas if the heights of the bins doesn't decrease monotonically, and there are no holes between bins, the first quantization step was smaller than the second one.

Another considerable result reported in [115] is that, if we suppose to know q_1, and after retrieving q_2 from the JPEG header, starting from a bin of the histogram h_2 in position p_2, is possible to derive the number $N(p_2)$ of bins in the original histogram contributing to the bin in p_2. It depends on the triple (q_1, q_2, p_2) and it's equal to[1]:

$$N(p_2) = q_1 \left(\left\lfloor \frac{q_2}{q_1} \left(p_2 + \frac{1}{2} \right) \right\rfloor - \left\lceil \frac{q_2}{q_1} \left(p_2 - \frac{1}{2} \right) \right\rceil + 1 \right) \tag{4.1}$$

It is then pointed out that $N(p_2)$ is a periodic function, with a period:

$$\wp = \frac{q_1}{gcd(q_1, q_2)} \tag{4.2}$$

Some of the above results have been also extended in case of video formats by Wang and Farid in 2006 [167] and 2009 [168].
In 2012 an improved Double Quantization detection method has been proposed by Thing et al. in [161], exploited in turn more recentely by NG et al. within a method to detect double compressed Facebook JPEG images [48].
As already mentioned we will report only papers that we consider mostly important for the topic of this thesis. We wish to point out that, although all the following works have the goal to reconstruct some (as much as possible) elements of the quantization matrix referred to previous JPEG quantization(s) to which the image has been subjected, not all of them start from the same scenario. Indeed, some papers move from the analysis of a JPEG image without the inner metadata (as happens, for example, if a JPEG images has been imported into Microsoft Powerpoint or Word documents by graphics programs, or if they have been manually erased from the forger), others from an image given in a uncompressed format (such as Bitmap[159] or Tagged Image File Format[49]) that has been previously JPEG compressed, others from a doubly compressed JPEG image (see Fig. 4.2). Besides, some works have the goal to determine the tampered parts in an image, and the retrieving of the coefficients of the first quantization matrix is only a step in the pipeline of the proposed approach. Since the common goal of all the approaches is to extract the quantization step of the JPEG image before its decompression, we identify this problem with the acronym QSE (Quantization Step Estimation). In almost all cases we tried to capture the main idea referred to our topic, sometimes giving its mathematical formulation and often ignoring other parts that we found not directly connected to our purpose. Despite other possible criteria, we decided to expose the works in a chronological order, since the problems addressed in every paper below are very closely connected and consequently all these approaches have, in some

[1] $\lfloor . \rfloor$ and $\lceil . \rceil$ are, respectevely, the *floor* and *ceil* functions.

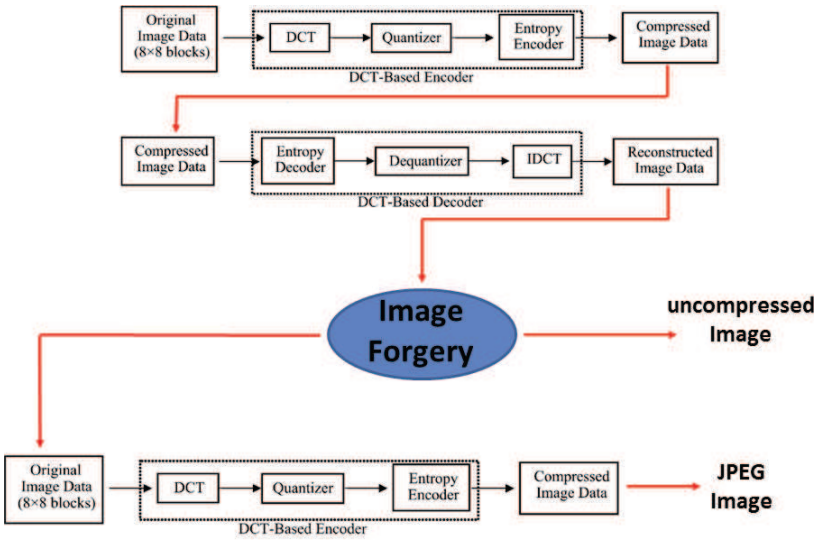

Figure 4.2: After being JPEG compressed, decompressed and subjected to some kind of forgery, an image could be JPEG-recompressed or saved in some other kind of uncompressed format. In both cases, the ability to retrieve (as much as possible of) the coefficients of the first JPEG compression is an important skill for forensics purposes.

way and with respect to their chorological order, inspired each other. A summarized list of the papers is given in Tab.4.1, in which the works are grouped together depending on their specific purpose.

4.2 History of a bitmap image with no prior information (2000 - 2003)

In [75] and [76], Fan and de Queiroz presented a method that, given an image in bitmap format is able to determine whether it has been previously JPEG-compressed, and further estimate which quantization matrix has been used. The method assumes that if there is no compression, the pixel differences across 8×8 block boundaries should be similar to those within blocks, while they should be different if the image has been JPEG-compressed. In particular, taking into account inter and intrablock pixel differences, it is possible to build two functions that, with reference to Fig. 4.3, are defined in the following way:

$$Z^{'}(i,j) = |A - B - C + D| \quad \text{and} \quad Z^{''}(i,j) = |E - F - G + H| \tag{4.3}$$

The energy of the difference between the histograms of these functions is then compared to a proper threshold, to deduce the presence of a prior compression. The method is capable of revealing artifacts also when very light JPEG compression is applied (i.e., with quality factor as high as 95). After detecting the compression signature, the authors

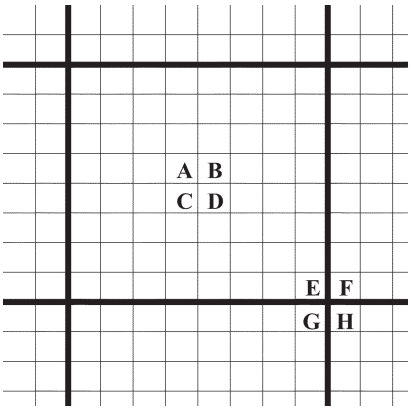

Figure 4.3: In [76] (from where this image has been taken), the authors propose to ascertain if the pixel differences across the boundaries of every 8×8 image block is similar to the one within the block.

presented a method for maximum likelihood estimation (MLE) of JPEG quantization steps and showed its reliability via experimental results. For their purpose they face the rounding and truncation errors, starting by the same observations exposed in Sections 3.4.2 and 3.5: the distribution of the former is Gaussian in the range $[-0,5 : 0,5)$ and the percentage of the latter inside every block is very low. Some of the results obtained in these papers formed the basis for the approach exploited in [128]. This work deserves to be quoted mainly for two reasons: it deals with color images, and it proposes (for the first time in multimedia forensics) an estimation of the lattice structure in the Discrete Cosine Transform domain for determining the color space, even if limited on the case when the quantization of DCT-coefficients is performed for a JPEG compressed image without downsampling of color components.

4.3 First approach to doubly compressed JPEG images (2003)

Expanding their previous works devoted to define steganalytics methods, Lukáš and Fridrich in [117] started to face the problem of the retrieval of the coefficients of the first quantization in a double compressed JPEG images. They proposed an alternative method based on the evaluation of the behavior of normalized histograms. Since this approach provides unsatisfactory results, they finally focused on a strategy that uses in sequence a set of Neural Network (NN) as a classifier. Their exposition of the method began observing that the question needs to be addressed separately, depending upon the different possibilities of relations between the two quantization steps:

- $q_1 = q_2 \cup [(q_1 < q_2) \wedge (\exists n \in \mathbb{N} : n * q_1 = q_2)]$;
- $q_1 > q_2$;
- $q_1 < q_2 \wedge (\nexists n \in \mathbb{N} : n * q_1 = q_2)$.

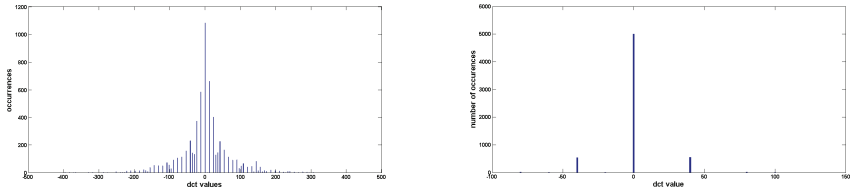

Figure 4.4: Histograms of a doubly compressed image after decompression. From an AC term of a low frequency (left histogram) a lot of information can be extracted, whereas in case of an AC term referred to high frequency coefficients (right histogram) the most part of dequantized coefficients are equal to 0.

This paper, which also has the goal to detect if a given JPEG image has been previously doubly compressed (*Double Compression Detection* problem), was the first to point out two aspects which have become milestones in this research field:

- since DCT is an orthogonal transform, changes in one coefficient should not affect the other ones. So it is possible to study separately every position in the 8×8 image block;
- in every block, approaching to the 64^{th} coefficient following the same zig-zag order showed in Fig. 3.3 for the JPEG entropy coding step, the amount of information that is possible to extract becomes progressively smaller. Indeed, as can be noted in Fig. 4.4, the left histogram referred to an AC term in position 2 (very low frequency) contains a big amount of information, whereas the right histogram, coming from the AC term in position 35, does not contain many useful information, since almost all the coefficients are equal to 0.

The main limitation of this paper lies in the fact that it only takes under consideration DCT coefficients in the first three positions of the block, that is not enough helpful to uniquely identify a quantization matrix. An important (often used in the following) property stated in the paper is that "the pattern of bins in the histogram of a doubly compressed JPEG image for a given (possibly referred to a low frequency) AC term can offer important hints for the identification of the primary quantization factor."

4.4 The approaches exploiting the Benford's law (2007)

In [88], the first digit law (Benford's law[101]) is applied by Fu et al. to estimate the JPEG-compression history for images in bitmap format, by means of a support vector machine (SVM) based classifier. In particular, the provided results include the detection of JPEG (either single or double) compression and the estimation of JPEG compression factor. The authors demonstrated that the probability distribution of the first digit of the DCT coefficients in original JPEG images (single-compressed) follows this Benford-like logarithmic law:

$$p(x) = Nlog_{10}\left(1 + \frac{1}{s + x^q}\right) \tag{4.4}$$

with $x = 1, 2, \ldots, 9$, N is a normalization factor, s and q are the model parameters. Consequently, they proposed a generalized form of the Benfords law to precisely describe the distributions of the original JPEG images with different Q-factors. Since the first digit of the DCT coefficients in double JPEG-compressed images doesn't follow the above mentioned law (in the paper is observed that the fitting provided by the generalized Benfords law is decreasingly accurate with the number of compression steps), its presence (or absence) can be used as a signature in a double JPEG processing detection algorithm. Like all the milestone papers, also this work has been deeply explored over the years. As an example, in [113] is discussed how the performances of this approach can be improved by examining the first digit distribution of each sub band of DCT coefficients independently, rather than analyzing the entire set at once. Again, Feng et al. in [83] outperformed the results given in the above paper with a multi-features detection method using both linear and non-linear classifiers. More recently, Hou et al. extended the above results by including also *zero* in the set of possible digits for the statistics of the first digit distribution[102]. In the same year the authors of [122] exposed an Antiforensic method to fool the statistics connected to the Benford's law in case of the detection of double compressed images. Another interesting question, detecting how many JPEG compressions have been applied to one image, is answered by the application of this statistical rule by Milani et at. in [123] in 2014. At the same time, in a work by Pasquini et al. [131] is proposed a binary decision test, based upon the Benford-Fourier theory, to distinguish the images that was previously JPEG compressed starting from images stored in an uncompressed format. Always leveraging the same theory, Pasquini et al. in [130] faced also multi (up to three) JPEG compressions , exposing a method for its identification starting from JPEG images. Their approach is also extended to the estimation of the quantization steps, passing through a training phase followed by a testing one, obtaining good results compared with [58], also for the challenging case of $q_1 < q_2$, even if limited to an aligned image grid. The difference between this scenario and a non-aligned one, more similar to what a forensics expert really have to face, is hightlighted in Sect. 4.10.

4.5 Attack to the doubly compressed JPEG images issue using a SVM (2008)

The work exposed in [133], by Pevny and Fridrich, it's an improved version of the NN developed in [117], where the histogram is also used to train an SVM and to make the same detection. More precisely, in this approach the double compression detector is based on a Support Vector machine (SVM) with Gaussian kernel, and the train is obtained with a collection of 9 DCT coefficients derived from the first order statistics of individual DCT modes of low frequency DCT coefficients. The algorithm not only detects doubly compressed images, but also can be used as a detector of the Primary Quantization Step, and for this purpose, a set of SVM-based multiclassifiers (a collection of binary classifiers) is used. This approach, however, similarly to the work of [83] has been tested only for secondary quality factors equal to 75 or 80, since these are the default quality factors of two famous steganalisys algorithms: F5[170] and OutGuess [139]. A third outcome exposed in the paper is the comparison between the retrieved

DCT coefficients and a set of whole quantization matrix, with the purpose of trying to find the "closest" (depending upon a proper metric) quantization table. In the paper the authors solve the query of the Double Compression Detection comparing the feature set proposed in [88] with their own, and training the classifiers on exactly the same images dataset.

4.6 Hunting for the JPEG ghosts (2009)

Although the paper by Farid [79] was not strictly dedicated to recover the quantization steps of the first quantization matrix, but primarily to the identification of the tampered regions (the so called "ghosts") in a double compressed JPEG image, we mention this paper since the core of its approach is somehow similar with the error function developed in our papers and exposed in Chapter 5. Indeed, the author proposes to estimate q_1 through a third quantization, by varying its correspondent step in a proper range and then computing the error between the DCT coefficients, before and after this operation, with the following map:

$$f_e(y_{i,j}^{(0)}, q_1, q_2, q_3) = \left| \left[\left[\left[\frac{y_{i,j}^{(0)}}{q_1} \right] \times \frac{q_1}{q_2} \right] \times \frac{q_2}{q_3} \right] \times q_3 - \left[\left[\frac{y_{i,j}^{(0)}}{q_1} \right] \times \frac{q_1}{q_2} \right] \times q_2 \right| \tag{4.5}$$

Extracting the local mimima of this error function, Farid stated that is possible to highlight the exact values q_1 and q_2.
Unfurtunately, as highlighted in [91] and exposed in Sect. 5.1, for the majority of the real cases the original quantization coefficient cannot be easily inferred.
In 2012, Zach et al. present a method that fully automates the detection of JPEG ghosts [175].

4.7 Extraction of information from a bitmap image that was previously JPEG compressed (2010)

In [118], a paper which we yet partially explored in Sect. 3.4, Luo et al. expose a method to identify quantization steps and quantization tables from Bitmap images that have been previously JPEG compressed. An interesting result presented here is that the de-quantized coefficients of a JPEG compression will be well preserved with the highest probability after JPEG recompression, also when compared with any others including the quantization table of ones (QF2 = 100), when the second compression has been exploited using the same quantization table of the first one ($Q_2 = Q_1$).
The strength of their approach lies in the fact that it works also when the test images don't have enough statistics (i.e., the tampered region within an image is just a small patch such as a face, some numbers on a plate, and so on), indeed the reported outcomes continue to be significant also when the size of the images is reduced to a block of 64×64 pixels, in case of the detection of the quantization table. For this purpose, first the proposed algorithm JPEG recompresses the image $X^{(1)}$ (a singly-compressed JPEG image) with all the possible quantization tables belonging to a known set with quality factors ranging from 1 to 100, obtaining 100 different decompressed version of $X^{(2)}$. At

this point the quality factor (QF) of $X^{(1)}$ is:

$$\arg max_i \left(R\left(X^{(1)}, X^{(2)}(i) \right), i = 1, 2, \ldots 100 \right) \tag{4.6}$$

where R is defines as a similarity measure between two images $X^{(1)}$ and $X^{(2)}$ with size of $M \times N$.
Once obtained the QF, the compression matrix is uniquely identified.
As can be noted, one big limitation of this paper is that it assumes that the primary quantization matrix belongs to a set of known matrices, whereas in a real scenario this is not generally true especially today, when, as clarified in Sect. 2.2, image acquisition devices often create on site their own best quantization tables.

4.8 JPEG images doubly compressed with the same quantization matrix (2010)

In [103], F. Huang et al. cope with the detection of double JPEG compression when the primary and secondary quantization matrix are the same. It's a challenging problem, since in this conditions the "characteristic framework" introduced by different quantization matrices (i.e., the behaviors shown in Fig. 4.1) is missing, causing the usual detection methods don't work in the proper way.
They start observing that, caused by the three kind of errors that arise in the JPEG compression/decompression pipeline, the number of different DCT coefficients in case of multiple compressions (recompressing a JPEG image over and over again) with the same quantization matrix, decreases as the number of compressions rises. To this aim, they define as C_n the rate of coefficient change between two subsequent JPEG quantization, which is dependent on the number of nonzero DCT coefficients and the different DCT coefficients between the quantization. Subsequently, they took about 4000 images of roughly equal size from three different dataset and doubly compressed them with the same quantization table. In this manner they can observe that, in case of single and double compression, the average value of C_1 is heavily depending on the chosen database.
Further considerations regarding the statistical propriety of the DCT terms, compared between subsequent compressions, allowed the authors to state that not only as the number of compressions increases the amount of different DCT coefficients decrease, but the same happens for the difference between two subsequent D_i (i.e., $D_n - D_{n+1} > D_{n+1} - D_{n+2}$). Exploiting the above considerations, the proposed algorithm first gets an estimate D of the different JPEG coefficients between the examined JPEG image J and its recompressed version $J^{'}$ obtained with the same quantization table. The next step expects to entropy decode $J^{'}$, randomly selects and modifies a "proper" amount of its DCT coefficients, modifies them randomly decreasing or increasing by 1 arbitrarily, and decodes the whole image again obtaining $J^{'}_m$. Subsequently the image is then decompressed and recompressed with the same quantization table to get $J^{''}_m$, and D^1_m is setted as the number of different DCT coefficients between these two images. The next two steps are repeated a certain number of times and an average value $\bar{D}_m$ is calculated.

Then the rule for discriminating between singly and doubly compressed image is:

$$\begin{cases} \bar{D}_m \geq D & \Longrightarrow \text{J is doubly compressed} \\ \bar{D}_m < D & \Longrightarrow \text{J is singly compressed} \end{cases} \tag{4.7}$$

Since the correct choice of the amount of DCT coefficients to modify is the key for the success of the method, a big part of the paper is devoted to the selection of this term. The results are quite significant: if the QF is no less than 90, the final detection accuracy rates are constantly higher than 90 percent for all the image dataset used. The authors also extended their approach to discriminate between single-triple or double-triple compressions, and declare that, assuming to find a suitable "proper" ratio their method can detect four times and further JPEG compressions.
In the following years, the same problem has been addressed in [120] and [152], whereas more recently Lui et al. in [116] proposed a method to detect the presence of forgery in images where the modified parts have been generated with the same quantization matrix of the background. In particular, [120] exposes a modified version of the Random Perturbation Strategy adopted in [103], obtaining good results especially for the detection of triply compressed JPEG images.

4.9 Analysis of JPEG images using the factor histogram (2011)

In [174], Yang et al. extract a statistic feature called "factor histogram" from the analysis of the procedure of double quantization. This characteristic describes the distribution of the factors being related to quantized DCT coefficients, and is used to detect double quantization and to estimate the primary quantization matrix in double compressed JPEG images. According with the authors, to derive the notion of factor histogram is necessary to start with a formula that represents the generic DCT term after the second quantization, taking into account all the kind of errors:

$$y_{i,j}^{(2)} = \left\lfloor \frac{y_{i,j}^{(1)} q_{i,j}^{(1)} + \epsilon_r + \epsilon_t}{q_{i,j}^{(2)}} \right\rfloor \tag{4.8}$$

Following considerations about the rounding function similar to the one that brought to Fig. 3.15, and neglecting the rounding/truncation errors, the authors come to state that the product $y_{i,j}^{(1)} \cdot q_{i,j}^{(1)}$ securely belong to the set of $q_{i,j}^{(2)}$ consecutive integers defined as:

$$D(y_{i,j}^{(2)}, q_{i,j}^{(2)}) = \left\{ \left\lceil \left(y_{i,j}^{(2)} - 0.5 \right) q_{i,j}^{(2)} \right\rceil + x | x = 0, 1, \ldots, q_{i,j}^{(2)} - 1 \right\} \tag{4.9}$$

At this point they factorize each integer in $D(y_{i,j}^{(2)}, q_{i,j}^{(2)})$, and collect all of the positive integer factors to form the factor set that is a constraint for the value range of the step size $q_{i,j}^{(2)}$, being defined as:

$$F(y_{i,j}^{(2)}, q_{i,j}^{(2)}) = \left\{ x | mod(x, y) = 0, y \in D(y_{i,j}^{(2)}, q_{i,j}^{(2)}), x > 0 \right\} \tag{4.10}$$

where $mod(\cdot,\cdot)$ indicates the modulo function. The next step lies in defining the factor histogram h_f as the histogram of the factor sequence given by a set of k different $F(y_{i,j}^{(2)^k}, q_{i,j}^{(2)})$, every one given by (4.10) varying $y_{i,j}^{(2)}$ in a a nonzero coefficient sequence of length k, in which each component has been doubly quantized with step size q_1 and q_2. Finally, the authors set up a kind of score assessment strategy associated with this factor sequence. Inside of this rank, for a doubly quantized sequence with $q_1 > q_2$ the factor histogram will achieve its maximum at q_1, thus allowing to detect the first compression step.
It is important to point out that this approach starts from two hypothesis: the first one, that allows to assert that $q_{i,j}^{(2)} \in F(y_{i,j}^{(2)}, q_{i,j}^{(2)})$, is that $q_{i,j}^{(1)} > q_{i,j}^{(2)}$. This means that the quality factor of the first quantization is assumed lower than the second one. This assumption also characterizes other approaches, as we will see, indeed the study of the case when $q_{i,j}^{(1)} < q_{i,j}^{(2)}$ is an open challenge for the scientific community also at the present time. The second (very restrictive in our opinion) conjecture, assumes the knowledge of the set of quantization matrix used for the first compression, that the authors called QMS (Quantization Matrix System) and represents the JPEG quantization matrices provided by a company (producing either cameras or photo editing software) inside its software. Even if the latter assumption can in some cases correspond to a real scenario, since every investigation is composed by scientific methods together with classical ones and so this information can be known by other ways, nevertheless for a fair comparison to the state of the art we think that it would be better to avoid any kind of hypothesis about such information.
Recently, in [173], almost the same group of the authors exposed another method based on the statistics of the factor histogram for estimating the JPEG compression history of bitmap images. In particular, the authors move from the observation that this feature decreases with the increase of its bin index for uncompressed bitmaps, whereas exhibits a local maximum at the bin index corresponding to the quantization step for JPEG decompressed bitmaps.

4.10 Aligned and non-aligned scenarios (2011 - 2012)

The papers [56] by Bianchi et al., and [58] by Bianchi and Piva, are closely related as stated by the the authors themselves. In [56], which in turn took the cue from [115], Bianchi et al. face with a particular scenario that they called Single Compression Forgery for JPEG images. This is the situation in which a part of a JPEG image is patched over an uncompressed one (copy-paste or cut/past operation) and the result is JPEG compressed. The core of the method is the use of Bayesian inference to assign to each DCT coefficient a probability of being doubly quantized, giving the possibility to build a probability map that for every part of the image tells if it is original or tampered. One of the parameters needed to calculate the probability is the quantization step of the first compression that in this case is iteratively estimated.
In [58], which is itself a refinement of [57] by the same authors, Bianchi et al. build a likelihood map to find the regions that have undergone to a double JPEG compression, starting from a scenario that is the same as described above. In particular, the authors observe that the distribution of the DCT coefficients of a tampered image, considering

the above scenario, can be modeled as a weighted summation of two hypotheses:

$$p\left(x; q_1, \alpha\right) = \alpha \cdot p\left(x|H_0\right) + (1-\alpha) \cdot p\left(x|H_1; q_1\right) \tag{4.11}$$

where α indicates how strong is the probability that the DCT coefficient has been single quantized (hypothesis H_0, $\Rightarrow$ it belong to a non tampered part), or doubly quantized (hypothesis H_1, $\Rightarrow$ it belong to a tampered part). As can be seen, among the parameters required to correctly identify this likelihood map and modeling the doubly compressed regions, q_1 (the quantization step of the primary compression) is crucial. The authors estimate q_1 using the EM (Expectation Maximization) algorithm over a set of candidates. This procedure is replicated for each of the 64 DCT coefficients that compose the first-compression matrix. Besides its results, the method is important because it takes into account two type of traces left by tampering in doubly-compressed JPEG images: aligned and non-aligned, something that was considered, to the best of our knowledge, only few times before[50, 65] and never after. These two scenarios, respectively referred as A-DJPG and NA-JPG, arise depending if the DCT grid of the portion of image pasted in a splicing or cloning operation is (or not) aligned with the one of the original image. Also in these papers is underlined the tested difficult to correctly estimate q_1 when it is $\leq q_2$. Indeed, their results are heavily affected from this problem, as they pointed out in their conclusions.

4.11 Tampering detection based upon the distribution of DCT coefficients (2014)

The work [166], by Wang et al., exposes a method for tampering detection based on the different distributions of DCT coefficients between tampered and non tampered regions. In their approach, the authors built up a statistical model (EM algorithm) in which the knowledge of q_1 is one of the four parameters required. Since they explore the scenario where a JPEG image I_0 is decompressed and then JPEG compressed again, they provide a way to determinate the first quantization step in doubly compressed JPEG images. Their considerations start from the expression of a generic double compressed DCT term without taking into consideration truncation and rounding errors:

$$y_{i,j}^{(2)} = \left\lfloor \left\lfloor \frac{y_{i,j}^{(0)}}{q_1} \right\rceil \frac{q_1}{q_2} \right\rfloor \tag{4.12}$$

The above term can be manipulated considering the propriety of the rounding function, coming to the following expression:

$$q_1 \left(\left\lceil \frac{q_2}{q_1} \left(y_{i,j}^{(2)} - \frac{1}{2} \right) \right\rceil - \frac{1}{2} \right) \leq y_{i,j}^{(0)} < q_1 \left(\left\lceil \frac{q_2}{q_1} \left(y_{i,j}^{(2)} + \frac{1}{2} \right) \right\rceil - \frac{1}{2} \right) \tag{4.13}$$

After this, the authors model the probability distribution of the absolute values of the DCT coefficients in a tampered image in the following way:

$$P(X = x) = \alpha_1 P(X_s = x) + \alpha_2 P(X_d = x) \tag{4.14}$$

where:

$$P(X_s = x) = \int_{q_2(x-\frac{1}{2})}^{q_2(x+\frac{1}{2})} \frac{\mu_1}{2} \exp(-\mu_1 x)\, dx \tag{4.15}$$

and

$$P(X_d = x) = \int_{q_1\left(\left\lceil \frac{q_2}{q_1}\left(y^{(2)}_{i,j}-\frac{1}{2}\right)\right\rceil-\frac{1}{2}\right)}^{q_1\left(\left\lceil \frac{q_2}{q_1}\left(y^{(2)}_{i,j}+\frac{1}{2}\right)\right\rceil-\frac{1}{2}\right)} \frac{\mu_2}{2} \exp(-\mu_2 x)\, dx \tag{4.16}$$

where α_1 and α_2 indicate respectively the portion of tampered and untampered image ($\alpha_1 + \alpha_2 = 1$), μ_i is the term that characterizes the Laplacian distribution of the AC terms (see (3.13)). From this statistical model the authors define a likelihood function and use the EM algorithm for the estimation of the unknown parameters. In doing so, they have also taken into account the truncation and rounding errors, referring to the work of Bianchi et al.[56]. Finally, we want to point out that also in this work the case $q_1 < q_2$ gives unsatisfactory results.

At the end of this section we expose the overview schema in Tab.4.1. It points out that JPEG is the most investigated image format, that statistical-probabilistic features are the most investigated compared to Machine Learning approaches, and finally that only a few number of papers are devoted to highlight tampered regions in images, whereas the majority of the works have the goal to clarify the existence of traces coming from past compressions.

Table 4.1: Overview of the methods exposed in Sect. 4.

Image Format	Mathematical Tool	Goal
Bitmap	MLE	Image compression history
[75, 76, 88, 118]	[75, 76]	[75, 76, 88, 118, 117]
JPEG	Neural Networks	[103, 174, 133, 58, 57]
[117, 133, 79, 103]	[117]	JPEG quantiz. matrix estimation
[174, 56, 58, 166]	SVM	[75, 76, 118, 133, 174]
	[88, 133]	[58, 57, 166]
	Probabilistic laws	Identification of tampered regions
	[88, 56, 58, 166]	[79, 58, 57, 166]
	Statistical features	
	[75, 76, 118, 133, 79]	
	[174, 103]	

5

A new approach for QSE in doubly compressed JPEG images

The problem is not the problem,
the problem is your attitude towards the problem.

Captain Jack Sparrow

This Chapter contains the work developed during my Phd studies, rearranged and adapted to the present exposition. Its three subsections are composed (in the same order) by the content of the following papers:

- Fausto Galvan, Giovanni Puglisi, Arcangelo R. Bruna and Sebastiano Battiato: *First quantization coefficient extraction from double compressed JPEG images.* Presented to International Conference on Image Analysis and Processing - ICIAP Naples (Italy), vol. 8156, pp 783 - 792, (2013).
- Giovanni Puglisi, Arcangelo R. Bruna, Fausto Galvan and Sebastiano Battiato: *First JPEG quantization matrix estimation based on histogram analysis.* Presented to the 20th International Conference on Image Processing - ICIP Melbourne (Australia), pp. 4502 - 4506, (2013).
- Fausto Galvan, G. Puglisi, A.R. Bruna, and Sebastiano Battiato. *First quantization matrix estimation from double compressed JPEG images.* In IEEE Transactions on Information Forensics and Security, 9(8):1299-1310, (2014).

The first paper contains the mathematical details related to the approach, and highlights how a fourth quantization allows in theory (which means in absence of the rounding

and truncation errors that arises in the "real" quantization/dequantization/quantization pipeline of a forgery in case of JPEG images) the extraction of the first quantization step. The need to correct the nasty influence of the noise on the results of the first paper in real cases, mainly due to the rounding step during the dequantization algorithm, encouraged us to search for new approaches of filtering on histograms. A first result in this direction is reported in the second work, that indeed has been devoted to develop a new filtering strategy with the aim to remove the noise introduced from the real pipeline. Further studies led us to define two different types of noise, that we called "split noise" and "residual noise". The third work is dedicated to the definition of these features and to their removal, together with the joint action of the error function yet introducted and developed in the first paper.

5.1 Implementation of a fourth quantization

Considering a single DCT coefficient $x_{i,j}^{(0)}$, the quantization steps q_1 (for the first quantization) and q_2 (second quantization), the value of the coefficient after a double quantization is given by [1] [2] :

$$y_{(q)i,j}^{(2)} = \left[\left[\frac{y_{i,j}^{(0)}}{q_1} \right] \times \frac{q_1}{q_2} \right] \tag{5.1}$$

As exposed in Sect. 4.6, to infer the value of q_1 Farid in [79] suggests to quantize again such value with a novel quantization coefficient (q_3), by varying its value in a proper range and searching the values in the (local) minima of an error function defined as follows[3] :

$$f_e(y_{i,j}^{(0)}, q_1, q_2, q_3) = \left| \left[\left[\left[\frac{y_{i,j}^{(0)}}{q_1} \right] \times \frac{q_1}{q_2} \right] \times \frac{q_2}{q_3} \right] \times q_3 - \left[\left[\frac{y_{i,j}^{(0)}}{q_1} \right] \times \frac{q_1}{q_2} \right] \times q_2 \right| \tag{5.2}$$

As an example, the typical outcome of (5.2) considering the DC term $q_1 = 23$ and $q_2 = 17$ is reported in Fig. 5.1(a). In this specific case (both coefficients are prime numbers) we obtain interesting results: both q_1 and q_2 can be easily found, since they correspond to the two evident local minima. Hence in this case the first quantization coefficient q_1 can be retrieved (q_2, as mentioned before, is often already available in the Exif metadata). Unfortunately, in a real scenario the original quantization coefficient cannot be easily inferred as proved by considering the following cases:

- Taking into account the quantization values used before ($q_1 = 23$, $q_2 = 17$) and the same input image, but varying q_3 in the range [1,70], the outcome is more complex to analyze than before. Several local minima arise and a strong one can be found in 65 (see Fig. 5.1(b)).
- By employing the same input image and q_3 in the range [1,30], but with different quantization steps $q_1 = 21$ and $q_2 = 12$ (they are both not prime numbers), the

[1] For sake of simplicity, in (5.1) truncation and rounding errors have not been considered. However, they have been taken into account in the design of the proposed approach.

[2] [.] indicates the *rounding* function

[3] |.|indicates the *abs* function

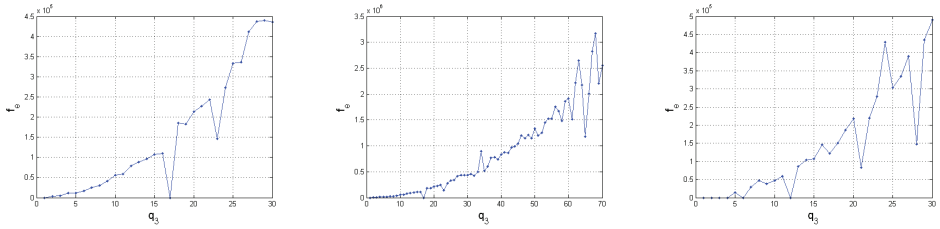

(a) (b) (c)

Figure 5.1: Examples of the error function values (2) with respect to q_3: (a) $q_1 = 23$, $q_2 = 17$ and q_3 is in the range [1,30]; (b) $q_1 = 23$, $q_2 = 17$ and q_3 is in the range [1,70]; (c) $q_1 = 21$, $q_2 = 12$ and q_3 is in the range [1,30].

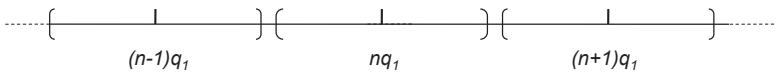

Figure 5.2: The effect of quantization and dequantization for coefficient q_1.

outcome reported in Fig. 5.1(c) is obtained. Without additional information about the input image, a wrong estimation could be performed ($q_1 = 28$ in this case).

When $q_3 = q_2$, the error function (5.2) is equal to 0. This motivates the absolute minima found in the previous examples.
Since we saw that obtaining a reliable q_1 estimation from (5.2) is a difficult task (too many cases have to be considered), we developed an alternative strategy which comprises a new error function:

$$f'_e(y^{(0)}_{i,j}, q_1, q_2, q_3) = \left| \left[\left[\left[\left[\frac{y^{(0)}_{i,j}}{q_1} \right] \times \frac{q_1}{q_2} \right] \times \frac{q_2}{q_3} \right] \times \frac{q_3}{q_2} \right] \times q_2 - \left[\left[\frac{y^{(0)}_{i,j}}{q_1} \right] \times \frac{q_1}{q_2} \right] \times q_2 \right| \quad (5.3)$$

To properly understand the rationale of (5.3), especially when $q_3 = q_1$, we have to better analyze the effect of a single quantization and dequantization step. If we examine the behavior of the following function:

$$\widehat{c} = \left| \frac{c}{q} \right| \times q \quad (5.4)$$

where c is an integer, we can note that if q is odd all integer numbers in $[nq - \lfloor \frac{q}{2} \rfloor, nq + \lfloor \frac{q}{2} \rfloor]$[4] [5] will be mapped in nq (with n a generic integer number). If q is even it maps in

[4] $\lfloor . \rfloor$ indicates the *floor* function
[5] in this and other cases, since [.] isn't within an expression, it indicates an interval

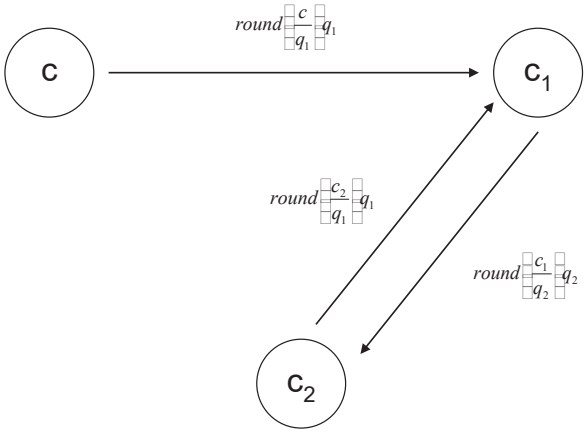

Figure 5.3: Scheme describing the effect of three quantization and dequantization with quantization steps q_1, q_2 and $q_3 = q_1$.

nq all the integer numbers in $[nq - \frac{q}{2}, nq + \frac{q}{2} - 1]$. From now on, in both cases, we call this range *range related* to nq.
The behaviour just described has been already pointed out in Sect. 3.4.1 and sketched in Fig. 3.15, in case of q even. As a consequence, we can say that (5.4) "groups" all integer numbers of its domain in multiples of q. We also observe that the maximum distance between a generic coefficient c and the corresponding $\widehat{c}$, obtained by the quantization and dequantization process, is $\frac{q}{2}$ if c is even, $\lfloor \frac{q}{2} \rfloor$ if c is odd.
Based on the above observation, analyzing three quantizations applied in sequence, with $q_2 < q_1$ and $q_3 = q_1$, like in the following:

$$\left[\left[\left[\frac{c}{q_1}\right] \times \frac{q_1}{q_2}\right] \times \frac{q_2}{q_1}\right] \times q_1 \tag{5.5}$$

we can observe this evolution:

- $c_1 = \left[\frac{c}{q_1}\right] \times q_1$ for the above observations leads to the situation shown in Fig. 5.2;
- $c_2 = \left[\frac{c_1}{q_2}\right] \times q_2$ maps multiples of q_1 in multiples of q_2. It is worth noting that, being $q_2 < q_1$, a generic nq_1 will be mapped in a multiple of q_2 (for example mq_2) whose distance from nq_1 will be less than or equal to $\frac{q_2}{2}$ (or $\lfloor \frac{q_2}{2} \rfloor$) if q_2 is odd), then in the range related to nq_1;
- at this point, $\left[\frac{c_2}{q_1}\right] \times q_1$ maps c_2 in nq_1 again, since as already pointed out, c_2 is in the range related to nq_1.

With the three steps above, we demonstrated that (see Fig. 5.3):

$$\left[\left[\left[\frac{c}{q_1}\right] \times \frac{q_1}{q_2}\right] \times \frac{q_2}{q_1}\right] \times q_1 = \left[\frac{c}{q_1}\right] \times q_1 \tag{5.6}$$

Therefore the error function in (5.3) is 0 when $q_3 = q_1$ regardless the c value. It is worth noting that in real conditions, due to rounding and truncation to eight bit integers, (5.3) is close to zero but not zero in $q_3 = q_1$. This can lead to the presence of multiple minima (a situation similar to the one exposed in Fig. 5.1(c)) and such behavior can be source of confusion and misunderstandments. This issue bring us to develop the following algorithm, detailed below for a generic frequency position $f_j \in [1, 2, ..., 64]$:

- from a double quantized image I_{DQ}, the DCT coefficients c_{DQ} are extracted.
- a set of candidate to be the right value of q_1 (C_{f_j}) is collected by simply considering (5.3) and selecting the strongest minima with the lowest values.
- by performing a proper cropping of the double compressed image, as proposed in [117], an estimation of the original DCT coefficients ($\widehat{c_{f_j}}$) is obtained.
- the above coefficients are used as input of a double compression procedure where the first quantization is performed by using a constant matrix with values from C_{f_j}, and the second one by simply using the already known values of the second quantization coefficients ($q_{2_{f_j}}$ values are present in the header data). At the end of this step a set of double quantized images are obtained ($I_{DQ_i},\ i \in [1, ..., |C_{f_j}|]$) related to the different first quantization candidates.
- equation (5.3) is computed for each candidate image I_{DQ_i} and the output is compared to the one obtained from I_{DQ} by simply using the mean absolute distance.
- the $\widehat{q_{1_{f_j}}}$ related to the closest image (with regard to the above defined distance) is selected as the correct one.

In order to prove the effectiveness of the proposed approach, several tests and comparisons have been performed. A first test has been conducted considering artificial data. Specifically, a random vector of 5000 elements has been built by using a uniform distribution in the range [-1023,1023]. The range corresponds to an input image within the range [0,255] in the spatial domain. Indeed, the output of the DCT transform, as it is defined, is three bits wider of the input bit depth and it is centered in zero. These simulated DCT coefficients are then used as input of the error function we proposed (5.3) by considering several pairs of quantization coefficients with $q_1 < q_2$. As can be easily seen from Figs. 5.4(a), 5.4(b) and 5.4(c), (5.3) has a global minimum (equal to zero) when $q_3 = q_1$. Moreover, q_1 value can be found in the range $q_3 \in]q_2, +\infty[$. It is worth noting that, sometimes, more than one local minimum can be found in the range $q_3 \in]q_2, +\infty[$. For example, this behavior can arise when q_1 is a multiple of q_2 (see Fig. 5.4(d)). However, even in this case, the correct q_1 value can be easily recovered. In fact, the additional minima are always between q_1 and q_2 and their positions depend on the common divisors between q_2 and q_3. Hence, in this case, q_1 is a multiple of q_2, the correct value is the maximum one.

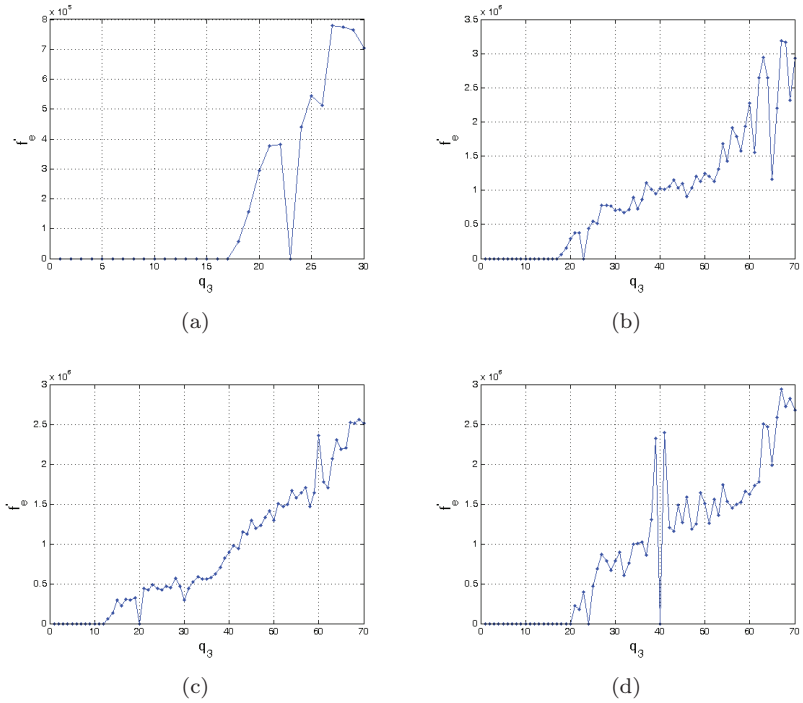

Figure 5.4: Examples of the error function values vs q_3, computed by using the proposed solution (5.3): (a) $q_1 = 23$, $q_2 = 17$ and q_3 is in the range [1,30]; (b) $q_1 = 23$, $q_2 = 17$ and q_3 is in the range [1,70]; (c) $q_1 = 20$, $q_2 = 12$ and q_3 is in the range [1,70]; $q_1 = 24$, $q_2 = 20$ and q_3 is in the range [1,70].

To further assess the performance of our approach, several tests have been conducted considering real doubly compressed images. We built up our dataset starting from a set of 24 uncompressed images from [43], that we double-compress using JPEG encoding functions provided by Matlab[36] considering quality factors (QF_1, QF_2) in the range from 50 to 100 at step of 10. Taking into account the condition $q_1 > q_2$ (i.e., $QF_1 < QF_2$), the final dataset contains 360 images. Tables in Fig. 5.5 report the average percentage of erroneously estimated q_1 values at varying of quality factor relative to the first 3, 6, 10 and 15 DCT coefficients. These values have been averaged over all images of our dataset, and the coefficients were considered in the usual zig-zag order exposed in Fig. 3.3. As expected, better results are usually obtained for higher QF_1 and QF_2 values corresponding to lower quantization, since the amount of data different from 0 is higher. Further analyses have been conducted in order to study the performance of the proposed approach with respect to the specific DCT coefficient. In Fig. 5.6 is reported the average percentage of erroneously estimated q_1 values at varying of the DCT coefficient (from low to high frequencies). These values are obtained averaging over all (QF_1,QF_2). As expected, the performance of the proposed solution degrades with DCT coefficients corresponding to high frequencies. To properly test the goodness

		QF_2				
		60	70	80	90	100
QF1	50	1,39%	0,00%	0,00%	0,00%	0,00%
	60		1,39%	1,39%	0,00%	0,00%
	70			0,00%	0,00%	0,00%
	80				1,39%	0,00%
	90					0,00%

(a)

		QF_2				
		60	70	80	90	100
QF1	50	2,08%	0,00%	0,00%	0,00%	0,00%
	60		4,17%	1,39%	0,00%	0,00%
	70			0,00%	0,00%	0,00%
	80				0,69%	0,00%
	90					0,00%

(b)

		QF_2				
		60	70	80	90	100
QF1	50	7,92%	0,00%	0,00%	0,00%	0,00%
	60		10,42%	10,42%	0,00%	0,00%
	70			0,00%	0,00%	0,00%
	80				0,42%	0,00%
	90					0,00%

(c)

		QF_2				
		60	70	80	90	100
QF1	50	19,44%	12,78%	0,56%	2.22%	5,83%
	60		24,17%	14,44%	0,00%	0,00%
	70			1,67%	0,00%	0,00%
	80				0,28%	0,00%
	90					0,00%

(d)

Figure 5.5: Percentage of erroneously estimated q_1 values at varying of quality factor (QF_1, QF_2) relative to the: (a) first 3 DCT coefficients, (b) first 6 DCT coefficients, (c) first 10 DCT coefficients, and (d) first 15 DCT coefficients, all related to the zig-zag order indicated in Fig. 3.3

of the proposed approach, we compared it with the method proposed in [79], where (5.2) is proposed instead of (5.3). As can be easily seen from Fig. 5.6, the proposed approach provides satisfactory results outperforming the older one.

5.2 First QSE extraction by histograms analysis

As already described in the introductory part of Sect. 4, and showed afterwards in Fig 4.1, double quantization introduces artefacts in the DCT coefficient histograms, that can be exploited to recover the FQS q_1 (q_2 is already present in the header). In more detail, considering as an example the image I (from [43]) and the corresponding histogram of a generic AC coefficient $x_{i,j}^{(0)}$, the histograms h_{DQi} obtained applying a double compression with several q_{1i} and a given q_2 are different and present predictable sequences (pattern) of zero (not zero) values as depicted in Fig. 5.7.
In consideration of what above exposed, since double JPEG compression modifies the histograms of the DCT coefficients depending on both first and second quantization factor (q_1 and q_2), the sequence of zero (and not zero) values of the histogram related to a double compressed image I_{DQ} provides useful information for the estimation of the first quantization factor q_1. Starting from the same initial distribution of DCT coefficients c_i, different histograms have been generated just considering several values of q_{1i} followed by a further quantization with q_2.
In this section we expose a method whose goal is the determination of first JPEG quantization coefficients (also in this approach, the initial hypothesis is that the second quantization factor is lower than the first one). The proposed solution analyses histograms of quantized DCT coefficients of double compressed JPEG images, exploiting their peculiarities. In particular, when the second compression is lighter than the first

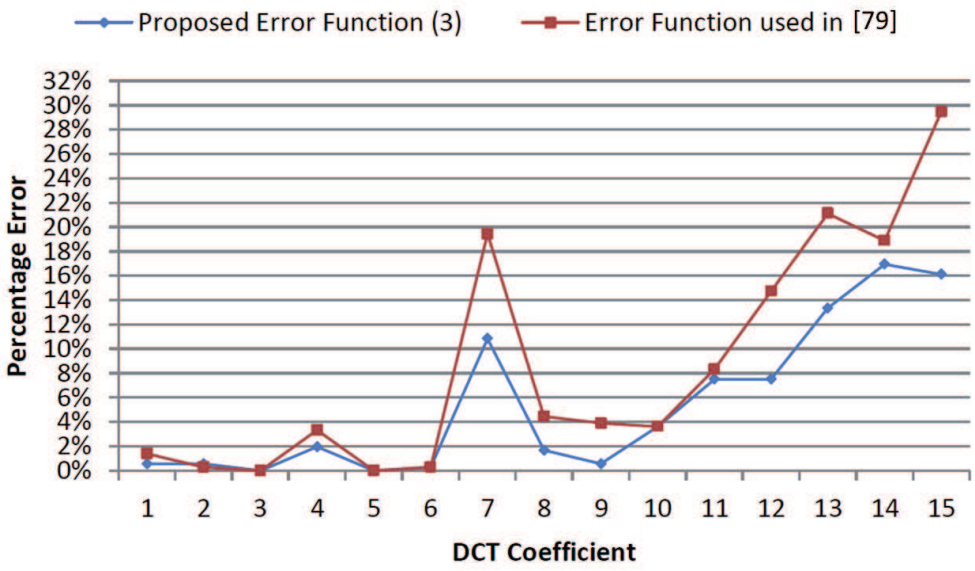

Figure 5.6: Percentage of erroneously estimated q_1 values at varying of DCT coefficient position (zig-zag scanning) considering the proposed error function (5.3) and the one presented in [79]. These values are obtained averaging over all (QF_1,QF_2) and images [43].

one we will see that it is possible to retrieve a pool of possible candidates for the first quantization factor making use of a proper simulation of the double compressed coefficient distribution with different first quantization values. This method can be used as stand-alone module (just to detect forgeries) or combined with other ones.
The overall schema of the algorithm is reported in Fig. 5.8, and it's composed by two main steps, executed for a generic frequency position $j \in [1, 2, ..., 64]$.
The first of them exploits a binary representation based on the pattern of zero (and not zero) values of the histograms to perform a first selection of a pool of q_1 candidates. Specifically, considered a wide range of initial possible values ($q_1 \in [q_{2+1}, ..., q_{max}]$), such selection method provides just a few candidates in the following way:

- from a double quantized image I_{DQ}, the DCT coefficients c_{DQ} are extracted;
- the histogram of the absolute value of DCT coefficient c_{f_j} is computed and refined, filtering out some unreliable values by simple trying to preserve the monotonicity of the distribution (this is applied only to AC coefficient usually characterized by Laplace distribution, as already exposed in Sect. 3.3.3);
- the histogram of the DC coefficient is filtered according to a threshold depending on the mean value of all not null bins;
- a binary vector is computed just considering the sequence of zero and not zero values of the filtered histogram;

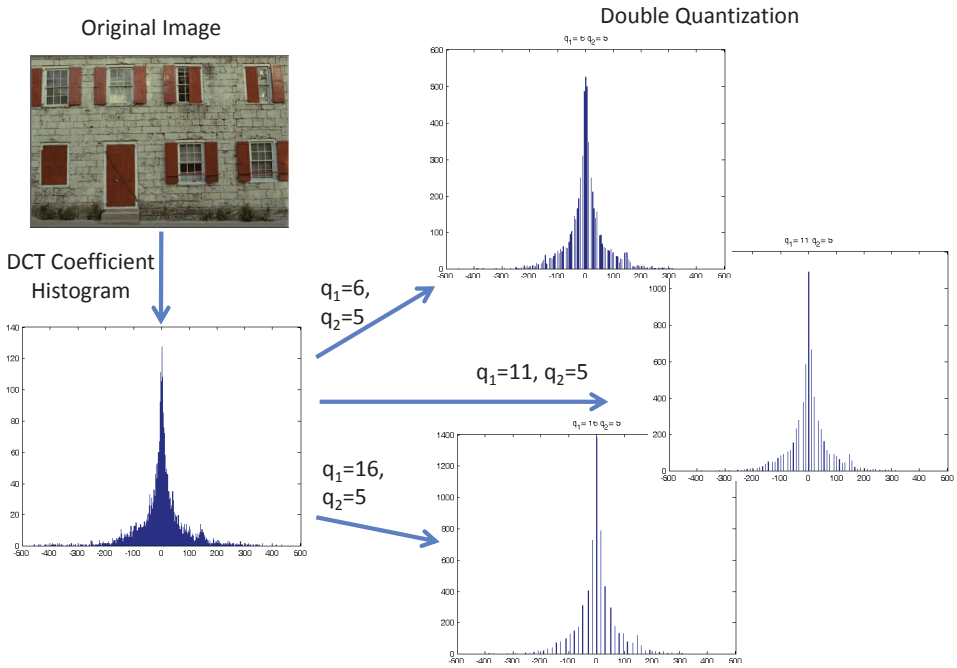

Figure 5.7: Examples of DCT coefficient histograms relative to double quantized images. Specifically, an image I taken from [43] has been double compressed with several q_{1i} and a fixed q_2. The final histograms show several differences and their analysis can be useful to recover compression history.

- a set of binary representation are then built for each $q_{1i_{f_j}}$ value exploiting information coming from the input (double compressed) image I_{DQ}. Specifically, as already proposed in [117], by performing a proper cropping of the double compressed image, an estimation of the original DCT coefficients can be obtained $(\widehat{c_{f_j}})$;
- the coefficients are then used as input of a double compression procedure where the first quantization is performed by using $q_{1i_{f_j}}$ and the second one by simply using the already known values of the second quantization steps. To better mimic double JPEG compression, some additional Gaussian noise [58] is added before the second quantization step;
- double quantized histograms are then refined to remove unreliable bins (trying to preserve the monotonicity of the distribution) and the binary representation is generated;
- based on the similarity between the generated representations and the one of the I_{DQ}, a set of $q_{1i_{f_j}}$ candidates are then selected (C_{f_j}). In particular for each $q_{1i_{f_j}}$

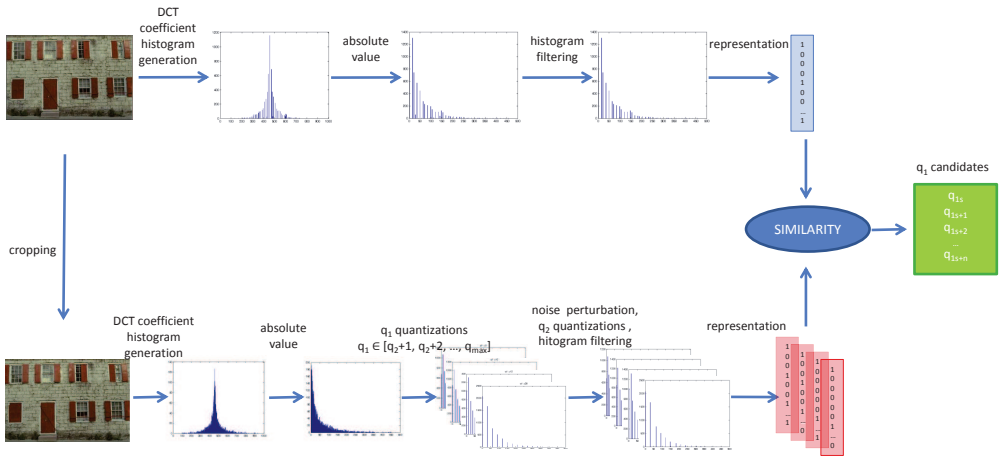

Figure 5.8: Candidate selection strategy. Starting form a wide set of q_1 candidates the proposed algorithm, by proper analyzing histogram properties, selects a short list of elements.

the sequence of zero (not zero) values represented as a binary sequence is compared by using the following similarity function:

$$F_s = \sum_{i=1}^{N}(B_{real}(i) * B_{sim}(i)) - \sum_{i=1}^{N}(B_{real}(i) \oplus B_{sim}(i)) \tag{5.7}$$

where B_{real} and B_{sim} are the N-bin binary representations related to the original input image I_{DQ} and the one corresponding to the simulated double compression respectively. Moreover $*$ and $\oplus$ represent logical AND and XOR operators.

In the latter and last step, devoted to estimate the correct q_1 from the candidate set, the whole histogram information is used instead of considering only the binary representation. Specifically, the refined histograms $H_{q_{1s}}$ related to the simulated double quantization with $q_{1s} \in C_{f_j}$ are compared with H_{real} obtained from I_{DQ} and the closest one is selected as follows:

$$\widehat{q_{1f_j}} = \min_{q_{1s} \in C_{f_j}} \sum_{i=1}^{N} \min(max_{diff}, |H_{real}(i) - H_{q_{1s}}(i)|) \tag{5.8}$$

where N is the number of bins of the histograms and max_{diff} is a threshold used to limit the contribution of a single difference in the overall distance computation. In order to prove the effectiveness of the proposed approach, several tests and comparisons have been performed considering real double compressed images[43], by using JPEG encoding functions provided by Matlab[36], a dataset of double compressed images has been built just considering quality factors (QF_1, QF_2) in the range 50 to 100 at step of 10. Taking into account the condition $q_1 > q_2$, the final dataset contains 360 images. All the tests have been performed with the same parameter setting (experimentally found). Specifically, the selection procedure (see Fig. 5.8) considers the best 8 candidates with

		QF2				
		60	70	80	90	100
QF1	50	0,00%	0,00%	0,00%	0,00%	0,00%
	60		0,00%	0,00%	0,00%	0,00%
	70			0,00%	0,00%	0,00%
	80				0,00%	0,00%
	90					0,00%

(a)

		QF2				
		60	70	80	90	100
QF1	50	1,39%	0.69%	0,00%	0,00%	0,00%
	60		0,00%	0.69%	0,00%	0,00%
	70			0,00%	0,00%	0,00%
	80				0,00%	0,00%
	90					0,00%

(b)

		QF2				
		60	70	80	90	100
QF1	50	2,08%	4,58%	0,00%	0,00%	0,00%
	60		1,25%	2,92%	0,00%	0,00%
	70			0,00%	0,00%	0,00%
	80				0,69%	0,00%
	90					0,00%

(c)

		QF2				
		60	70	80	90	100
QF1	50	4,44%	7,78%	1,94%	1,11%	0,00%
	60		5,56%	8,06%	0,28%	0,00%
	70			0,00%	0,28%	0,00%
	80				0,00%	0,00%
	90					0,00%

(d)

Figure 5.9: Percentage of erroneously estimated q_1 values at varying of quality factor (QF_1, QF_2) relative to the: (a) first 3 DCT coefficients, (b) first 6 DCT coefficients, (c) first 10 DCT coefficients, and (d) first 15 DCT coefficients, all related to the zig-zag order indicated in Fig. 3.3

respect to the similarity function (5.7). Moreover, q_{max} and max_{diff} have been set to 30 and 50 respectively. Tables in Fig. 5.9 report the average percentage of erroneously estimated q_1 values at varying of quality factor relative to the first 3, 6, 10 and 15 DCT coefficients. These values have been averaged over all images [43]. The coefficients were considered in zig-zag order that, as explained in Sect. 3.2 is used in JPEG standard to sort the coefficients from the lowest frequency (DC) to the highest frequencies in a 1D vector. As expected, better results are usually obtained for higher QF_1 and QF_2 quality factor corresponding to lower quantization. Further analyses have been conducted in order to study the performance of the proposed approach with respect to each specific DCT coefficient. In Fig. 5.11 is reported the average percentage of erroneously estimated q_1 values at varying of the DCT coefficient (from low to high frequencies). These values are obtained averaging over all (QF_1,QF_2). As expected the performance of the proposed solution degrades with DCT coefficients corresponding to highest frequencies. In Fig. 5.10 is highlighted the improvement obtained with the present approach compared to the one exposed in Sect. 5.1. To further assess the effectiveness of the proposed approach, a comparison with two state of the art techniques has been performed, by selecting a methods based upon histogram comparisons [117] and one exploiting multiple DCT coefficient compression properties [79].

5.3 A new QSE approach together with an improved histogram filtering strategy

Although the proof of concept of the proposed approach has been partially presented in Sect. 5.1, in the present work we have improved that algorithm, including a modified version of the histogram filtering strategy proposed in Sect. 5.2.

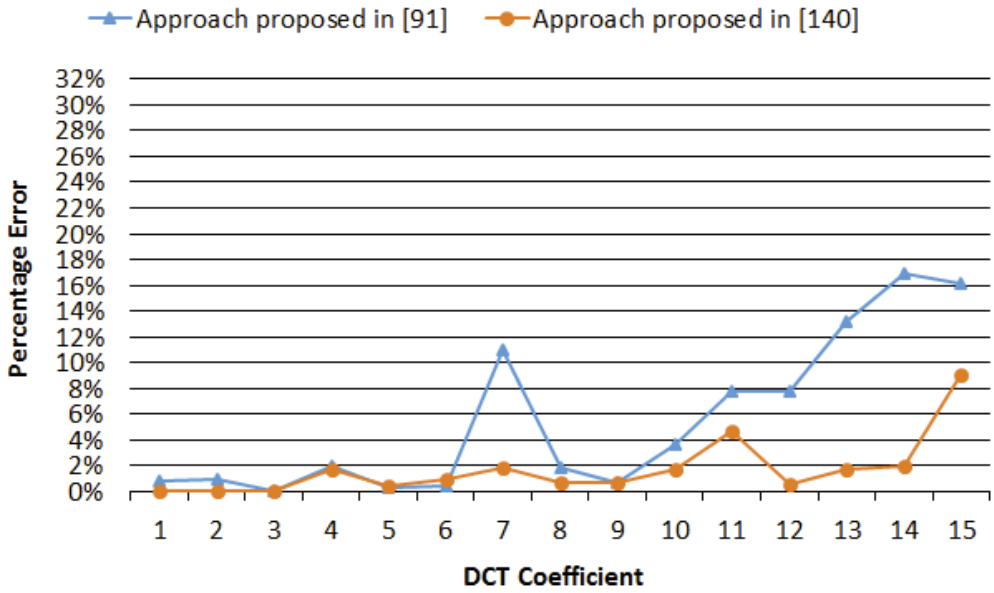

Figure 5.10: Comparison between the results of the method exposed in Sect. 5.1 and the ones of the approach given in Sect.5.2

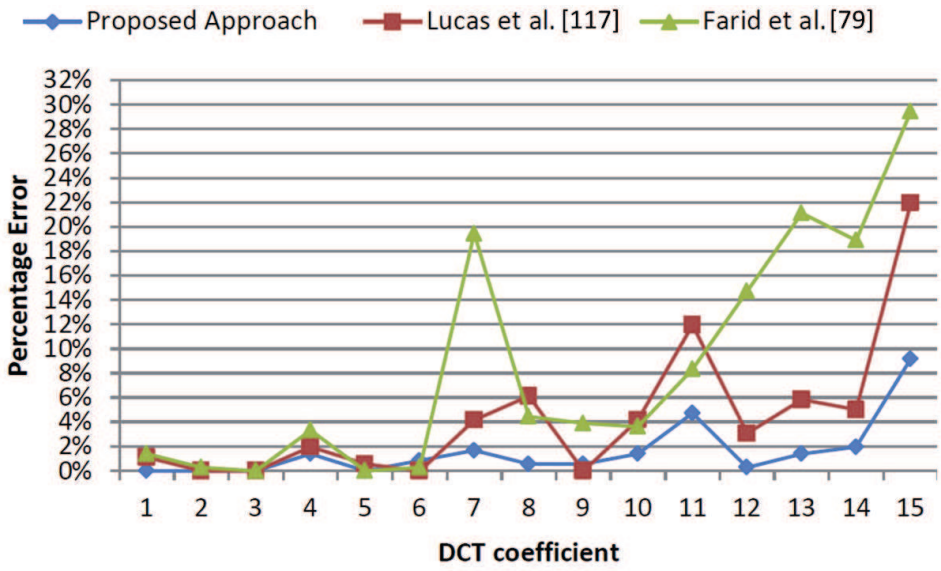

Figure 5.11: Percentage of erroneously estimated q_1 values at varying of DCT coefficient position considering the proposed approach and state of the art methods ([117], [79]). These values are obtained averaging over all (QF_1,QF_2) and images [43].

In the following analysis, only 8-bit grayscale images are considered. For sake of simplicity, considering a single DCT coefficient $y_{i,j}^{(0)}$ and the related quantization steps q_1

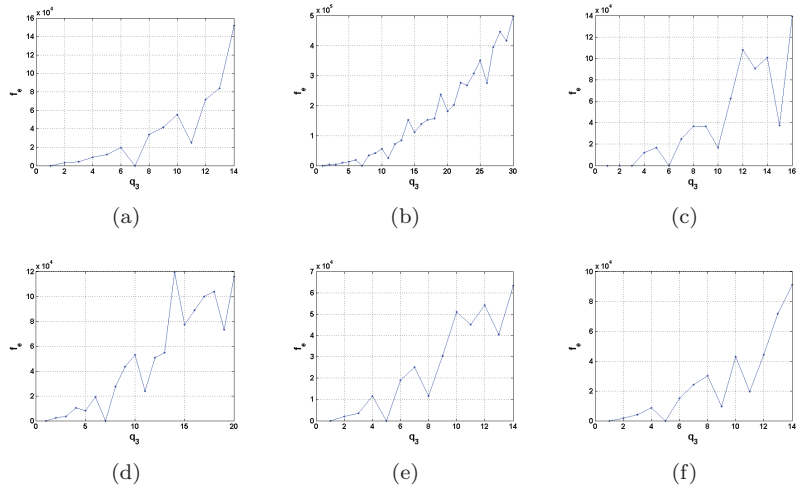

Figure 5.12: In the upper row three examples of the error function values (4.5) for an image of the same dataset used in [43], with respect to q_3 for the DC term: (a) $q_1 = 11$, $q_2 = 7$ and $q_3 \in \{1, 2, \ldots, 14\}$; (b) $q_1 = 11$, $q_2 = 7$ and $q_3 \in \{1, 2, \ldots, 30\}$; (c) $q_1 = 10$, $q_2 = 6$ and $q_3 \in \{1, 2, \ldots, 16\}$. In the lower row three examples of values obtained by (4.5) for the same image, with respect to q_3 for some AC term: (d) (1,0) term, $q_1 = 11$, $q_2 = 7$ and $q_3 \in \{1, 2, \ldots, 20\}$; (e) (2,0) term, $q_1 = 8$, $q_2 = 5$ and $q_3 \in \{1, 2, \ldots, 14\}$; (f) (3,0) term, $q_1 = 9$, $q_2 = 5$ and $q_3 \in \{1, 2, \ldots, 14\}$.

(first quantization) and q_2 (second quantization), the value of each coefficient after a double compression can be modeled as:

$$y_{i,j}^{(2)} = \left[\left(\left[\frac{y_{i,j}^{(0)}}{q_1} \right] q_1 + e \right) \frac{1}{q_2} \right] \tag{5.9}$$

where, unlike from the notation used in (5.1), we added the term e to represent the error introduced by several operations, such as color conversions (YCbCr to RGB and vice versa), rounding and truncation of the values to eight bit integers, etc. It is important to note that the errors above can be due to some processing in different domains (e.g., spatial domain). As described in the above sections, the function proposed in [79] is not able to work in real conditions. The main reason is that it doesn't take into account the noise error e of Eq. (5.9). Considering then a real scenario, a method able to cope with the aforementioned problems has been built. Specifically, as shown in Fig. 5.13 the proposed approach consists of the following main steps:

- DCT Histogram Filtering: A deep analysis on the consequences of both quantization and rounding error has been performed. While indeed the former is well known, the rounding error e in Eq. (5.9) manifests itself as peaks spread around the multiples of the quantization step q, as exposed in [118], and has been modeled as an approximate Gaussian noise (see Sect. 3.4.2). As we will explain in more detail later, these joint phenomenons will affect the behavior of the second

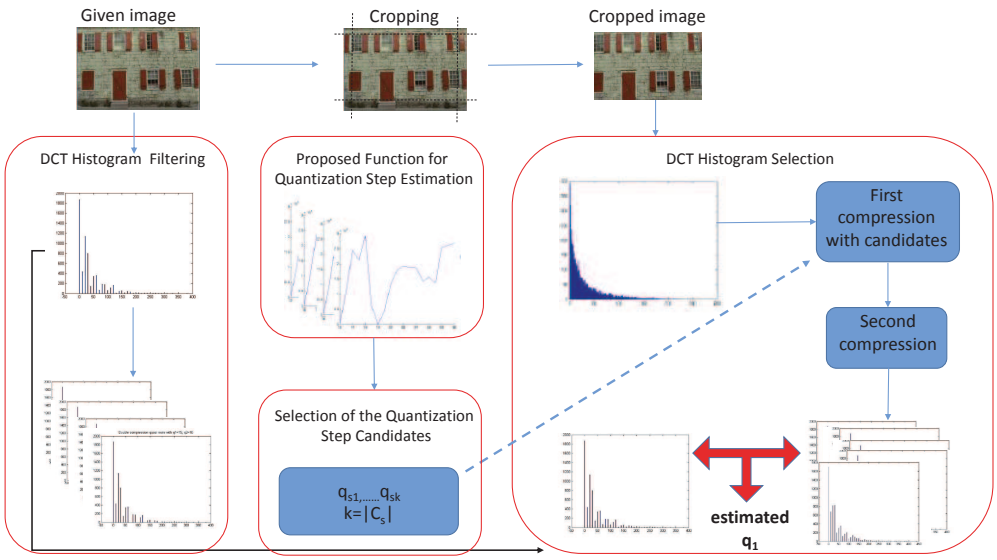

Figure 5.13: Proposed approach scheme. Starting from an image I, exploiting the effects of successive quantizations, it estimates the quantization steps of the first quantization q_1. First, the histogram of the absolute value of DCT coefficients is filtered, then a proper function able to detect the first quantization step is evaluated and a set of candidates is selected. Later, considering the DCT coefficients related to a cropped version of the original image, the double quantization is simulated with the candidates previously computed. Finally, comparing the histogram of the original image with the simulated ones the first quantization step q_1 is estimated.

quantization step, thus the magnitude of the DCT coefficients, and consequently its statistics. The filtering must then face two kind of noise: the "split noise" and the "residual noise", with the aim to bring the histogram as if the rounding error did not have impact. This module actually provides a set of filtered histograms $H_{filt_{q_{1i}}}$ (one for each quantization step $q_{1i} \in \{q_{1min}, q_{1min}+1, \ldots, q_{1max}\}$).

- Proposed Function for Quantization Step Estimation: once the histogram has been filtered, removing (or reducing) the error e, the error function exploited in Sect. 5.1 is actually evaluated over all the histograms $H_{filt_{q_{1i}}}$, generating a set of output $f_{out_{q_{1i}}}$.

- Selection of the Quantization Step Candidates: starting from the set of output $f_{out_{q_{1i}}}$, a limited number of first quantization candidates ($q_{1s} \in C_s$) is selected exploiting the q_1 localization property of the proposed error function.

- DCT Histogram Based Selection: the previous modules actually provide a series of q_1 candidates to be considered for further evaluations. The double quantization process is then simulated to consider the candidates provided by the other blocks and the best one exploiting directly histogram values is finally selected.

The above mentioned steps are detailed in the following subsections.

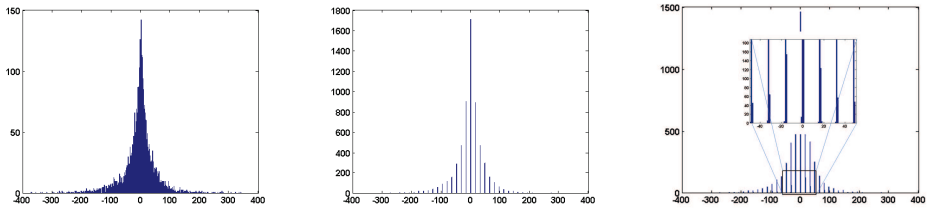

(a) (b) (c)

Figure 5.14: Real DCT coefficient histograms: (a) histogram related to the original image, (b) histogram related to the single compressed image, (c) histogram related to the DCT coefficients just before the second quantization (color conversions, rounding and truncation of the values to eight bit integers have been already performed). A detail was also overimposed for better visualization of the error e of Eq. (5.9).

5.3.1 DCT Histogram Filtering

Exploiting the effects of successive quantizations followed by dequantizations without considering the error factor e in Eq. (5.9), allows to easily manipulate the involved equations, but the performances of these approaches considerably degrades when real cases are considered. To cope with this problem, a deep analysis of the properties of this source of error has been performed. As explained before, it is introduced by several operations, such as color conversions (YCbCr to RGB and vice versa), rounding and truncation of the values to eight bit integers, etc. An example of real DCT coefficient histograms is reported in Fig. 5.14. The histogram depicted in Fig. 5.14(c) actually shows the DCT coefficient distribution just before the application of the second quantization. Once the image is compressed again, several scenarios can arise depending on the values of the first and second quantization steps. A typical scenario is the one reported in Fig. 5.15(a) and Fig. 5.15(c) where only a small perturbation (i.e., elements in a wrong bin) is propagated in the final histogram. On the contrary, in some specific conditions related to the q_1 and q_2 values a worst scenario can arise. As shown in Fig. 5.15(b) and Fig. 5.15(d) the original information can be quite equally split into two neighboring bins where one of them is a wrong one. This undesirable situation appears when a bin of the first quantization (i.e., in position mq_1) is situated exactly halfway between two consecutive bins coming from the second quantization (i.e., in position nq_2 and $(n+1)q_2$). Specifically, this effect arises when two consecutive multiples of q_2 are related to a generic multiple of q_1 as follows:

$$mq_1 = \frac{nq_2 + (n+1)q_2}{2}, \qquad n, m \in \mathbb{N}^+ \tag{5.10}$$

This behavior should be then taken into account in the design of algorithms aiming to exploit the effects of double quantizations. To properly cope with the noise e in Eq. (5.9) a filtering strategy has been developed. We have designed an approach based on two steps (see Fig. 5.16): the first one is devoted to filter the "split noise" (i.e., the one shown in Fig. 5.15(d)), whereas the second one deals with the residual noise

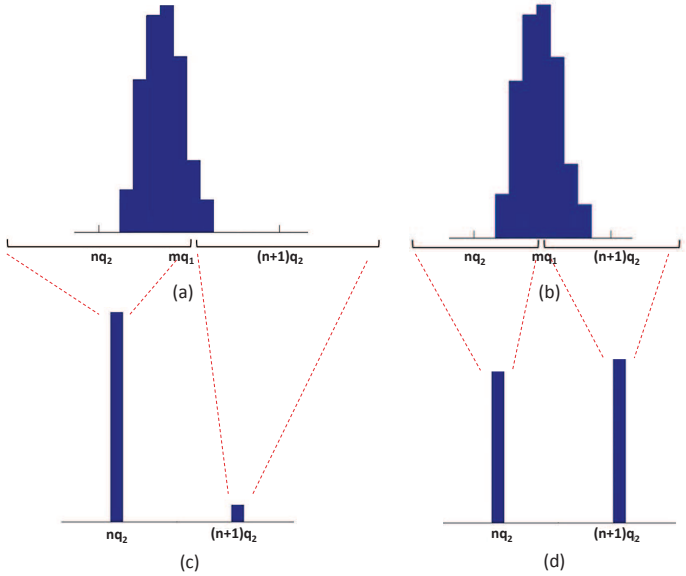

Figure 5.15: Depending on the values of the first and the second quantization values different situations can arise. Specifically, the effect of the error e in the final histogram can be limited (c) or difficult to deal with (d).

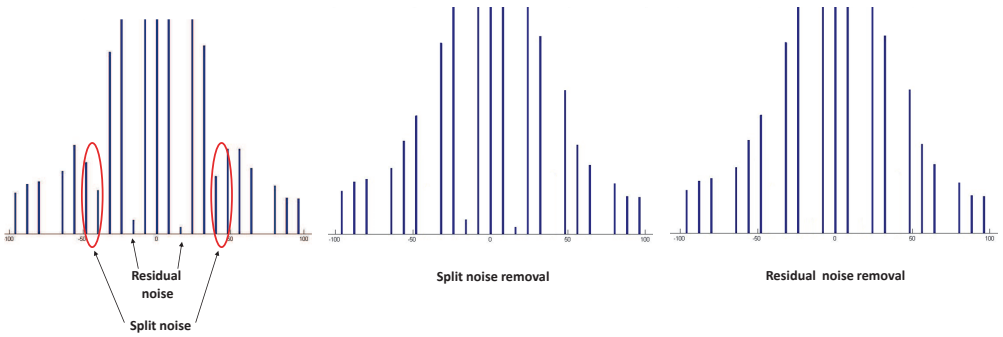

Figure 5.16: Example of histogram filtering. First wrong bins on the second quantization histogram are detected by using the Eq. (5.10) and then they are moved to the correct locations. Later, the residual error is removed exploiting the monotonicity of the DCT coefficient distribution (see Algorithm 1).

(Fig. 5.15(c)). Considering a specific pair of quantization steps q_1 and q_2 we design a filtering strategy that first detects the wrong bins on the second quantization histogram by using the Eq. (5.10) and then moves bin elements from the wrong to the correct ones. It is worth noting that the correct q_1 value is actually unknown and its estimation is the aim of the proposed approach. Several filtering are then performed considering a set of first quantization steps in the range $q_{1i} \in \{q_{1min}, q_{1min}+1, \ldots, q_{1max}\}$. The

Algorithm 1: AC coefficients histogram filtering

Input:
H_{in}: input histogram of absolute values of DCT coefficients
N_{bins}: number of bins of H_{in}
Th_{filt}: threshold used to measure the similarity between bins
Output:
H_{filt}: filtered histogram
begin
  $H_{tmp} = H_{in}$
  $i_{max_{old}} = 1$
  while $i_{max_{old}} != N_{bins}$ **do**
    $[v_{max}, i_{max}] = max(H_{tmp})$
    for $i = i_{max_{old}} + 1$ **to** $i_{max} - 1$ **do**
      $v_{curr} = H_{in}[i]$
      if $v_{curr} > v_{max} \cdot Th_{filt}$ **then**
        $H_{filt}[i] = v_{curr}$
      else
        $H_{filt}[i] = 0$
      $H_{tmp}[i] = -1$
    $H_{tmp}[i_{max}] = -1$
    $H_{filt}[i_{max}] = H_{in}[i_{max}]$
    $i_{max_{old}} = i_{max}$

actual selection of the correct value will be performed later (see section 5.3.3) employing further analyses and tests. Once the "split filter" has been performed, the residual noise is taken into account to remove further impurities (Fig. 5.14). Specifically, a filtering strategy based on the preservation of the monotonicity of the DCT coefficient distribution is employed (see Algorithm 1). As already exposed in Sect. 3.3.3, AC coefficients are usually characterized by Laplace distribution. Initially, the histogram of absolute value of DCT coefficients is considered. Both bin index (i_{max}) and value (v_{max}) related to the maximum element of the histogram are then considered. All the values of the bins with index lower than i_{max} are compared with v_{max} and the ones below a certain relative threshold (Th_{filt}) are discarded. Once this filtering is performed, a novel interval of the histogram is considered again and the same algorithm is applied (search of the maximum, filtering, etc.).
This filtering works properly only for AC coefficients due to the monotonicity of their distribution. A different kind of filtering is then applied to DC coefficients. Specifically, all the values below an adaptive threshold (e.g., the mean value) are simply discarded. Due to the "split filter", this filtering process provides to the following modules a series of filtered histograms $H_{filt_{q_{1i}}}$, one for each involved first quantization step $q_{1i} \in \{q_{1min}, q_{1min}+1, \ldots, q_{1max}\}$. Further details about the setting of the range of variation of q_{1i} will be provided in section 5.3.4.

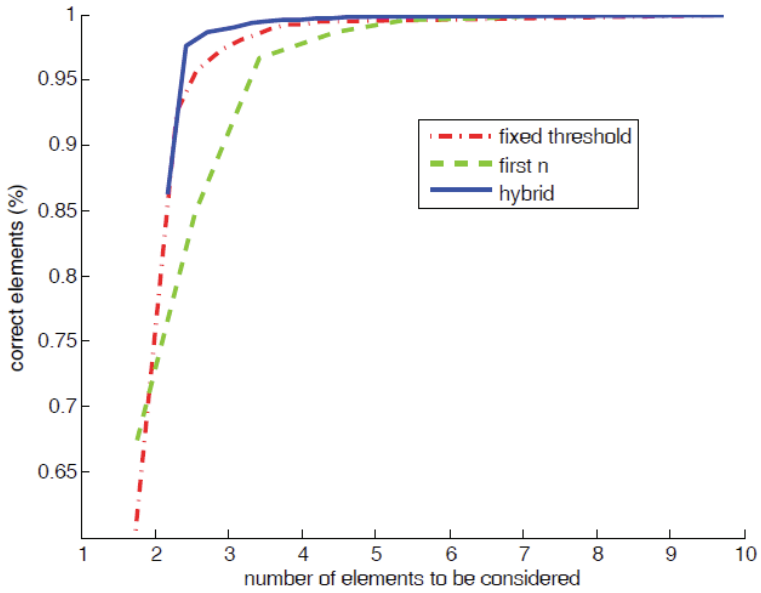

Figure 5.17: Percentage of first quantization steps correctly included into the candidate set with respect to the number of elements considered in the candidate set. These results have been computed considering the three considered strategies at varying of their parameters (T_{fix}; n; T_{fix_h}) and have been obtained as average over all frequencies (the first 15 DCT coefficients in zig-zag order) and considered images.

5.3.2 Selection of the Quantization Step Candidates

As described in a previous subsection, due to the split filtering, the information related to the original histogram of a specific DCT frequency is tested considering different hypotheses related to the first quantization steps $q_{1i} \in \{q_{1min}, q_{1min}+1, \ldots, q_{1max}\}$. Each function $f_{out_{q_{1i}}}$ is then related to a specific q_{1i} value. The main idea, allowing us selecting a limited set of first quantization candidates, is related to the properties of the proposed error function (5.3).
Whenever the filtering is performed with the correct first quantization step, $f_{out_{q_{1i}}}$ is close to zero when $q_3 = q_{1i}$. On the contrary, when the first quantization is not the correct one, this property usually is not verified. This behavior allows to design a simple strategy of candidate selection. Specifically, considering a single DCT frequency, each $f_{out_{q_{1i}}}$ is evaluated in $q_3 = q_{1i}$ (where q_{1i} is the first quantization step related to the $f_{out_{q_{1i}}}$). If this value is close to zero (i.e., less than a threshold T), it is added to the set of candidates C_s otherwise it is discarded. The final estimation is then performed among the limited set exploiting directly the histogram values as detailed in the following section. A crucial parameter that could impact the effectiveness of the proposed candidate selection strategy is the threshold T that determines the acceptance of the q_{1i} value. Choosing a low value, several correct elements could be lost (especially for higher DCT coefficients). On the other hand, higher values could include many

false candidates that degrade the effectiveness of the overall strategy. Moreover, the value of $f_{out_{q_{1i}}}$ when $q_3 = q_{1i}$ depends on many factors such as the DCT frequency under examination and the actual content of the input image. To properly tune this parameter a series of tests has been then performed, using images taken from [43]. Double compression has been then performed by using standard JPEG encoding, and a dataset of double compressed images have been built just considering quality factors (QF_1, QF_2) in the range 50 to 100 at steps of 10. Taking into account the condition $q_1 > q_2$, the final dataset contains 360 images. Three different strategies have been compared:

- fixed threshold: a fixed threshold T_{fix} is selected without considering the dependency with respect to the frequency f_j and the content of the input histogram.
- first n: the values of $f_{out_{q_{1i}}}$ are sorted in increasing order. The n^{th} value is then retained as threshold.
- hybrid: the threshold is computed as the sum of the minimum value of $f_{out_{q_{1i}}}$ and a fixed threshold (T_{fix_h}).

Each strategy has been tested at varying of their involved parameters: $T_{fix} \in [100, 50000]$, $n \in [1, 8]$, $T_{fix_h} \in [100, 50000]$ The percentage of first quantization steps correctly included into the candidate set has been plot with respect to the number of elements considered in the candidate set (see Fig. 5.8). These results have been obtained considering the average with respect to the image number and the considered frequencies (the first 15 DCT coefficients in zig-zag order in our test). As can be easily seen from Fig. 5.17 the hybrid approach provides the best performances. It is able to cope better than the other strategies with the content of the specific histogram.

5.3.3 DCT Histogram Selection

The modules presented above actually provide a series of first quantization candidates that have to be considered for further evaluations. The DCT Histogram Selection step, exploiting directly the information related to the histogram values estimates the q_1 value. In order to select the correct first quantization step, we exploit information coming from the original double compressed image I_{DQ}. We start with the extraction of DCT coefficients c_{DQ}, followed by a rough estimation of the original DCT coefficients obtained through a proper cropping of the double compressed image, as already proposed in [117]. These coefficients are then used as input of a double compression procedure, where the first quantization is performed by using $q_{1s} \in C_s$ whereas the second one using the already known values of the second quantization step (q_2 values are present in the header data). To estimate the correct q_1 from the candidate set, the whole histogram information is exploited. Specifically, the histograms $H_{q_{1s}}$ related to the simulated double quantization with $q_{1s} \in C_s$ are compared with H_{real} obtained from I_{DQ}. The closest one is selected according to the following criterion:

$$\widehat{q_1} = \min_{q_{1s} \in C_s} \sum_{i=1}^{N} \min(max_{diff}, |H_{real}(i) - H_{q_{1s}}(i)|) \tag{5.11}$$

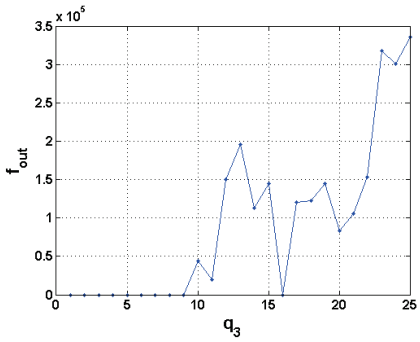

(a)

16	11	10	16	24	40	51	61
12	12	14	19	26	58	60	55
14	13	16	24	40	57	69	56
14	17	22	29	51	87	80	62
18	22	37	56	68	109	103	77
24	35	55	64	81	104	113	92
49	64	78	87	103	121	120	101
72	92	95	98	112	100	103	99

(b)

Figure 5.18: Criteria for the selection of the range $\{q_{1min}, q_{1min}+1, \ldots, q_{1max}\}$: (a) error function (5.3) for an AC term in case of $q_1 = 16$, $q_2 = 9$ and $q_3 \in \{1, 2, \ldots, 25\}$. We can note that, for every $q_3 \leq q_2$, the result is 0. (b) The compression matrix for $QF = 50$, according with the original JPEG standard. The first 15 terms considering the order used in the entropy coding of the JPEG algorithm are underlined. The maximum expected compression step is 24.

where N is the number of bins of the histograms and max_{diff} is a threshold used to limit the contribution of a single difference in the overall distance computation.

5.3.4 Definition of the Range of Variability of q_3

To properly set the range of variability of the third quantization step the outcome of Eq. (5.3) should be better analyzed.
Specifically, in case of $q_3 \leq q_2$, the proposed function is always equal to 0. Indeed in this situation, starting from bins located in multiples of q_2, $\left[\frac{c_2}{q_3}\right] q_3$ will drive the bins in multiples of q_3 that belong to the range related to nq_2. For this reason, the fourth quantization step with $q = q_2$ will drive again the bins in multiples of q_2. In Fig. 5.18 a) we can see an example of the behavior of Eq. (5.3) in case of $q_1 = 16$ and $q_2 = 9$. For this reason, we always consider $q_2 + 1$ as the term q_{1min}. The compression matrix defined by the IJG [164] for the quality factor 50 (the lower one considered in this work, i.e. the matrix with the higher quantization steps for every position) is the one showed in Fig. 5.18 b). Since we extended our study to its first 15 positions following the zig-zag order used in the JPEG algorithm during the entropy coding, the higher quantization step (in position (0,4)) is 24. For this reason, considering the need to visualize also the trend after this value, and what exposed in Sect. 3.3.2, we set q_{1max} to 30.

5.3.5 Experimental Results

To assess the performances of the proposed approach, several tests have been conducted considering real double compressed images taken from two different sources. A dataset of 110 uncompressed images has been collected considering different cameras (Canon D40, Canon D50 e Canon Mark3) with different resolutions. Moreover, a certain variability in terms of image content has been taken into account in the image acquisition.

The considered dataset (Canon D40D50MK3 Dataset from here on) contains: people, landscapes, coasts, mountains, animals, flowers, buildings, foods, bridges, trees, etc. A cropping of size 1024×1024 of the central part of each image has been then selected in order to speed up the tests.
Starting from the cropped images, applying JPEG encoding functions provided by Matlab[36] with standard JPEG quantization tables proposed by IJG (Independent JPEG Group) [34], a dataset of double compressed images ha been built just considering quality factors (QF_1, QF_2) in the range 50 to 100 at steps of 10. Taking into account the condition $q_1 > q_2$ (i.e., $QF_2 > QF_1$ in our tests), the final dataset contains 1650 images. Results are then reported with respect to quality factors instead of the specific quantization steps. This methodology simplifies the analysis of the results, since a single parameter (quality factor) describes a quantization matrix with 64 quantization steps usually having different values and related to different frequencies. As an example, the quantization matrix for $QF = 50$ is reported in Fig. 5.18(b).
Table 5.1 reports the average percentage of erroneously estimated q_1 values at varying of quality factor, relative to the first 15 DCT coefficients considered in zig-zag order. This order, used in the standard JPEG, allows sorting the coefficients from the lowest frequency (DC) to the highest frequencies in a 1D vector. The estimation error of the proposed approach is close to zero for the DCT coefficients related to low frequency in the DCT domain and does not significantly depend on the specific quality factor employed for the first and second quantization. On the contrary, for higher frequencies, the estimation error is strictly correlated with the quality factors. Specifically, better results are usually obtained for higher QF_1 and QF_2 values corresponding to lower quantization. Further analyses have been conducted in order to study the performance of the proposed approach with respect to the specific DCT coefficient. In Fig. 5.19 the percentage error in the estimation of q_1, at varying of the DCT coefficients from low to high frequencies, is reported. These errors are average values obtained considering all the combinations of (QF_1, QF_2) indicated in Table 5.1. As expected the performance of the proposed solution degrades with DCT coefficients corresponding to the highest frequencies. The proposed approach estimates with high accuracy the first 10 coefficients with an error usually lower than 2%. The estimation of the other DCT coefficients (higher than 10^{th}) is actually reliable only considering high QF_2 values. It is worth noting that the results related to some frequencies (4^{th}, 7^{th}, 11^{th}) seem to differ with respect to the trend of the curve error. This behavior depends on the cropping procedure employed in the DCT Histogram Selection step (see section 5.3.3). First quantization actually introduces blocking artifacts, especially if lower quality factor are employed, between blocks that cannot be removed by simple cropping and influences the frequency content of the image. Specifically, the frequencies of positions 4^{th}, 7^{th}, 11^{th} are related to horizontal and vertical edges and are pretty sensitive to the aforementioned kind of artifacts. The method has been compared with the algorithms proposed in [58, 91, 117]. Specifically, the original code (available online) related to Bianchi et al. [58], has been considered whereas the method based on the direct comparison of histograms described in [117] has been reimplemented. Finally, to further validate the effectiveness of the proposed function (5.3), the approach proposed in [91] has been considered by using Eq. (4.5) proposed in [80] instead of Eq. (5.3). All techniques have been tested considering the first quantization step in the range $[1, 30]$. Moreover, the following parameter setting

Table 5.1: Percentage of errously estimated q_1 values at varying of quality factor (QF_1, QF_2) relative to the first 15 DCT coefficients in zig-zag order. Every coefficient is indicated with respect to its position in the 8×8 image block.(0,0) is the DC term.

(0,0)	QF2 60	70	80	90	100
QF1 50	0,00%	0,00%	0,00%	0,00%	0,00%
60		0,91%	0,00%	0,00%	0,00%
70			0,91%	0,00%	0,91%
80				0,00%	0,00%
90					0,00%

(1,0)	QF2 60	70	80	90	100
QF1 50	0,00%	0,00%	0,00%	0,00%	0,00%
60		0,00%	0,00%	0,00%	0,00%
70			0,00%	0,00%	0,00%
80				0,00%	0,00%
90					0,00%

(2,0)	QF2 60	70	80	90	100
QF1 50	0,00%	0,00%	0,00%	0,00%	0,00%
60		1,82%	0,00%	0,00%	0,00%
70			0,00%	0,00%	0,00%
80				0,00%	0,00%
90					0,00%

(3,0)	QF2 60	70	80	90	100
QF1 50	1,82%	1,82%	0,00%	0,00%	0,00%
60		1,82%	1,82%	0,00%	0,00%
70			0,00%	0,00%	0,00%
80				0,00%	0,00%
90					0,00%

(4,0)	QF2 60	70	80	90	100
QF1 50	0,00%	0,00%	0,91%	0,00%	0,00%
60		0,00%	0,00%	0,00%	0,00%
70			0,00%	0,00%	0,00%
80				0,00%	0,00%
90					0,00%

(0,1)	QF2 60	70	80	90	100
QF1 50	0,00%	0,00%	0,00%	0,00%	0,91%
60		0,91%	0,00%	0,00%	0,00%
70			0,91%	0,00%	0,00%
80				0,00%	0,00%
90					0,00%

(1,1)	QF2 60	70	80	90	100
QF1 50	12,73%	16,36%	0,91%	0,00%	0,00%
60		1,82%	1,82%	0,00%	0,00%
70			0,00%	0,00%	0,00%
80				0,00%	0,00%
90					0,00%

(2,1)	QF2 60	70	80	90	100
QF1 50	2,73%	4,55%	0,00%	0,00%	0,00%
60		0,91%	0,91%	0,00%	0,00%
70			0,00%	0,00%	0,00%
80				0,00%	0,00%
90					0,00%

(3,1)	QF2 60	70	80	90	100
QF1 50	0,91%	0,91%	0,00%	0,91%	0,00%
60		0,91%	0,00%	0,00%	0,00%
70			0,00%	0,00%	0,00%
80				0,00%	0,00%
90					0,00%

(0,2)	QF2 60	70	80	90	100
QF1 50	3,64%	5,45%	0,00%	0,91%	0,00%
60		3,64%	2,73%	0,00%	0,00%
70			0,00%	0,00%	0,00%
80				0,00%	0,00%
90					0,00%

(1,2)	QF2 60	70	80	90	100
QF1 50	10,91%	58,18%	15,45%	3,64%	0,00%
60		6,36%	25,45%	0,91%	0,00%
70			10,00%	0,91%	0,00%
80				0,00%	0,00%
90					0,00%

(2,2)	QF2 60	70	80	90	100
QF1 50	14,55%	2,73%	54,55%	0,00%	0,00%
60		16,36%	10,91%	0,91%	0,00%
70			18,18%	0,00%	0,00%
80				0,00%	0,00%
90					0,00%

(0,3)	QF2 60	70	80	90	100
QF1 50	20,00%	22,73%	0,00%	3,64%	0,91%
60		1,82%	8,18%	1,82%	0,00%
70			0,00%	0,00%	0,00%
80				0,00%	0,00%
90					0,00%

(1,3)	QF2 60	70	80	90	100
QF1 50	12,73%	9,09%	19,09%	4,55%	0,00%
60		47,27%	7,27%	1,82%	0,00%
70			1,82%	1,82%	0,00%
80				0,00%	0,00%
90					0,00%

(0,4)	QF2 60	70	80	90	100
QF1 50	20,91%	16,36%	20,00%	13,64%	0,91%
60		50,00%	47,27%	10,00%	0,00%
70			4,55%	6,36%	0,00%
80				0,91%	0,00%
90					0,00%

has been used: histogram filtering $Th_{filt} = 0.35$ (see Sect. 5.3.1), hybrid strategy with $T_{fix_h} = 5000$ for AC coefficients and $T_{fix_h} = 100000$ for DC coefficient (see Sect. 5.3.2), $max_{diff} = 100$ (see section 5.3.3). The cropping has been performed by removing both the first and the last 4 rows and columns. It is worth noting that all the parameter settings related to the proposed approach have been performed on the dataset [43]. As already underlined in Sect. 5.1, the function proposed in [80] has a poor q_1 localization property that degrades its performances. Moreover, the filtering step (see section 5.3.1) allows to considerably improve the performances of the proposed approach with respect to the method in [91] that does not cope with error e in Eq. (5.9).The direct histogram comparison proposed in [117], without any filtering and candidate selection, is not able to deal with the low quality data related to higher frequencies. Although Bianchi et al. [58] consider in their model the noise e of Eq. (5.9) they actually do not perform any kind of filtering. The combination of a filtering strategy with a function having a good q_1-localization property, allows us outperforming the other state-of-the-art approaches (see Fig. 5.19) both for low and high frequencies.
To further confirm the effectiveness of the proposed approach, additional tests have

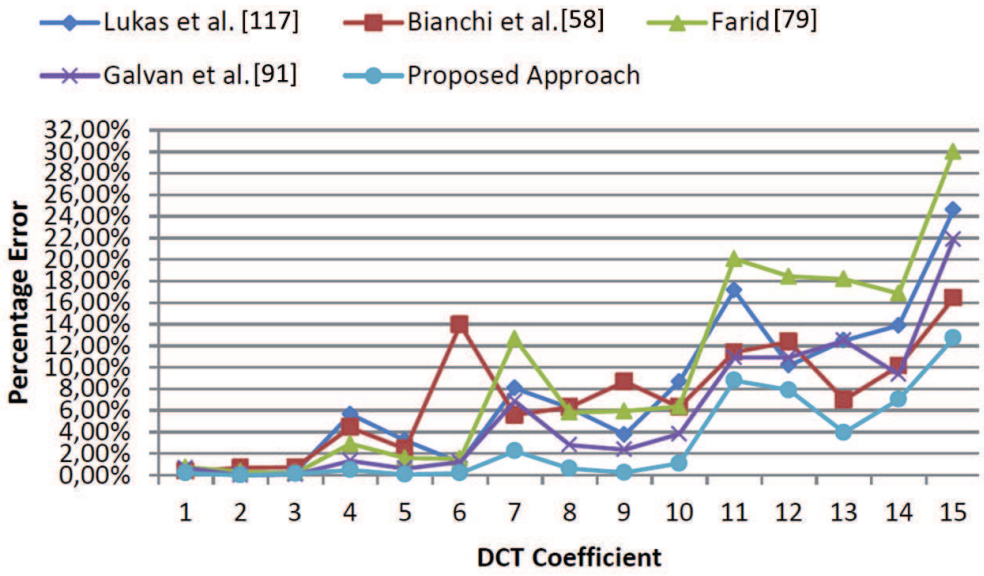

Figure 5.19: Percentage of erroneously estimated q_1 values at varying of DCT coefficient position (zig-zag scanning) considering several state-of-the-art approaches. These values are obtained averaging over all (QF_1,QF_2) and images from the Canon D40D50MK3 Dataset.

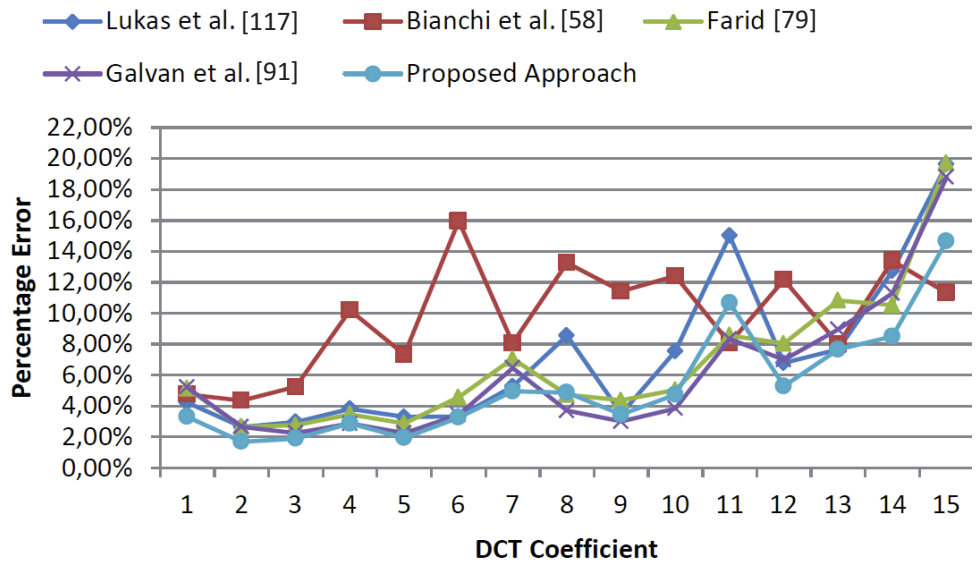

Figure 5.20: Percentage of erroneously estimated q_1 values at varying of DCT coefficient position (zig-zag scanning) considering several state-of-the-art approaches. These values are obtained averaging over all (QF_1,QF_2) and images from the UCID (v2) dataset.

been performed on the Uncompressed Colour Image Database (UCID) standard dataset [148]. Specifically, the UCID (v2) contains 1338 uncompressed TIFF images with a certain variability in terms of scene content (natural, man-made objects, indoor, outdoor, etc.). Moreover, image sizes are 512×384 or 384×512. A novel compressed dataset has then been built, with the same methodology explained before: quality factors (QF_1, QF_2) in the range 50 to 100 at steps of 10 and $q_1 > q_2$. The final dataset contains 20070 double compressed images. As can be easily seen from Fig. 5.20, the proposed solution outperforms, almost everywhere, the state-of-the-art approaches. It is worth noting that the performances of the considered methods in this test are lower than the ones shown in Fig. 5.19. Indeed, the outcomes of the considered approaches depend on the resolution of the image under analysis. If the image size is low, few JPEG blocks can be collected and the reliability of the analysis could be low. In the first test, performed on the Canon D40D50MK3 Dataset, 16384 JPEG blocks are collected per image, whereas in the UCID (v2) Dataset the number of blocks was only 3072. However, working with small images is not the common scenario, and also nowadays images have bigger resolution compared to the ones used in our tests. Moreover, in a tampering scenario in which a patch is pasted over a portion of the original image, the above considerations are still valid. The unmodified regions will undergo to a double compression and, even if the pasted part is significantly smaller compared to the image, the number of available blocks to perform a correct estimation can be enough.

6

Open problems and conclusions

It is important that legislation keeps pace with scientific progress.

Robert Winston

So far, after some theoretical background we reported a list of the main papers that gave the stronger feedback for the area of Image Forensics that is the subject of this thesis, followed by our own contribute to the topic. Nevertheless, this work wouldn't be complete without having touched some aspects that, although somewhat minor, could have a strong impact on the robustness of a method and on the credibility of the proposed outputs.
Indeed, the ideal "to do list" for testing every presented Image Forensics approach for a real scenario is composed by checking out all the following points:

- which is the sensibility of the results on the variation of different quantization tables (that means Quality Factor) used to JPEG compress the image?
- how robust are results on the variation of the DataSet of images used for the tests?
- which is the sensibility of the results on the variation of the resolution of the images?
- how the computational time of every method impacts on its usability?
- how differs the outcomes considering both aligned and not-aligned scenarios?
- how robust are the results to the state-of-the-art Antiforensics methods?

In the following we briefly point out some of the above aspects. We are conscious that everyone of them would deserve to be explored in more detail, but this is out of the purposes of this work.

6.1 The choice of the right Dataset

The need of standardization yet exposed in Sect. 3.3 returns when we take under consideration the databases used in the tests exposed in the papers listed in the previous sections. In these works, the authors referred about the dataset(s) used to check the robustness of their methods. The most frequently cited is the UCID (Uncompressed Color Image Dataset)[148], but also SUN Database[172], Dresden Image Dataset[93], BOSS Image Database[51], NRCS Photo Gallery[37], Kodak Dataset[38], CASIA Tampered Image Detection Evaluation Database[39] and BOWS-2[40] are considered.
This plethora of source is a big obstacle to a correct and fair comparison between the different approaches. Besides, whereas in some works the authors use two or more different sets of images to control the robustness of the proposed approach (i.e., two in [90] and [100], even five in [118]) in some other we noted that the authors tested their method with only one image (i.e., [48, 120]), or created themselves their own dataset (see [56, 65, 86]), or also in some cases (i.e., see [58]) the authors didn't indicate from where the images were taken. To this purpose, in Tab. 6.1 are listed all the choices made by the authors of the papers exposed in Sect. 4 reguarding the datasets used for testing their approaches.
For what exposed discussed above, it is clear that there is not only the need of a shared dataset, but is also necessary to answer to other questions, i.e. which is the minimum amount of images required to give an adequate level of robustness to a proposed method? But more than this, in case of an approach devoted to detect image forgeries, we may ask for a dataset of forged images yet including a set of different resolutions and a set of different kind of patches pasted over the original image, and so on. Moreover, in the case of QSE a proper combination of subsequent quantization parameters (q_1, q_2, ...) should be properly assessed, also considering the real scenario where the involved parameters are not well known [124].
In the paper by Torralba ed al.[162] we found good suggestions about how to create a fair dataset and in general about the fairly use of some existing sets of images. About the first point as an example is suggested to collect the images automatically, instead of in a manual and supervised way. For the latter point is argued that to detect potential sources of bias (or at least to find out the main problematic issues quickly and early, not years after the dataset has been released) it would be better to run any brand-new dataset on a given battery of tests.
Recently, the problem of a common dataset where to fairly compare the verious approaches is exploited by the RAISE dataset [41]. It is composed by a collection of 8156 high-resolution RAW downloadable unprocessed images, taken from seven different scenarios. Time will tell if this purpose will become a landmark.

6.2 Computational time

As a rule, every new algorithm proposed to the scientific community is evaluated also considering its computational time. In case of Image Forensics instead, this is not a point taken under consideration. The reason of this lies in the use that a forensic expert will do of the method, in particular the fact that he acts not on the crime scene but after the event. In general any investigation is divided in two stages. The first (where

Table 6.1: Database used for every method exposed in Sect. 4.

Paper	Composition of the Database
[75, 76]	7 images from an unspecified source
[117]	Training set: 100 JPEG images from various datasets 5 different cameras
[88]	1338 uncompressed images from UCID 198 RAW images from a private dataset 1 camera
[133]	Unspecified
[79]	1000 uncompressed (TIFF) images from UCID From indoor and outdoor Dimension of 512 x 384
[118]	1000 images from COREL, NJIT, NRCS, SYSU and UCID Dimensions from 256 x 256 to 8 x 8
[103]	Images from UCID, NRCS and a private dataset
[174]	2000 color images from COREL and NRCS
[56]	100 uncompressed (TIFF) images from a private dataset Heterogeneous scene content 3 different cameras Dimensions of 1024 x 1024
[58]	Uncompressed (TIFF) images from UCID Dimensions of 384 x 512
[166]	1338 uncompressed (TIFF) images from a private dataset 110 RAW images from a private dataset From indoor and outdoor 3 different cameras Dimensions of 512 x 384 Different resolutions

the image forensics expert rarely is one of the crew) includes the moments in which the crime is accomplished and the police, if present, must take action to prevent it from being led to more serious consequences, or to collect evidences. The second is the phase that begins when the crime is discovered and denounced, after which the law begins to take its course. In this moment the scientific approach for the correct readability of the investigative cues, give to the expert the possibility to answer to the various questions that arise upon a visual document. For example: is this image original? Has it been tampered? In case of positive answer, where and how? Has this image been taken from that device? and so on. These questions, that generally regard few images, are transmitted to the expert and generally the time allowed to him by the public executor amounts to 2/3 weeks.
In this scenario, there is a difference between the time taken to test the methods over an entire dataset (possibly some days), that is what the researcher must do before the validation of his method, and the computational time reported by some papers[166] ($\sim 0,5$ seconds for every image) that took for the application of this method to every image, that is what we must take care about. These considerations let understand that, from the investigative point of view, this topic could be of no interest.
An exception to what stated above can be done when investigators have the need to examine an huge amount of images as quickly as possible. As an example, in the investigations that followed the Boston bombing in 2013 the FBI's call for help caused law enforcement agencies had the disponibility of thousands of footages uploaded by citizens, which sent in what amounted to 29 terabytes of data[42]. In those fundamental moments, a fast algorithm to check the originality of the uploaded images before using them for investigative purposes is undoubtedly desirable.

6.3 Antiforensics

Trying to hide the traces of a malicious action, deleting them or preventing their discovery, is a behavior that has always characterized attackers. Also in Computer Forensics, as its methods come out from the scientific community, we witness to the contemporary flowering of approaches intended to make the first ineffective[98, 132]. Even if this natural phenomenon is somewhat desirable, given that in general it allows the development and growth of any science, it would be preferable if, in cases of forensics approaches, anti-forensics methods wouldn't develop to the same speed as their opponent, but the enormous ease to find the details of any scientific discovery makes this hope very difficult to be satisfied. Also for Image/Video Forensics area, several authors exposed ways to fool the forensics analysis of a visual document, both hiding the traces of a forgery and possibly trying to delete them. In [143] Redi et al. exposed a complete list of possible anti-forensics approaches, followed and supplemented two years later by the work of Piva [135]. From this survey on, restricting our discussion to the DCT domain since there are other areas of Image Forensics which developed their own Antiforensics methods[94, 155, 165], we can cite the work of Fan et al.[73], where after having pointed out the potential vulnerability of the quantization table estimation based detector, the authors proposed a method to fool JPEG forensic detectors based upon optimizing an objective function considering both the anti-forensic terms and a natural image statistical model. In the same year Sreelakshmi et al.[154] proposed an anti-forensic technique

based on the removal of the compression fingerprints of JPEG compression (the blocking artifacts and the characteristic behavior of the histograms of the DCT terms), Comesana et al.[66] exposed an approach to fool the histogram-based Image Forensics methods, and also recently Fan et al. in [74] exposed a method with the purpose to hide the information detectable by histograms-based Image Forensics algorithms.
As the Forensics methods generates the Antiforensics ones, these latter have stimulated the creation and development of a set of approaches, which are known as Counter-Antiforensics. This sub-area of Image Forensics has the aim to discover the information about JPEG compression history after the action of an anti-forensics pipeline, considering both the fingerprints that were not deleted and the ones left by the previous anti forensics attack itself. About the bibliography in this challenging field we want to remember the ones exposed by Lai et al[108], Li et al.[114], Valenzise et al.[163] and the interesting approach devoted to merge together Image Forensics and Counter-Antiforensics methods given by Fontani et al. in [87].

6.4 Final considerations

This thesis, and in particular Chapter 5 that forms its core part, exposes an Image Forensic approach in the DCT domain devoted to retrieve the coefficients of the first quantization in a doubly compressed JPEG image, since the second round of the JPEG algorithm delete all the metadata referred to the first quantization. We saw that the proposed method obtains good performances, also compared with other state of the art methods, even if limited to the case of $q_1 > q_2$.
The introductory part, that highlight some of the reasons why the images are becoming more and more central in our everyday life, is followed by an important section which has the purpose to define the Image/Video Forensics science in the Italian legal context. The following technical part starts with some close details on the JPEG compression algorithm and the Discrete Cosine Transform, continuing with the list, the definitions and the critical discussions of the various kind of errors that characterize a forgery pipeline in case of JPEG images. Before the main part, the thesis contains a detailed list of the state of the art approaches in the field covered by the work. The end takes into consideration some aspects which, even somehow boundary, can have a big influence upon the robustness and the practical applications of every Image Forensics method.
Both in the case in which the results of this work will serve as a stand-alone tool, or as a part of a forensics analysis pipeline, or even if it will be of inspiration for future approaches, our desire to have made a contribution to the scientific growth will be fulfilled.

Bibliography

[1] http://ampedsoftware.com/company.

[2] http://www.factshunt.com/2014/01/world-wide-internet-usage-facts-and.html [Online accessed on October 30^{th}, 2014].

[3] http://thesocietypages.org/cyborgology/2010/12/06/wikileaks-and-our-liquid-modernity/ [Online accessed on July 1^{st}, 2014].

[4] http://www.technologyreview.com/photoessay/533556/auras-theres-an-app-for-that/ [Online accessed on December 29^{th}, 2014].

[5] http://messaggeroveneto.gelocal.it/udine/cronaca/2014/02/19/news/ci-sono-340-telecamere-per-vigilare-su-udine-1.8698695 [Online accessed on July 25^{th}, 2015].

[6] http://www.qumu.com/blog/2014/01/14/[Online accessed on July 16^{nd}, 2015].

[7] http://www.fourandsix.com/photo-tampering-history/tag/photojournalism-ethics?currentPage=5 [Online accessed on March 13^{th}, 2014].

[8] http://www.fourandsix.com/photo-tampering-history/tag/politics?currentPage=8 [Online accessed on March 13^{th}, 2014].

[9] http://www.worldpressphoto.org/collection/photo/2013[Online accessed on July 26^{nd}, 2015].

[10] http://www.flcgil.it/rassegna-stampa/nazionale/truccate-le-foto-delle-cellule-il-prof-universitario-sotto-accusa.flc[Online accessed on July 16^{nd}, 2015].

[11] http://w3techs.com/technologies/overview/images_format/all [Online accessed on March 10^{th}, 2014].

[12] http://w3techs.com/technologies/overview/image_format/all[Online accessed on July 16^{nd}, 2015].

[13] http://www.rewindproject.eu/[Online accessed on November 10^{th}, 2015].

[14] https://www.s-five.eu/mediawiki/index.php[Online accessed on November 10^{th}, 2015].

[15] http://revealproject.eu/[Online accessed on November 10^{th}, 2015].

[16] http://maven-project.eu/[Online accessed on November 10^{th}, 2015].

[17] http://thehackernews.com/2015/06/Stegosploit-malware.html[Online accessed on July 16^{nd}, 2015].

[18] http://renatodisa.com/2015/07/31/[Online accessed on September 29^{nd}, 2015].

[19] http://www.transperfectlegal.com/solutions/forensic[Online accessed on July 21^{nd}, 2015].

[20] http://www.altalex.com/documents/codici-altalex/2014/10/30/codice-di-procedura-penale [Online accessed on July 26^{th}, 2014].

[21] http://www.processig8.org/Udienze_2025/Ud._20143/143_motivazioni-03_25.html[Online accessed on July 20^{nd}, 2015].

[22] http://www.aes.org/tmpFiles/aessc/20150721/aes43-2000-r2010-i.pdf [Online accessed on March 13^{th}, 2014].

[23] http://www.ilgiornaledeimarinai.it/squali-tutta-la-verita/ [Online accessed on May 16^{th}, 2014].

[24] http://www.photoshop.com/ [Online accessed on July 28^{th}, 2015].

[25] https://www.fbi.gov/about-us/lab/forensic-science-communications/fsc/oct2005/index.htm/standards/2005_10_standards01.htm[Online accessed on July 15^{nd}, 2015].

[26] http://www.fourandsix.com/photo-tampering-history/[Online accessed on March 17^{nd}, 2015].

[27] https://www.swgit.org/[Online accessed on March 15^{nd}, 2015].

[28] http://www.fbi.gov/about-us/lab/forensic-science-communications/fsc/oct2005/index.htm/[Online accessed on March 19^{nd}, 2015].

[29] http://www.ijg.org/[Online accessed on December 7^{th}, 2015].

[30] http://en.wikipedia.org/wiki/{JPEG} [Online accessed on January 25^{th}, 2015].

[31] http://www.photome.de/ [Online accessed on August 1^{st}, 2015].

[32] http://exifeditorapp.com/ [Online accessed on August 1^{st}, 2015].

[33] http://www.cs.cf.ac.uk/Dave/Multimedia/node231.html [Online accessed on March 17^{th}, 2014].

[34] http://www.infai.org/jpeg [Online accessed on February 22^{nd}, 2015].

[35] http://www.adobe.com/ [Online accessed on February 23^{nd}, 2015].

[36] `http://it.mathworks.com/` [Online accessed on August 19^{th}, 2015].

[37] `http://photogallery.nrcs.usda.gov/res/sites/photogallery/` [Online accessed on May 1^{st}, 2015].

[38] `http://r0k.us/graphics/kodak/` [Online accessed on May 1^{st}, 2015].

[39] `http://forensics.idealtest.org/` [Online accessed on May 1^{st}, 2015].

[40] `http://bows2.ec-lille.fr/` [Online accessed on May 1^{st}, 2015].

[41] `http://mmlab.science.unitn.it/RAISE/` [Online accessed on September 05^{th}, 2015].

[42] `http://edition.cnn.com/2015/03/09/us/boston-marathon-bombing-trial/` [Online accessed on May 19^{nd}, 2015].

[43] Dataset Eastman Kodak Company: PhotoCD PCD0992, http://r0k.us/graphics/kodak/.

[44] AA.VV. *Enciclopedia del Diritto*. Giuffré Editore, 2008.

[45] Nasir Ahmed. How i came up with the discrete cosine transform. *Digital Signal Processing*, 1(1):4–5, 1991.

[46] Nasir Ahmed, T. Natarajan, and Kamisetty R. Rao. Discrete cosine transform. *Computers, IEEE Transactions on*, 100(1):90–93, 1974.

[47] Ali N Akansu and Paul R Haddad. *Multiresolution signal decomposition: transforms, subbands, and wavelets*. Academic Press, 2000.

[48] NG Allan, Lei Pan, and Yang Xiang. A novel method for detecting double compressed facebook JPEG images. In *Applications and Techniques in Information Security*, pages 191–198. Springer, 2014.

[49] Adobe Developers Association et al. Tiff revision 6.0. *Mountain View, Cal.: Adobe Systems*, 1992.

[50] Mauro Barni, Andrea Costanzo, and Lara Sabatini. Identification of cut & paste tampering by means of double-JPEG detection and image segmentation. In *Circuits and Systems (ISCAS), Proceedings of 2010 IEEE International Symposium on*, pages 1687–1690. IEEE, 2010.

[51] Patrick Bas, Tomáš Filler, and Tomáš Pevnỳ. Break Our Steganographic System: The Ins and Outs of Organizing BOSS. In *Information Hiding*, pages 59–70. Springer, 2011.

[52] Sebastiano Battiato, Arcangelo Ranieri Bruna, Giuseppe Messina, and Giovanni Puglisi. *Image processing for embedded devices*. Bentham Science Publishers, 2010.

[53] Sebastiano Battiato, Fausto Galvan, Martino Jerian, and Matteo Salcuni. Linee guida per l'autenticazione forense di immagini. *IISFA Memberbook*, pages 125–176, 2013.

[54] Sebastiano Battiato, Massimo Mancuso, Angelo Bosco, and Mirko Guarnera. Psychovisual and statistical optimization of quantization tables for DCT compression engines. In *Image Analysis and Processing, 2001. Proceedings. 11th International Conference on*, pages 602–606. IEEE, 2001.

[55] Nicole Beebe. Digital forensic research: The good, the bad and the unaddressed. In *Advances in digital forensics V*, pages 17–36. Springer, 2009.

[56] Tiziano Bianchi, Alessia De Rosa, and Alessandro Piva. Improved DCT coefficient analysis for forgery localization in JPEG images. In *Acoustics, Speech and Signal Processing (ICASSP), 2011 IEEE International Conference on*, pages 2444–2447. IEEE, 2011.

[57] Tiziano Bianchi and Alessandro Piva. Detection of non-aligned double JPEG compression with estimation of primary compression parameters. In *18th IEEE International Conference on Image Processing (ICIP), 2011*, pages 1929–1932. IEEE, 2011.

[58] Tiziano Bianchi and Alessandro Piva. Image forgery localization via block-grained analysis of JPEG artifacts. *Information Forensics and Security, IEEE Transactions on*, 7(3):1003–1017, 2012.

[59] Li Bin, Ng Tian-Tsong, Li Xiaolong, Tan Shunquan, and Huang Jiwu. Revealing the trace of high-quality JPEG compression through quantization noise analysis. *Information Forensics and Security, IEEE Transactions on*, 10(3):558–573, 2015.

[60] JK Bowmaker and HJk Dartnall. Visual pigments of rods and cones in a human retina. *The Journal of physiology*, 298(1):501–511, 1980.

[61] Arthur Brisbane. Speakers give sound advice. *Syracuse Post Standard*, 18, 1911.

[62] Brian Carrier and Eugene H. Spafford. Getting physical with the digital investigation process. *International Journal of digital evidence*, 2(2):1–20, 2003.

[63] Eoghan Casey. *Digital evidence and computer crime: Forensic science, computers, and the internet*. Academic press, 2011.

[64] Joon-Hyuk Chang, Jong Won Shin, Nam Soo Kim, and Sanjit K Mitra. Image probability distribution based on generalized gamma function. *Signal Processing Letters, IEEE*, 12(4):325–328, 2005.

[65] Yi-Lei Chen and Chiou-Ting Hsu. Detecting recompression of JPEG images via periodicity analysis of compression artifacts for tampering detection. *Information Forensics and Security, IEEE Transactions on*, 6(2):396–406, 2011.

[66] Pedro Comesana-Alfaro and Fernando Pérez-González. Optimal counterforensics for histogram-based forensics. In *Proc. IEEE Int. Conf. Acoust., Speech, and Signal Process*, pages 3048–3052, 2013.

[67] Alan J Cooper. Improved photo response non-uniformity (prnu) based source camera identification. *Forensic science international*, 226(1):132–141, 2013.

[68] Davide Cozzolino, Diego Gragnaniello, and Luisa Verdoliva. Image forgery localization through the fusion of camera-based, feature-based and pixel-based techniques. In *IEEE International Conference on Image Processing (ICIP), 2014*, pages 5302–5306. IEEE, 2014.

[69] Alessia De Rosa, Alessandro Piva, Marco Fontani, and Massimo Iuliani. Investigating multimedia contents. In *Security Technology (ICCST), 2014 International Carnahan Conference on*, pages 1–6. IEEE, 2014.

[70] Nilanjan Dey, Debalina Biswas, Anamitra Bardhan Roy, Achintya Das, and Sheli Sinha Chaudhuri. DWT-DCT-SVD based blind watermarking technique of gray image in electrooculogram signal. In *ISDA*, pages 680–685, 2012.

[71] Ahmet Emir Dirik and Ahmet Karaküçük. Forensic use of photo response nonuniformity of imaging sensors and a counter method. *Optics express*, 22(1):470–482, 2014.

[72] Japan Electronics and Information Technology Industries Association. Exchangeable image file format for digital still cameras: Exif version 2.2. technical report. 2002.

[73] Wei Fan, Kai Wang, François Cayre, and Zhang Xiong. JPEG anti-forensics using non-parametric DCT quantization noise estimation and natural image statistics. In *Proceedings of the first ACM workshop on Information hiding and multimedia security*, pages 117–122. ACM, 2013.

[74] Wei Fan, Kai Wang, Francois Cayre, and Zhang Xiong. JPEG anti-forensics with improved tradeoff between forensic undetectability and image quality. *Information Forensics and Security, IEEE Transactions on*, 9(8):1211–1226, 2014.

[75] Zhigang Fan and Ricardo de Queiroz. Maximum likelihood estimation of JPEG quantization table in the identification of bitmap compression history. In *Image Processing, 2000. Proceedings. 2000 International Conference on*, volume 1, pages 948–951. IEEE, 2000.

[76] Zhigang Fan and Ricardo L. de Queiroz. Identification of bitmap compression history: JPEG detection and quantizer estimation. *Image Processing, IEEE Transactions on*, 12(2):230–235, 2003.

[77] Hany Farid. Digital image ballistics from JPEG quantization. *Department of Computer Science, Dartmouth College, Tech. Rep. TR2006-583*, 2006.

[78] Hany Farid. Digital image ballistics from JPEG quantization: A followup study. *Department of Computer Science, Dartmouth College, Tech. Rep. TR2008-638*, 2008.

[79] Hany Farid. Exposing digital forgeries from JPEG ghosts. *Information Forensics and Security, IEEE Transactions on*, 4(1):154–160, 2009.

[80] Hany Farid. Image forgery detection. *Signal Processing Magazine, IEEE*, 26(2):16–25, 2009.

[81] Giovanni M. Farinella, Daniele Ravì, Valeria Tomaselli, Mirko Guarnera, and Sebastiano Battiato. Representing scenes for real-time context classification on mobile devices. *Pattern Recognition*, 48(4):1086–1100, 2015.

[82] Giovanni Maria Farinella and Sebastiano Battiato. Scene classification in compressed and constrained domain. *Computer Vision, IET*, 5(5):320–334, 2011.

[83] Xiaoying Feng and Gwenaël Doërr. JPEG recompression detection. In *IS&T/SPIE Electronic Imaging*, pages 75410J–75410J. International Society for Optics and Photonics, 2010.

[84] Gianni Fenu and Fabrizio Solinas. Computer forensics between the italian legislation and pragmatic questions. *International Journal of Cyber-Security and Digital Forensics (IJCSDF)*, 2(1):9–24, 2013.

[85] Hans Fischer. *A history of the central limit theorem: from classical to modern probability theory*. Springer Science & Business Media, 2010.

[86] Marco Fontani, Enrique Argones-Rua, Carmela Troncoso, and Mauro Barni. The watchful forensic analyst: Multi-clue information fusion with background knowledge. In *Information Forensics and Security (WIFS), 2013 IEEE International Workshop on*, pages 120–125. IEEE, 2013.

[87] Marco Fontani, Alessandro Bonchi, Alessandro Piva, and Mauro Barni. Countering anti-forensics by means of data fusion. In *IS&T/SPIE Electronic Imaging*, pages 90280Z–90280Z. International Society for Optics and Photonics, 2014.

[88] Dongdong Fu, Yun Q Shi, and Wei Su. A generalized benford's law for JPEG coefficients and its applications in image forensics. In *Electronic Imaging 2007*, pages 65051L–65051L. International Society for Optics and Photonics, 2007.

[89] Hei Tao Fung and Kevin J. Parker. Design of image-adaptive quantization tables for JPEG. *Journal of Electronic Imaging*, 4(2):144–150, 1995.

[90] Fausto Galvan, Giovanni Puglisi, A Bruna, and Sebastiano Battiato. First quantization matrix estimation from double compressed JPEG images. *IEEE Transactions on Information Forensics and Security*, 9(8):1299–1310, 2014.

[91] Fausto Galvan, Giovanni Puglisi, Arcangelo R. Bruna, and Sebastiano Battiato. First quantization coefficient extraction from double compressed JPEG images. In *International Conference on Image Analysis and Processing–ICIAP 2013*, volume 8156, pages 783–792. Springer, 2013.

[92] Thomas Gloe. Demystifying histograms of multi-quantised DCT coefficients. In *Multimedia and Expo (ICME), 2011 IEEE International Conference on*, pages 1–6. IEEE, 2011.

[93] Thomas Gloe and Rainer Böhme. The dresden image database for benchmarking digital image forensics. *Journal of Digital Forensic Practice*, 3(2-4):150–159, 2010.

[94] Miroslav Goljan, Jessica Fridrich, and Mo Chen. Defending against fingerprint-copy attack in sensor-based camera identification. *Information Forensics and Security, IEEE Transactions on*, 6(1):227–236, 2011.

[95] Rafael C. Gonzalez and E. Richard. Woods, digital image processing. *ed: Prentice Hall Press, ISBN 0-201-18075-8*, 2002.

[96] Robert M. Gray. *Entropy and information theory*. Springer Science & Business Media, 2011.

[97] Eric Hamilton. JPEG file interchange format. *C-Cube Microsystems*, 1992.

[98] Ryan Harris. Arriving at an anti-forensics consensus: Examining how to define and control the anti-forensics problem. *digital investigation*, 3:44–49, 2006.

[99] Junfeng He, Zhouchen Lin, Lifeng Wang, and Xiaoou Tang. Detecting doctored JPEG images via DCT coefficient analysis. In *Computer Vision–ECCV 2006*, pages 423–435. Springer, 2006.

[100] Zhongwei He, Wei Lu, Wei Sun, and Jiwu Huang. Digital image splicing detection based on markov features in DCT and DWT domain. *Pattern Recognition*, 45(12):4292–4299, 2012.

[101] Theodore P Hill. A statistical derivation of the significant-digit law. *Statistical Science*, pages 354–363, 1995.

[102] Wei Hou, Zhe Ji, Xin Jin, and Xing Li. Double JPEG compression detection base on extended first digit features of DCT coefficients. *International Journal of Information and Education Technology*, 3(5):512–515, 2013.

[103] Fangjun Huang, Jiwu Huang, and Yun Qing Shi. Detecting double JPEG compression with the same quantization matrix. *Information Forensics and Security, IEEE Transactions on*, 5(4):848–856, 2010.

[104] Mei Jiansheng, Li Sukang, and Tan Xiaomei. A digital watermarking algorithm based on DCT and DWT. In *Proceedings of the 2009 International Symposium on Web Information Systems and Applications*, pages 104–107. Citeseer, 2009.

[105] Eric Kee, Michael K. Johnson, and Hany. Farid. Digital image authentication from JPEG headers. *IEEE Transactions on Information Forensics and Security*, 6(3):1066–1075, 2011.

[106] Syed Ali Khayam. The discrete cosine transform (DCT): theory and application. *Michigan State University*, 2003.

[107] Jesse D Kornblum. Using JPEG quantization tables to identify imagery processed by software. *Digital Investigation*, 5:S21–S25, 2008.

[108] ShiYue Lai and Rainer Böhme. Countering counter-forensics: The case of JPEG compression. In *Information Hiding*, pages 285–298. Springer, 2011.

[109] Edmund Y. Lam. Analysis of the DCT coefficient distributions for document coding. *Signal Processing Letters, IEEE*, 11(2):97–100, 2004.

[110] Edmund Y. Lam and Joseph W. Goodman. A mathematical analysis of the DCT coefficient distributions for images. *Image Processing, IEEE Transactions on*, 9(10):1661–1666, 2000.

[111] Alan Leger, Joan L Mitchell, and Yasuhiro Yamazaki. Still picture compression algorithms evaluated for international standardisation. In *Global Telecommunications Conference, 1988, and Exhibition.'Communications for the Information Age.'Conference Record, GLOBECOM'88., IEEE*, pages 1028–1032. IEEE, 1988.

[112] Bin Li, Tian-Tsong Ng, Xiaolong Li, Shunquan Tan, and Jiwu Huang. JPEG noises beyond the first compression cycle. *Technical Report TR2014-001, Shenzhen University, Tech. Rep.*, 2014.

[113] Bin Li, Yun Q Shi, and Jiwu Huang. Detecting doubly compressed JPEG images by using mode based first digit features. In *Multimedia Signal Processing, 2008 IEEE 10th Workshop on*, pages 730–735. IEEE, 2008.

[114] Haodong Li, Weiqi Luo, and Jiwu Huang. Countering anti-JPEG compression forensics. In *19th IEEE International Conference on Image Processing (ICIP), 2012*, pages 241–244. IEEE, 2012.

[115] Zhouchen Lin, Junfeng He, Xiaoou Tang, and Chi-Keung Tang. Fast, automatic and fine-grained tampered JPEG image detection via DCT coefficient analysis. *Pattern Recognition*, 42(11):2492–2501, 2009.

[116] Qingzhong Liu, Andrew H Sung, Zhongxue Chen, and Lei Chen. Exposing image tampering with the same quantization matrix. In *Multimedia Data Mining and Analytics*, pages 327–343. Springer, 2015.

[117] Jan Lukáš and Jessica Fridrich. Estimation of primary quantization matrix in double compressed JPEG images. In *Proc. Digital Forensic Research Workshop*, pages 5–8, 2003.

[118] Weiqi Luo, Jiwu Huang, and Guoping Qiu. JPEG error analysis and its applications to digital image forensics. *Information Forensics and Security, IEEE Transactions on*, 5(3):480–491, 2010.

[119] Babak Mahdian and Stanislav Saic. Detecting double compressed JPEG images. *3rd International Conference on Imaging for Crime Detection and Prevention (ICDP-09), London, U.K*, 2009.

[120] S Manimurugan and Jose B. A novel method for detecting triple JPEG ompression with the same quantization matrix. *International Journal of Engineering Trends and Technology*, 3(2):94–97, 2012.

[121] Rebecca Mercuri. Courtroom considerations in digital image forensics. In *Digital Image Forensics*, pages 313–325. Springer, 2013.

[122] Simone Milani, Marco Tagliasacchi, and Stefano Tubaro. Antiforensics attacks to benford's law for the detection of double compressed images. In *Acoustics, Speech and Signal Processing (ICASSP), 2013 IEEE International Conference on*, pages 3053–3057. IEEE, 2013.

[123] Simone Milani, Marco Tagliasacchi, and Stefano Tubaro. Discriminating multiple JPEG compressions using first digit features. *APSIPA Transactions on Signal and Information Processing*, 3:e19, 2014.

[124] Marco Moltisanti, Antonino Paratore, Sebastiano Battiato, and Luigi Saravo. Image manipulation on facebook for forensics evidence. In *Image Analysis and ProcessingICIAP 2015*, pages 506–517. Springer, 2015.

[125] F Muller. Distribution shape of two-dimensional DCT coefficients of natural images. *Electronics Letters*, 29(22):1935–1936, 1993.

[126] Hitomi Murakami, Yoshinori Hatori, and Hide Yamamoto. Comparison between dpcm and hadamard transform coding in the composite coding of the NTSC color TV signal. *Communications, IEEE Transactions on*, 30(3):469–479, 1982.

[127] Robert A.. Nash, Kimberley A. Wade, and D. Stephen Lindsay. Digitally manipulating memory: Effects of doctored videos and imagination in distorting beliefs and memories. *Memory & cognition*, 37(4):414–424, 2009.

[128] Ramesh N. Neelamani, Ricardo De Queiroz, Zhigang Fan, Sanjeeb Dash, and Richard G. Baraniuk. JPEG compression history estimation for color images. *Image Processing, IEEE Transactions on*, 15(6):1365–1378, 2006.

[129] Arooj Nissar and AH Mir. Classification of steganalysis techniques: A study. *Digital Signal Processing*, 20(6):1758–1770, 2010.

[130] Cecilia Pasquini, Giulia Boato, and Fernando Perez-Gonzalez. Multiple JPEG compression detection by means of benford-fourier coefficients. In *Parallel Computing Technologies (PARCOMPTECH), 2015 National Conference on*, pages 113–118. IEEE, 2015.

[131] Cecilia Pasquini, Fernando Pérez-González, and Giulia Boato. A benford-fourier jpeg compression detector. In *IEEE International Conference on Image Processing (ICIP), 2014*, pages 5322–5326. IEEE, 2014.

[132] Christian SJ Peron and Michael Legary. Digital anti-forensics: emerging trends in data transformation techniques. In *Proceedings of ECCE'05 E-Crime and Computer Conference*, 2005.

[133] Tomas Pevny and Jessica Fridrich. Detection of double-compression in JPEG images for applications in steganography. *Information Forensics and Security, IEEE Transactions on*, 3(2):247–258, 2008.

[134] Mark A. Pinsky. *Introduction to Fourier analysis and wavelets*. Brooks/Cole Pacific Grove, 2002.

[135] Alessandro Piva. An overview on image forensics. *ISRN Signal Processing*, 2013, 2013.

[136] Alin C Popescu and Hany Farid. Statistical tools for digital forensics. In *Information Hiding*, pages 128–147. Springer, 2005.

[137] William K Pratt. Digital image processing john wiley & sons. *New York*, 1191:491–556, 1978.

[138] NISO Press. Understanding metadata. *National Information Standards*, 20, 2004.

[139] Niels Provos. Defending against statistical steganalysis. In *Usenix Security Symposium*, volume 10, pages 323–336, 2001.

[140] Giovanni Puglisi, Arcangelo R. Bruna, Fausto Galvan, and Sebastiano Battiato. First jpeg quantization matrix estimation based on histogram analysis. In *20th IEEE International Conference on Image Processing (ICIP), 2013*, pages 4502–4506. IEEE, 2013.

[141] Atul Puri and Andria H Wong. Spatial-domain resolution-scalable video coding. In *Visual Communications' 93*, pages 718–729. International Society for Optics and Photonics, 1993.

[142] T Recommendation. 81: Digital compression and coding of continuous-tone still imagesrequirements and guidelines. Technical report, Technical report, CCITT, 1992.

[143] Judith A. Redi, Wiem Taktak, and Jean-Luc Dugelay. Digital image forensics: a booklet for beginners. *Multimedia Tools and Applications*, 51(1):133–162, 2011.

[144] Randall C. Reininger and Jerry D. Gibson. Distributions of the two-dimensional DCT coefficients for images. *Communications, IEEE Transactions on*, 31(6):835–839, 1983.

[145] Mark A. Robertson and Robert L. Stevenson. DCT quantization noise in compressed images. *Circuits and Systems for Video Technology, IEEE Transactions on*, 15(1):27–38, 2005.

[146] Nuno Roma and Leonel Sousa. A tutorial overview on the properties of the discrete cosine transform for encoded image and video processing. *Signal Processing*, 91(11):2443–2464, 2011.

[147] Dario LM Sacchi, Franca Agnoli, and Elizabeth F. Loftus. Changing history: Doctored photographs affect memory for past public events. *Applied Cognitive Psychology*, 21(8):1005–1022, 2007.

[148] Gerald Schaefer and Michal Stich. Ucid: an uncompressed color image database. In *Electronic Imaging 2004*, pages 472–480. International Society for Optics and Photonics, 2003.

[149] Victor Schetinger, Manuel M Oliveira, Roberto da Silva, and Tiago J Carvalho. Humans are easily fooled by digital images. *arXiv preprint arXiv:1509.05301*, 2015.

[150] Abduljabbar Shaamala, Shahidan M. Abdullah, and Azizah A. Manaf. Study of the effect DCT and DWT domains on the imperceptibility and robustness of genetic watermarking. *IJCSI International Journal of Computer Science Issues*, 8(5), 2011.

[151] David J Sheskin. *Handbook of parametric and nonparametric statistical procedures*. crc Press, 2003.

[152] Milani Simone, Tagliasacchi Marco, and Tubaro Stefano. Segmentation-based motion compensation for enhanced video coding. In *Acoustics, Speech and Signal Processing (ICASSP), 2012 IEEE International Conference on (ICASSP 2012)*, March 2012.

[153] Fabrizio Solinas. Technical and legal perspectives on forensics scenario. 2014.

[154] MS Sreelakshmi and D. Venkataraman. Image compression using anti-forensics method. *International Journal of Computer Science, Engineering & Applications*, 3(1), 2013.

[155] Matthew C. Stamm, W Sabrina Lin, and KJ Ray Liu. Temporal forensics and anti-forensics for motion compensated video. *IEEE Transactions on Information Forensics and Security*, 7(4):1315–1329, 2012.

[156] Matthew C Stamm and KJ Ray Liu. Anti-forensics of digital image compression. *Information Forensics and Security, IEEE Transactions on*, 6(3):1050–1065, 2011.

[157] Matthew C Stamm, Steven K Tjoa, W Sabrina Lin, and KJ Ray Liu. Undetectable image tampering through JPEG compression anti-forensics. In *17th IEEE International Conference on Image Processing (ICIP), 2010*, pages 2109–2112. IEEE, 2010.

[158] Gilbert Strang. The discrete cosine transform. *SIAM review*, 41(1):135–147, 1999.

[159] Tom Swan. *Inside Windows File Formats*. Sams, 1993.

[160] T Thai, Rémi Cogranne, and Florent Retraint. Statistical model of quantized DCT coefficients: Application in the steganalysis of jsteg algorithm. 2014.

[161] Vrizlynn LL Thing, Yu Chen, and Carmen Cheh. An improved double compression detection method for JPEG image forensics. In *Proceedings of the 2012 IEEE International Symposium on Multimedia*, pages 290–297. IEEE Computer Society, 2012.

[162] Antonio Torralba and Alexei A. Efros. Unbiased look at dataset bias. In *Computer Vision and Pattern Recognition (CVPR), 2011 IEEE Conference on*, pages 1521–1528. IEEE, 2011.

[163] Giuseppe Valenzise, Marco Tagliasacchi, and Stefano Tubaro. Revealing the traces of JPEG compression anti-forensics. *Information Forensics and Security, IEEE Transactions on*, 8(2):335–349, 2013.

[164] Gregory K. Wallace. The JPEG still picture compression standard. *Communications of the ACM*, 34(4):30–44, 1991.

[165] Meijuan Wang, Zhenyong Chen, Wei Fan, and Zhang Xiong. Countering anti-forensics to wavelet-based compression.

[166] Wei Wang, Jing Dong, and Tieniu Tan. Exploring DCT coefficient quantization effects for local tampering detection. *IEEE Transactions on Information Forensics and Security*, 9(10):1653–1666, 2014.

[167] Weihong Wang and Hany Farid. Exposing digital forgeries in video by detecting double MPEG compression. In *Proceedings of the 8th workshop on Multimedia and security*, pages 37–47. ACM, 2006.

[168] Weihong Wang and Hany Farid. Exposing digital forgeries in video by detecting double quantization. In *Proceedings of the 11th ACM workshop on Multimedia and security*, pages 39–48. ACM, 2009.

[169] Andrew B. Watson. Image compression using the discrete cosine transform. *Mathematical Journal*, 4(1):81.

[170] Andreas Westfeld and A Pfitzmann. High capacity despite better steganalysis (f5–a steganographic algorithm). In *Information Hiding, 4th International Workshop*, volume 2137, pages 289–302, 2001.

[171] Bernard Widrow, Istvan Kollar, and Ming-Chang Liu. Statistical theory of quantization. *IEEE Transactions on Instrumentation and Measurement*, 45(2):353–361, 1996.

[172] Jianxiong Xiao, James Hays, Krista A Ehinger, Aude Oliva, and Antonio Torralba. Sun database: Large-scale scene recognition from abbey to zoo. In *Computer vision and pattern recognition (CVPR), 2010 IEEE conference on*, pages 3485–3492. IEEE, 2010.

[173] Jianquan Yang, Guopu Zhu, Jiwu Huang, and Xi Zhao. Estimating JPEG compression history of bitmaps based on factor histogram. *Digital Signal Processing*, 2015.

[174] Jianquan Yang, Guopu Zhua, and Jiwu Huangb. Detecting doubly compressed JPEG images by factor histogram. *Asia Pacific Signal and Information Processing Association - Annual Summit and Conference (APSIPA ASC 2011), Xi'an, China*, 2011.

[175] Fabian Zach, Christian Riess, and Elli Angelopoulou. *Automated image forgery detection through classification of JPEG ghosts*. Springer, 2012.